Processing and Flavoring

MEAT ANALOGUES

SILVIA J. E. SNEL

SILVIA J.E. SNEL
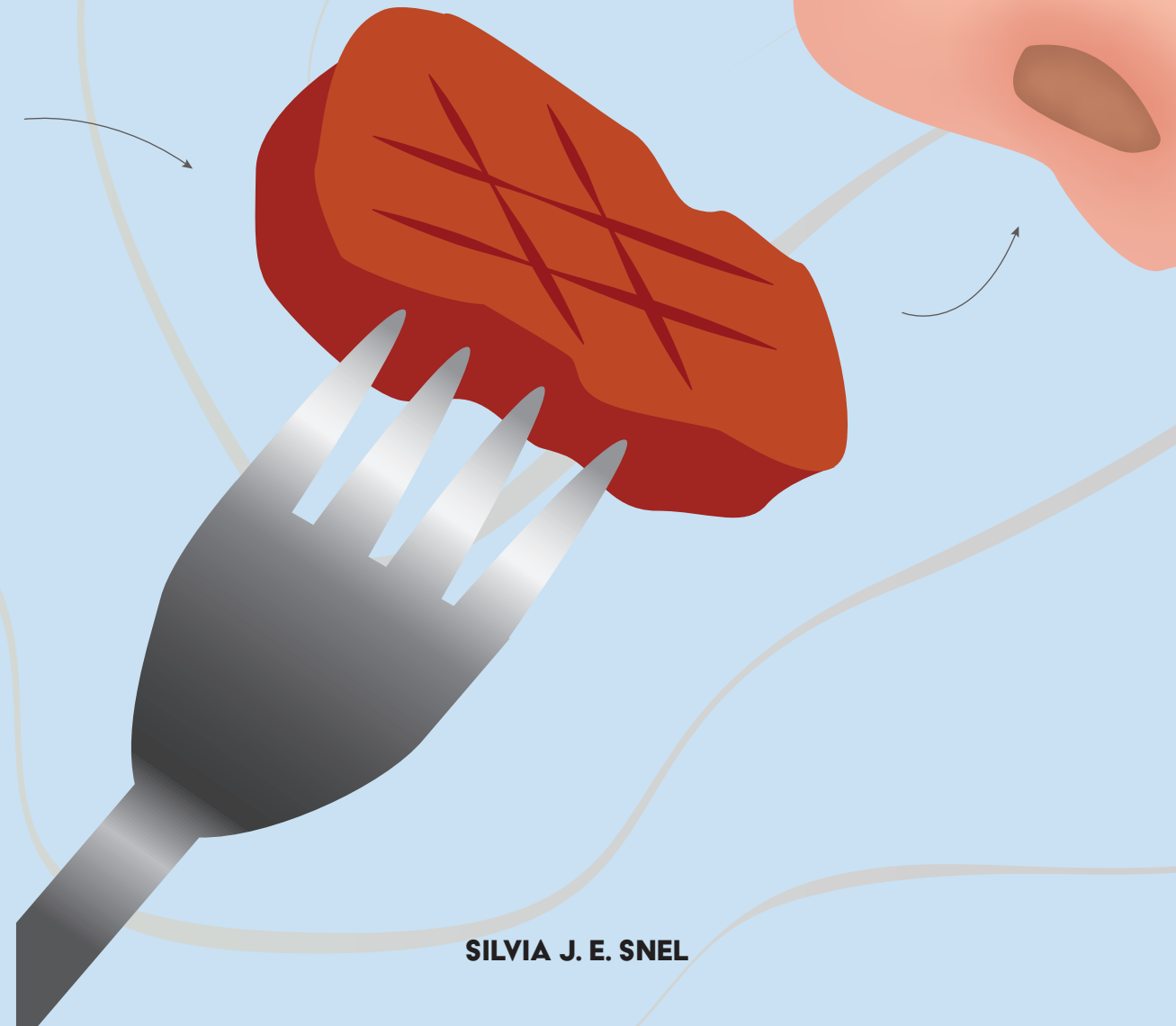
Propositions

1. For the development of next generation meat analogues, it is necessary to develop dedicated equipment, such as the rotating die.
   (this thesis)
2. The addition of flavors to plant proteins while extruding is not efficient.
   (this thesis)
3. Beyond meat analogues, preserving plant-based traditional recipes offers sustainable solutions for global challenges of hunger and the climate crisis.
4. In our pursuit of sustainability, the current emphasis on technological innovation overshadows the vital need for behavioral changes in consumption patterns.
5. Experienced lab technicians are under rewarded despite being essential for PhD students to thrive.
6. Encouraging parents of adult children that moved out to become foster parents can both address the shortage of foster families and provide a solution for empty nest syndrome.
7. To be better prepared for the defense, all PhD's could benefit from learning Karate.

Propositions belonging to the thesis, entitled

Processing and flavoring meat analogues

Silvia J. E. Snel

Wageningen, 3 November 2023

Processing and flavoring meat analogues

Silvia J. E. Snel

Processing and flavoring meat analogues

Silvia J. E. Snel

Thesis

submitted in fulfilment of the requirements for the degree of doctor

at Wageningen University

by the authority of the Rector Magnificus,

Prof. Dr A.P.J. Mol,

in the presence of the

Thesis committee appointed by the Academic Board

to be defended in public

on Friday 3 November 2023

at 4 p.m. in the Omnia Auditorium.

Table of contents

Chapter 1

General introduction

Meat analogues are meant to replace meat in the human diet. Such replacement is described to reduce the environmental burden of human diets (Smetana et al., 2023). Consumer acceptance of meat analogues is enhanced by a high similarity in texture and flavor to meat, according to several studies (Hoek et al., 2011; Michel et al., 2021). However, even today, it is challenging to create products that are both similar in texture and taste compared to a broad range of meat products.

1.1   Production of current Meat analogues

A first step in the creation of a meat analogues is the transformation of plant proteins into anisotropic, fibrous meat products (Dekkers et al., 2018). Many industrial processes to texturize plant proteins into fibrous meat analogues are based on extrusion cooking (Cornet et al., 2021), but mixing and coagulation is also used and studied (Dobson et al., 2023; Kweldam et al., 2011).

Extrusion cooking was discovered as an effective way to transform defatted soy flour, a by-product from soy oil, into meat extenders (Puski & Konwinski, 1976). Extrusion cooking is performed with an extruder comprising two co-rotating screws in a heated barrel, in which the wet and dry ingredients are mixed and pushed into a die (Figure 1.1). The heated barrel is divided into different sections, and the temperature is increased to around 120-150 °C. The co-rotating screws induce shear with rates up to 2000 s-1 at the screw tips (Emin & Schuchmann, 2013). The moisture content in the low moisture process is typically 30% and the obtained product is then a result of expansion after leaving a short die. Expansion at the die exit takes place as a result of the pressure build-up in the extruder barrel, causing a pressure drop upon product exiting the die leading to rapid moisture evaporation from the product (Alam et al., 2016). After extrusion, the product is further dried to 6-10 % to allow a long shelf life (Puski & Konwinski, 1976). These dried products are hydrated before they can be used in, for example, hamburgers, nuggets, and sausages.

The invention of a long cooling die allowed the production of meat analogues with a higher moisture content (Cheftel et al., 1992, Figure 1.1). At the end of the extruder barrel, the protein mixture is pushed through a long cooling die to cool the protein mixture to below 100 °C, which prevents moisture release and expansion when the product exists the die. The moisture content is generally between 50-70 %, and the product is not dried after the process, allowing for immediate use as a meat analogue. The products made with high moisture extrusion cooking are less spongy, and have a more distinctive meat-like, dense structure (Samard et al., 2019). Products produced under high moisture conditions can be used for products like chicken strips. Shear in the cooling die has been pointed out as an important parameter for structure formation but the actual shear rates and stresses are directly dependent on the die dimensions and throughput (Cornet et al., 2021).
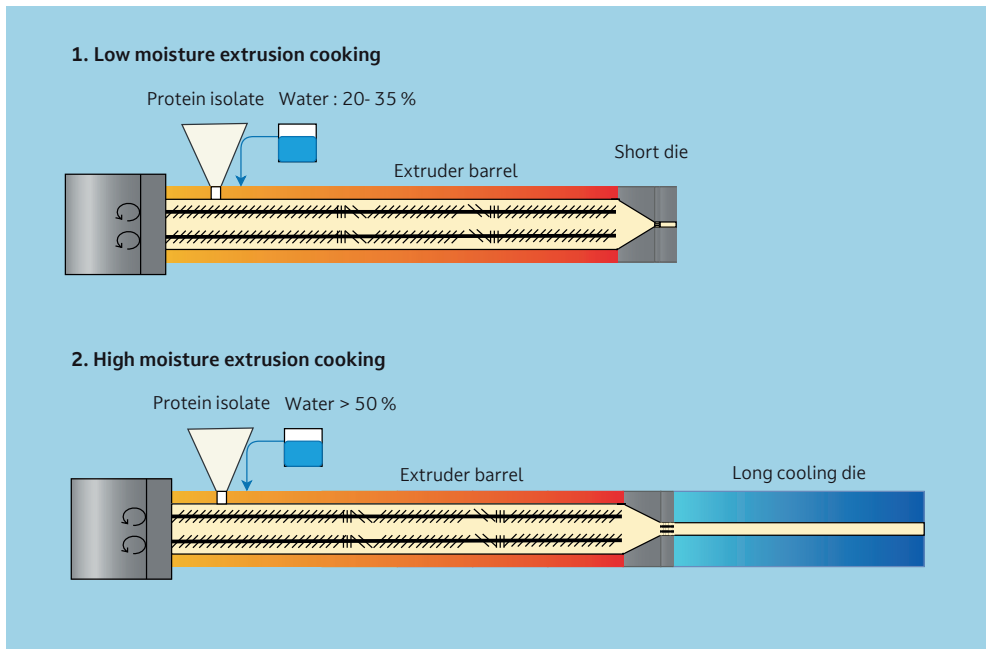
Figure 1.1: Schematic representation of low and high moisture extrusion cooking. Adapted from (S. H. V. Cornet, Snel, et al., 2021).

1.2 Developments in creation of meat analogues

The complexity of extrusion cooking, the fact that the equipment is expensive and the limited possibilities to alter product shape and structure due to the constrained die design have stimulated the development of novel processing techniques for meat analogues. Contrary to extrusion, those techniques have not been applied yet industrially, or just on limited scale.

1.2.1 Shear Cell

The shear cell was initially developed to mimic extrusion-like conditions (Van Den Einde et al., 2003). Later, it was discovered that the shear cell technology could be used as a novel structuring method (Manski et al., 2007). It is a batch operated process for which the protein and water are mixed externally before it is placed in the heated cone-in-cone design. The shear cell consists out of two cones, an upper static cone, and a rotating bottom cone. The lower cone rotates and induces a shear stress, while the cones are both heated to temperatures of 130-160 °C, after which a cooling step is performed without rotation. It should be noted that the mechanical energy input needed to make a structure is much lower compared to extrusion (Krintiras et al., 2016), suggesting that the process based on shear cell is milder than extrusion.

1.2.2 Spinning

Another technique for creating aligned proteins is spinning. Spinning can be performed either as wet spinning or electrospinning. In the former, the viscous biopolymer solution is pushed out of a spinneret into a coagulating bath (Dekkers et al., 2018). The combination of soy protein isolate with sodium alginate has proven successful in forming edible spun fibers in a calcium chloride bath (Cui et al., 2022). A drawback of wet spinning is the creation of large water wastes, and the difficulty to assemble the fibers into a food product on industrial scale. For electrospinning, very thin fibrils are produced by placing a high voltage over a polymer solution, inducing a Taylor cone formation that results in a spun thread (Nieuwland et al., 2014). This technique was applied to spin pea and common pea protein isolates with added solvents (Aguilar-Vázquez et al., 2020). However, the solvents used are toxic and might end up in the fibrils partly (Aguilar-Vázquez et al., 2020). The replacement of the toxic solvent, or its complete removal from the fibrils is still a challenge that has to be solved in order to produce food-grade fibrils.

1.2.3 3D printing

The three-dimension (3D) printing of plant proteins into meat analogues is the recently developed technique (Voon et al., 2019). A printable mixture of ingredients is pushed through nozzle. After printing, often a post processing step is performed, such as baking or cooking. A 3D printer combined with air-heating was able to create solid structures instantly from a combination of soy, gluten, and rice protein (Qiu et al., 2023). However, as it is a more novel technique, scalability for food production is still a challenge. A current advancement is combine multiple printers, which also enables printing 'protein', 'blood', and 'fat' simultaneously (Ben-Shitrit et al., 2022).

1.2.4 Mixing of ingredients

Mixing and coagulation is a technique that is already applied to structure milk proteins into meat analogues (Kweldam et al., 2011). Similarly, a recent study showed the potential of mixing and stretching of zein domains in a protein-starch network to develop fibrous meat analogues without applying high temperatures or extensive shear (Dobson et al., 2023). Zein was plasticized with acetic acid and mixed with PPI and waxy maize starches and subsequently manually extended to induce elongation of the zein domains (Dobson et al., 2023). Another mixing technique involved coarcevate formation of potato protein with gellan gum at acidic pH as a route to make vegan chicken-like products (Ryu et al., 2023).

1.2.5 Combining technologies for better products

Instead of developing a new technology, it is also interesting to explore possibilities for combining technologies. For example, a small-scale twin-screw extruder can be combined with a moving plateau to simulate 3D printing (Kim et al., 2021). A micro-compounder, resembling a tiny single-screw extruder could also be combined with 3D printing (Tingle, 2022). The printed protein bundles could be printed simultaneously with a hydrocolloid to

'glue' them together. Spinning can be used to make fibrils that can be added to a protein mix in high moisture extrusion or shear cell. Another route is to modify the die of an extruder to create additional shear that can be modified independently. It can be expected that more combinations of technology will be proposed in near future.

1.3   Ingredients to make meat analogues; effect of minor ingredients

Soy protein isolate (SPI) and soy protein concentrate (SPC) are the most common ingredients used for meat analogues (Kyriakopoulou et al., 2021). However, leguminous protein sources, such as pea, are gaining more attention and have been used in meat analogues as well (Geistlinger, 2015; Osen, 2017). Vital wheat gluten (VWG) can be added to leguminous proteins to induce a fibrous structure (Cornet, Bühler, et al., 2021). Apart from gluten, also hydrocolloids are added to induce structure formation in an ingredient that otherwise would not create fibrous textures (Dekkers, Hamoen, et al., 2018; Schreuders et al., 2022). The effect of hydrocolloids is explained by considering thermo-mechanical incompatibility of the protein and hydrocolloid (Grinberg & Tolstoguzov, 1997). This incompatibility leads to two phases. In such two-phase blends it is possible to elongate the dispersed phase under shear, which is thought to be responsible for the fibrous appearance of a product (Dekkers et al., 2016). When screening different hydrocolloids, it was found that xanthan gum could be used to make a more pronounced fibrous product using pea protein isolate (PPI)-VWG blends (Taghian Dinani et al., 2023). However, not all hydrocolloids induce a fibrous product when added to an protein isolate.Processing of these beldns blends can also lead to isotropic products or macroscopic phase separation. The latter was for example observed when processing blends of SPI and cellulose in the shear cell (Schreuders et al., 2022).

### 1.3.1   Flavoring meat analogues

In addition to creating the best structure, the flavoring of meat analogues remains challenging. Plant proteins have off-flavors that are naturally present, arise during the isolation procedure and can develop during processes such as extrusion (Wang et al., 2022). Furthermore, the effective addition of flavor to meat analogues is hindered by interactions between flavors and plant proteins (Reineccius, 2022). The protein-flavor interactions reduce the flavor release and perception when eating the product (Hansen & Heinis, 1991) The interactions between flavors and proteins depend on the chemical class of the flavor molecules, the protein source and processing history (Guichard, 2002). Examples of flavor classes used for flavoring protein blends are esters, ketones, and aldehydes. Esters and ketones can interact with the protein through non-covalent interactions, such as hydrophobic interactions and hydrogen bonds (Wang & Arntfield, 2016). Apart from non-covalent interactions, aldehydes can also interact through covalent reactions, mainly adduct formation (Fenaille et al., 2003). In addition, the high temperatures during extrusion can lead to increased volatility and possibly degradation of flavors (Khio et al., 2012).

Flavors do not only influence taste, but they could also influence the structuring potential of ingredients. There might be a direct effect, but also the flavor solvent, such as oil, will affect the final product structure.

1.4   Aim and thesis Outline

The aim of this thesis is to increase understanding of the effects of processing and minor ingredients including flavors on the structuring process of dense protein blends. To reach this aim the following objectives are defined.

1.   To demonstrate potential of a rotating die attached to an extruder;
2.   To study effect of minor components on the structuring potential of SPI;
3.   To quantify flavor binding to proteinaceous ingredients that are used or have potential for use in meat analogues.
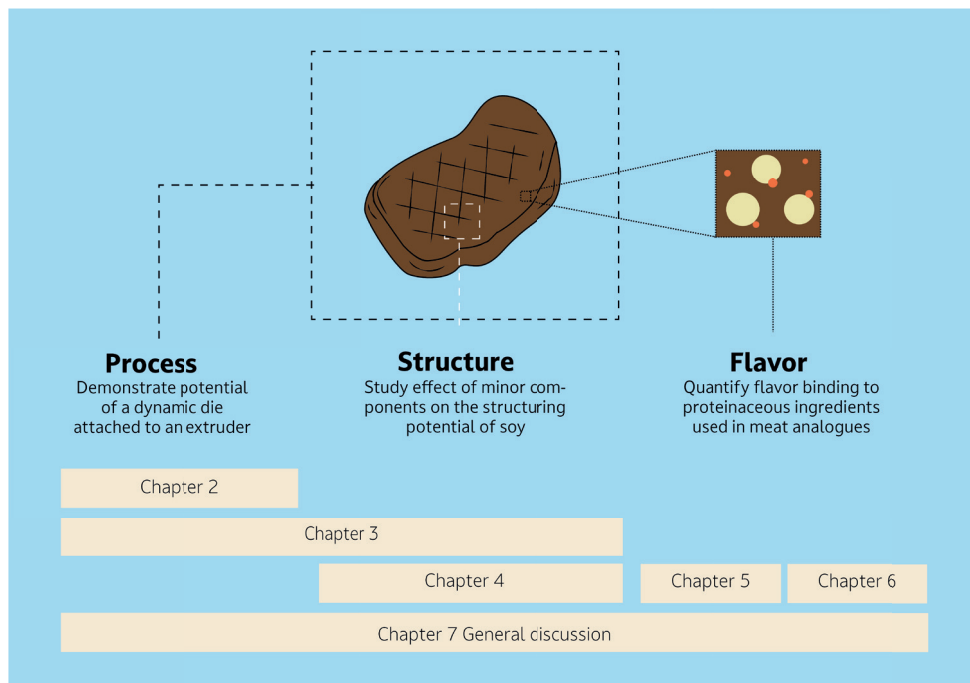
Figure 1.2 Graphical representation of the outline of the thesis, and how the aims are covered in the different chapters

In **Chapter 2** a new extrusion die is introduced that allows the implementation of shear as an independent parameter during high moisture extrusion cooking. A so-called rotating cooling die is therefore constructed and connected to a twin-screw extruder. Common ingredients for meat analogues, which are pea protein isolate (PPI), soy protein concentrate (SPC), vital wheat gluten (VWG), and blends of PPI/SPC with VWG are explored for their potential to make fibrous products with this set-up. The fibrous products produced at different shear rates

are compared on their visual texture, microstructure, hardness, and anisotropy.

The same rotating die is used in **Chapter 3** to test the rework potential of SPI- and PPI-based fibrous products. The fibrous products are freeze-dried, ground, and processed again in a second extrusion step. The obtained products are analyzed in terms of their hardness, anisotropic cutting strength and visual texture. Furthermore, rheological behavior, solubility and WHC of the freeze-dried powders are measured.

In **Chapter 4** the shear cell is used to observe the structuring potential of four different pectins in a SPI-based meat analogue. In this manner, we obtain a better understanding of the role of minor components, their interactions with SPI and the importance of phase separation as a principle for structuring meat analogues. The sugar composition and functionality of the pectins are studied. Products obtained with blends of SPI and pectins are compared on macro- and micro-texture, void fraction, fracture behavior and anisotropy. Furthermore, the rheological properties of the SPI-pectin blends are studied with a strain amplitude sweep.

Chapter 5 introduces the flavoring aspect of meat analogues. In this chapter, esters and ketones of different chain lengths are added to protein dispersions with different protein concentrations. Protein isolates of pea, soy, chickpea and fava bean are studied on their ability to retain flavors and are compared with whey protein as a control. The obtained results are captured in a flavor model that delivers values for fitting parameters to describe and predict the flavor retention in protein blends.

The same flavor model is implemented again in **Chapter 6** with mono-unsaturated and saturated aldehydes. Because aldehydes can covalently interact with proteins, a covalent interaction parameter is added to the flavor retention model. This allows comparisons between hydrophobic and covalent interactions.

Chapter 7 reviews all results and insights obtained in this thesis. It describes the effect of flavor on structuring potential of soy. Finally, the chapter ends with a future outlook.

References

Aguilar-Vázquez, G., Ortiz-Frade, L., Figueroa-Cárdenas, J. D., López-Rubio, A., & Mendoza, S. (2020). Electrospinnability study of pea (Pisum sativum) and common bean (Phaseolus vulgaris L.) using the conformational and rheological behavior of their protein isolates. *Polymer Testing*, *81*(July 2019). https://doi.org/10.1016/j.polymertesting.2019.106217

Alam, M. S., Kaur, J., Khaira, H., & Gupta, K. (2016). Extrusion and Extruded Products: Changes in Quality Attributes as Affected by Extrusion Process Parameters: A Review. *Critical Reviews in Food Science and Nutrition*, *56*(3), 445–473. https://doi.org/10.1080/10408398.2013.779568

Ben-Shitrit, E., Tomsov, A., Mandelik, D., Dikovsky, D., & Silberstein, S. (2022). *Meat analogues and methods of producing the same* (Patent No. US20220125072A1).

Cheftel, J. C., Kitagawa, M., & Queguiner, C. (1992). New Protein Texturization Processes by Extrusion Cooking at High Moisture Levels. *Food Reviews International*, *8*(2), 235–275. https://doi.org/10.1080/87559129209540940

Cornet, S. H. V., Bühler, J. M., Gonçalves, R., Bruins, M. E., van der Sman, R. G. M., & van der Goot, A. (2021). Apparent universality of leguminous proteins in swelling and fibre formation when mixed with gluten. *Food Hydrocolloids*, *120*. https://doi.org/10.1016/j.foodhyd.2021.106788

Cornet, S. H. V., Snel, S. J. E., Schreuders, F. K. G., Van der Sman, R. G. M., Beyrer, M., & Van der Goot, A. J. (2021). Thermo-mechanical processing of plant proteins using shear cell and high-moisture extrusion cooking. *Critical Reviews in Food Science and Nutrition*, *0*(0), 1–18. https://doi.org/10.1080/10408398.2020.1864618

Cui, B., Liang, H., Li, J., Zhou, B., Chen, W., Liu, J., & Li, B. (2022). Development and characterization of edible plant-based fibers using a wet-spinning technique. *Food Hydrocolloids*, *133*. https://doi.org/10.1016/j.foodhyd.2022.107965

Dekkers, B. L., Boom, R. M., & van der Goot, A. J. (2018). Structuring processes for meat analogues. *Trends in Food Science and Technology*, *81*, 25–36. https://doi.org/10.1016/j.tifs.2018.08.011

Dekkers, B. L., Nikiforidis, C. V., & van der Goot, A. J. (2016). Shear-induced fibrous structure formation from a pectin/SPI blend. *Innovative Food Science and Emerging Technologies*, *36*, 193–200. https://doi.org/10.1016/j.ifset.2016.07.003

Dobson, S., Stobbs, J., Laredo, T., & Marangoni, A. G. (2023). A facile strategy for plant protein fiber formation without extrusion or shear processing. *Innovative Food Science and Emerging Technologies*, *86*. https://doi.org/10.1016/j.ifset.2023.103385

Emin, M. A., & Schuchmann, H. P. (2013). Analysis of the dispersive mixing efficiency in a twin-screw extrusion processing of starch based matrix. *Journal of Food Engineering*, *115*(1), 132–143. https://doi.org/10.1016/j.jfoodeng.2012.10.008

Fenaille, F., Guy, P. A., & Tabet, J. C. (2003). Study of protein modification by 4-hydroxy-2-nonenal and other short chain aldehydes analyzed by electrospray ionization tandem mass spectrometry. *Journal of the American Society for Mass Spectrometry*, *14*(3), 215–226. https://doi.org/10.1016/S1044-0305(02)00911-X

Geistlinger, T. (2015). *Plant based meat structured protein products* (Patent No. US20150296834A1).

Grinberg, V. Y., & Tolstoguzov, V. B. (1997). Thermodynamic incompatibility of proteins and polysaccharides in solutions. *Food Hydrocolloids*, *11*(2), 145–158. https://doi.org/10.1016/S0268-005X(97)80022-7

Guichard, E. (2002). Interactions between flavor compounds and food ingredients and their influence on flavor perception. *Food Reviews International*, *18*(1), 49–70. https://doi.org/10.1081/FRI-120003417

Hansen, A. P., & Heinis, J. J. (1991). Decrease of Vanillin Flavor Perception in the Presence of Casein and Whey Proteins. *Journal of Dairy Science*, *74*(9), 2936–2940. https://doi.org/10.3168/jds.S0022-0302(91)78477-4

Hoek, A. C., Luning, P. A., Weijzen, P., Engels, W., Kok, F. J., & de Graaf, C. (2011). Replacement of meat by meat substitutes. A survey on person- and product-related factors in consumer acceptance. *Appetite*, *56*(3), 662–673. https://doi.org/10.1016/j.appet.2011.02.001

Khio, S. W., Cheong, M. W., Zhou, W., Curran, P., & Yu, B. (2012). Characterization of the volatility of flavor

compounds in alcoholic beverages through headspace solid-phase microextraction (HS-SPME) and mathematical modeling. *Journal of Food Science*, *77*(1). https://doi.org/10.1111/j.1750-3841.2011.02474.x

Krintiras, G. A., Gadea Diaz, J., Van Der Goot, A. J., Stankiewicz, A. I., & Stefanidis, G. D. (2016). On the use of the Couette Cell technology for large scale production of textured soy-based meat replacers. *Journal of Food Engineering*, *169*, 205–213. https://doi.org/10.1016/j.jfoodeng.2015.08.021

Kweldam, A. C., Kweldam, G., & Kweldam, A. C. (2011). *Method for the preparation of a meat substitute product, meat substitute product obtained with the method and ready to consume meat substitute product* (Patent No. US20110244090A1).

Manski, J. M., van der Goot, A. J., & Boom, R. M. (2007). Formation of fibrous materials from dense calcium caseinate dipersions. *Biomacromolecules*, *8*(4), 1271–1279. https://doi.org/10.1021/bm061008p

Michel, F., Hartmann, C., & Siegrist, M. (2021). Consumers' associations, perceptions and acceptance of meat and plant-based meat alternatives. *Food Quality and Preference*, *87*(August 2020), 104063. https://doi.org/10.1016/j.foodqual.2020.104063

Nieuwland, M., Geerdink, P., Brier, P., Van Den Eijnden, P., Henket, J. T. M. M., Langelaan, M. L. P., Stroeks, N., Van Deventer, H. C., & Martin, A. H. (2014). Food-grade electrospinning of proteins. *Innovative Food Science and Emerging Technologies*, *20*, 269–275. https://doi.org/10.1016/j.ifset.2014.07.006

Osen, R. (2017). *Texturization of pea protein isolates using high moisture extrusion cooking* [PhD, TU Munich]. https://d-nb.info/116838026X/34

Puski, G., & Konwinski, A. H. (1976). *Process of making a soy-based meat substitute* (Patent No. 494,099). United States Patent.

Qiu, Y., McClements, D. J., Chen, J., Li, C., Liu, C., & Dai, T. (2023). Construction of 3D printed meat analogs from plant-based proteins: Improving the printing performance of soy protein- and gluten-based pastes facilitated by rice protein. *Food Research International*, *167*. https://doi.org/10.1016/j.foodres.2023.112635

Ryu, J., Xiang, X., Hu, X., Rosenfeld, S. E., Qin, D., Zhou, H., & McClements, D. J. (2023). Assembly of plant-based meat analogs using soft matter physics: A coacervation-shearing-gelation approach. *Food Hydrocolloids*, *142*. https://doi.org/10.1016/j.foodhyd.2023.108817

Samard, S., Gu, B. Y., & Ryu, G. H. (2019). Effects of extrusion types, screw speed and addition of wheat gluten on physicochemical characteristics and cooking stability of meat analogues. *Journal of the Science of Food and Agriculture*, *99*(11), 4922–4931. https://doi.org/10.1002/jsfa.9722

Schreuders, F. K. G., Schlangen, M., Bodnár, I., Erni, P., Boom, R. M., & van der Goot, A. J. (2022). Structure formation and non-linear rheology of blends of plant proteins with pectin and cellulose. *Food Hydrocolloids*, *124*(October 2021). https://doi.org/10.1016/j.foodhyd.2021.107327

Taghian Dinani, S., Broekema, N. L., Boom, R., & van der Goot, A. J. (2023). Investigation potential of hydrocolloids in meat analogue preparation. *Food Hydrocolloids*, *135*. https://doi.org/10.1016/j.foodhyd.2022.108199

Tingle, C. , M. K. , Z. A. J. , M. B. J. & U. J. (2022). (2022). Texturization of pea protein isolate by micro compounding. *Submitted*, *163*(November 2022), 112250. https://doi.org/10.1016/j.foodres.2022.112250

Van Den Einde, R. M., Van Der Goot, A. J., & Boom, R. M. (2003). Understanding Molecular Weight Reduction of Starch during Heating-shearing Processes. *Journal of Food Science*, *68*(8), 2396–2404. https://doi.org/10.1111/j.1365-2621.2003.tb07036.x

Voon, S. L., An, J., Wong, G., Zhang, Y., & Chua, C. K. (2019). 3D food printing: a categorised review of inks and their development. In *Virtual and Physical Prototyping* (Vol. 14, Issue 3, pp. 203–218). Taylor and Francis Ltd. https://doi.org/10.1080/17452759.2019.1603508

Wang, K., & Arntfield, S. D. (2016). Probing the molecular forces involved in binding of selected volatile flavour compounds to salt-extracted pea proteins. *Food Chemistry*, *211*, 235–242. https://doi.org/10.1016/j.foodchem.2016.05.062

1

Chapter 2

Novel rotating die coupled to a twin-screw extruder as a new route to produce meat analogues with soy, pea and gluten

Abstract

Modern plant-based meat analogues should have a pronounced fibrous structure as an important characteristic. In this study, we demonstrate that the combination of high moisture extrusion (HME) with well-defined shear during cooling is a new process to make fibrous products using common meat analogue ingredients. The shear was applied via a cooling die attached to the extruder that was specially designed for that purpose. The in-house developed rotating cooling die consists of two sequential rotating inner cylinders with a separate drive-unit in an outer cylinder that can be thermo-regulated. Three rotational speeds of the inner cylinder, 45, 75 and 105 min^{-1}, were tested for pea protein isolate, soy protein concentrate, vital wheat gluten and blends of pea or soy with gluten.

A large effect on macro- and micro-texture and anisotropy index was found when the concentration of gluten was increased. The different ingredients and blends had different optimal conditions and reacted differently to the applied shear. Interestingly, the angle of the fibers observed in the samples differed at the different rotational speeds. This was attributed to the shear thinning behavior of the plant proteins and the velocity gradient in the rotating die, arising from the temperature and viscosity gradient.

The ability to change the shear rate as an independent parameter in the rotating cooling die is unique and allows texture adjustments during processing. This is an important improvement for industrial HME and opens new product design possibilities.

2.1   Introduction

Livestock production poses a significant burden on the environment (Steinfeld et al., 2006). Furthermore, increased welfare and urbanization will increase the consumption of animal products of the growing world population (FAO, 2017). Therefore, it is often suggested to replace animal protein with plant proteins for both the climate and food security (Aiking & de Boer, 2018; Chaudhary et al., 2018; González et al., 2011; Pimentel & Pimentel, 2003; Scarborough et al., 2012; Stehfest et al., 2009). A possible route to reduce the consumption of animal-based products, such as meat, is to create plant-based alternatives that are highly similar in texture and taste to meat, such as meat analogues (Aiking & de Boer, 2018; Michel et al., 2021).

Currently, different techniques are available to structure plant proteins into fibrous products (Dekkers, Boom, et al., 2018). These techniques include high moisture extrusion (HME) (Pietsch et al., 2019) and the use of simple shear devices, such as the Couette cell (Krintiras et al., 2016).

Both HME and shear devices combine thermo-mechanical processing and a cooling step to mix, melt, structure and solidify plant protein products (Cornet, Snel, et al., 2021). During HME, plant-based ingredients and water are placed in the extruder barrel where heat, shear and pressure are applied to the product, which is moved forward by co-rotating screws (Emin & Schuchmann, 2017). The product is then pushed into a long cooling die, which is used to prevent expansion of the product at the die exit (Cheftel et al., 1992). The cooling die is also referred to as the section where the orientation and structure formation of the protein phase takes place (Akdogan, 1999). Shearing devices, such as the Couette cell, lead to fibrous products via a batch process. The Couette cell consists of a rotating inner cylinder placed in a static cylinder. The rotation of the inner cylinder results in well-defined shear. This shear in combination with heating aligns the protein phase resulting in fibrous products (Krintiras et al., 2016). The deformation in the Couette cell and extruder die is considered essential for the structure formation (Cornet, Snel, et al., 2021). In the Couette cell, shear is controlled by adjusting the rotational speed. The shear in the cooling die, however, is directly correlated with the throughput.

The combination of the well-defined shear of the Couette cell with HME could open new possibilities to combine the benefits of both processes. The combination will enhance the possibilities of HME to create novel food structures and to fine-tune the final texture. We have therefore developed a novel extrusion die in-house that allows the application of the well-defined shear on materials mixed and heated in the extruder in a continuous matter. Instead of a static rectangular die, the new die consists of a cylinder with two rotating inner parts (Beyrer et al., 2022).

In this paper, we show the possibilities of the rotating die to make fibrous products. We hypothesize that adjusting the shear in the cooling die could lead to different extrudate

structures. Furthermore, we examine if the influence of the shear adjustments depends on the materials processed, which are pea protein isolate (PPI), soy protein concentrate (SPC), vital wheat gluten (VWG) and blends of PPI/SPC with VWG. Those ingredients are commonly used ingredients in HME (Kyriakopoulou et al., 2019).

2.2   Methods and Materials

2.2.1   Materials
Pea protein isolate (PPI, NUTRALYS° F85M) and vital wheat gluten (VWG, VITEN°) were obtained from Roquette Frères S.A. (Lestrem, France). Soy protein concentrate (SPC, ALPHA° 8) was obtained from Solae (St. Louis, MO, USA). PPI contained at least 83 wt% protein, SPC 67% and VWG 83% (N x 6.25, indicated by supplier). The moisture contents of the powders were measured with a moisture analyzer (Mettler Toledo, Ohio, United States). Moisture contents were 7.42 ± 0.11, 10.31 ± 0.13 and 6.82 ± 0.07 for PPI, SPC and VWG respectively. Salt fortified with iodine was obtained from Schweizer Salinen AG (Pratteln, Switzerland).

2.2.2   Preparation of ingredient blends
Blends of PPI or SPC with VWG were prepared with a total dry matter content of 40% in the ratios 40:0, 28:12, 20:20, 12:28 and 0:40. Furthermore, 1.8% salt was included in all dry blends, thus salt concentration was 0.7% in the final product. Salt was added for industrial relevance, since salt is often present in commercial meat analogues (Kyriakopoulou et al., 2019). Besides, its additions could lead to more fibrous products when produced in the shearing device (Dinani Taghian et al., 2022) Blends were mixed with a MP50 screw mixer (Prodima Mixers SA) at the highest speed for 10 min.

2.2.3   High moisture extrusion cooking with new rotating die
Extrusion experiments were performed using a Clextral Evolum 25 twin-screw extruder (Clextral, Firminy, France), which has a screw diameter of 25 mm and a length/diameter ratio of 40. The extruder barrel consisted of 10 sections, which can be heated separately with an electric cartridge heating system.

A novel extrusion die was developed in-house (Beyrer et al., 2022), and attached to the extruder (Figure 2.1). A cylindrical breaker plate with 31 holes with a diameter of 3 mm was placed just in between the barrel and the die to align the flow of the product before entering the die. The rotating die composed of a static outer (e) and a rotating inner cylinder (c) (Figure 2.1). The inner cylinder (c) had a diameter of 12 cm and was placed inside the outer cylinder (e, diameter = 14 cm). A cone-shaped diffuser (d) at the die inlet allowed the product to flow in smoothly. The length of the die was 59 cm and it consisted of two sections (length was 40 cm and 19 cm for section 1 and 2 respectively). The sections were separately driven by two motors (JS-Technik GmbH, Germany), as depicted in Figure 2.2, allowing the inner parts to have different rotational speeds in the two sections. The inclusion of two sections

made it possible to create a broad range of shear rate and temperature patterns. For example, the first section could be kept at a higher temperature and shear, to allow texture formation, while the second section could be cooled and operated at low shear to set the texture. The rotational speed was regulated with a frequency converter (b). A channel around the cylinder was connected with two water baths (one for each section) to control the temperatures (f). The water bath connected to the first section was set to 85 °C using a thermoregulator HB60 (Huber, Germany). The water bath connected to the second section was cooled with tap water (10 °C). In the first section, the rotational speed was set to 45, 75 or 105 min^{-1}, while the second section rotated at 0.5 min^{-1}.

The barrel temperatures of the 10 sections were set at 30, 50, 70, 90, 100, 120, 130, 145, 145 and 125 °C respectively. The screw speed was set at 240 rpm. A twin-screw gravimetric feeder type KCM (K-tron, Niederlenz, Switzerland) was used to feed the dry ingredients into the extruder at a feeding rate of 6 kg/h. Water was injected in the second section with a water pump (DKM) at 9 kg/h to aim for moisture contents of 63-64% in the extrudates for PPI, SPC and blend samples. For VWG samples, moisture content was set to 50% and the moisture of the extrudate 54-56%. The moisture content of the samples was measured as a control with a moisture analyzer (Mettler Toledo, Ohio, United States).

The total residence time of the process was estimated by adding carmine (Sigma-Aldrich, St.Louis, USA) directly in section 1 of the barrel and timing until the product came out red. For the rotating die, the residence time can be calculated:

$$t_{res} = \frac{\pi \left(r_o^2 - r_i^2 \right) L}{Q} \qquad\qquad 2.1$$

in which r_i and r_o are the radii of the inner and outer cylinder respectively, L is the length of the die and Q is the volumetric flow.
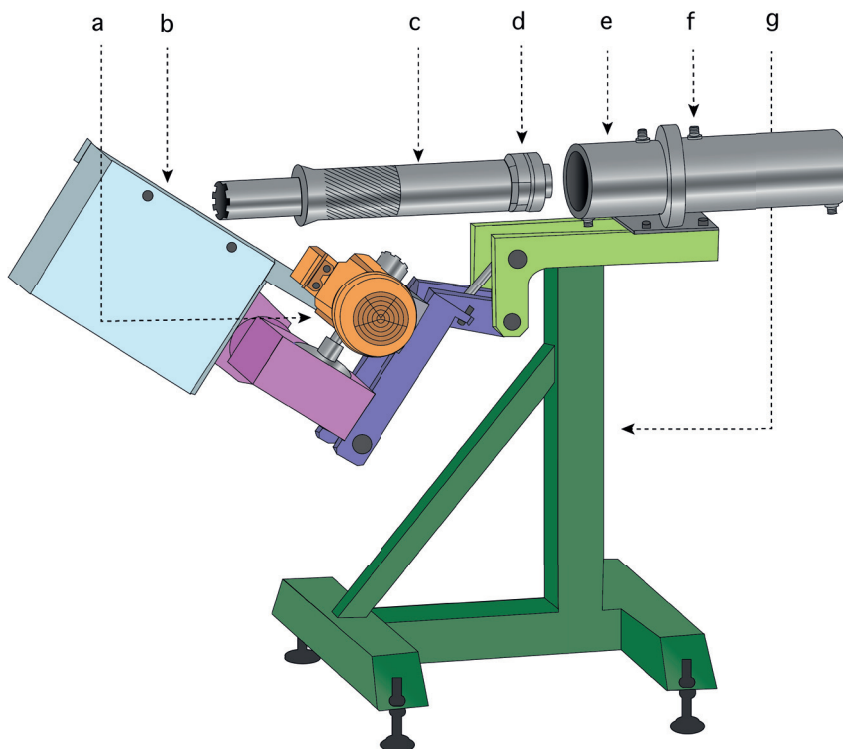
Figure 2.1: Schematic representation of the rotating die, when unmounted. The material flows from the extruder (right) in the die, a = motor, b = frequency converter, c = inner cylinder, d = diffuser, e = outer cylinder, f = water connection, g = supporting frame
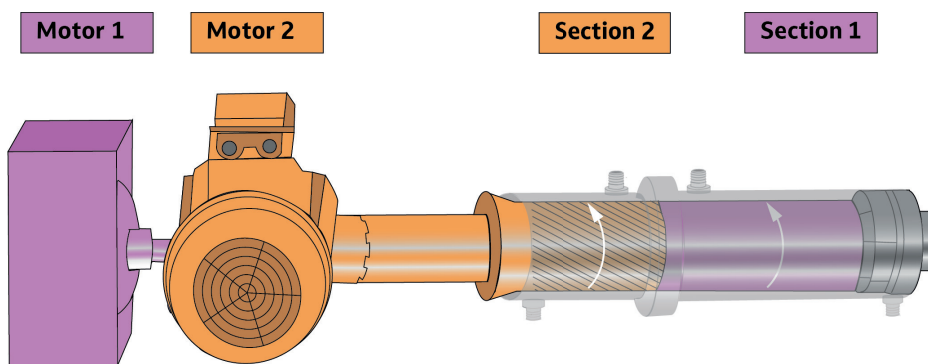

Figure 2.2: Graphical representation of the rotating die. Section 1 (purple) is connected to motor 1 with a long inner axis, which is placed inside section 2 (orange) and the axis of section 2. Section 2 is connected to motor 2. Both motors can be separately regulated to achieve desired rotational speed, indicated with solid arrows. Heating for the two sections was regulated separately to 85 and 10 °C respectively.
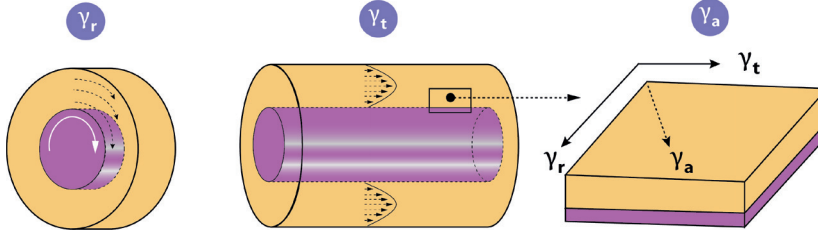
Figure 2.3: Graphical representation of the two types of shear stresses present in the the rotating die, and the total vector shear. From left to right: the shear in the direction of the rotation of the inner cylinder ($\dot\gamma r$), the shear in the direction of the throughput ($\dot\gamma t$) and the total apparent shear rate ($\dot\gamma a$)

2.2.4 Applied shear

In the die, the product is subjected to shear flow. The design of the rotating die generates three different shear stresses that are important to consider (Figure 2.3). The first two shear stresses are in the direction of rotation and are dependent on each section's rotational speed. The third shear stress is in the direction of the flow and is thus determined by the throughput. This shear is present in a static cooling die as well.

The apparent shear rate $\dot\gamma$ can be defined as follows:

$$\dot\gamma = \frac{\nu}{h} \qquad 2.2$$

in which ν is the velocity and h the gap height.

For the apparent shear rate in the direction of throughput, we expect a laminar flow with a maximum velocity at half gap height, thus:

$$\dot\gamma = \frac{\nu_{max}}{h/2} \qquad 2.3$$

then, we can approach the ν_{max} as $2\nu_{average}$ and calculate the average velocity:

$$\nu_{average} = \frac{Q}{A} \qquad 2.4$$

in which Q is the volumetric flow and A the area. This results in the equation for shear rate in direction of throughput:

$$\dot\gamma_t = \frac{8Q}{\pi\left(r_o^2 - r_i^2\right)h} \qquad 2.5$$

in which r_i and r_o are the radii of the inner and outer cylinder respectively. The volumetric flow is given by:

$$Q_{net} = M/\rho_{product} \qquad\qquad 2.6$$

in which M is the product feed rate and $\rho_{product}$ is the density of the product and was approximated as 1090 kg/m^3 for products with a dry matter content of 40 wt%.

For the apparent shear rate in the direction of rotation, we can assume ν is equal to Ω r and thus equation 2.2 becomes:

$$\dot{\gamma}_r = \frac{2\pi\nu\bar{r}}{h} \qquad\qquad 2.7$$

where v is the rotational speed and $\bar{r}$ is the average radius, or $(r_o + r_i)\,/2$. The total apparent shear rate, $\dot{\gamma}_a$, can be calculated as a vector shear:

$$\dot{\gamma}_a = \sqrt{\dot{\gamma_t}^2 + \dot{\gamma_r}^2} \qquad\qquad 2.8$$

However, since $\dot{\gamma_t}$ is negligible compared to $\dot{\gamma_r}$, we can approach the total shear as:

$$\dot{\gamma}_a \approx \dot{\gamma}_r \qquad\qquad 2.9$$

2.2.5   Sampling of samples for analysis

A large sample in the shape of a hollow tube was obtained, which was cut manually. The thickness of the sample was always equal to the gap width, 1 cm, meaning that no expansion took place. The cuts were transferred into a plastic bag, which was sealed and quickly cooled to -20 °C with a blast freezer (Electrolux, Sweden). Before analysis, samples were defrosted overnight and kept at ambient temperature during all the measurements, except for confocal laser scanning microscopy.

A sharp knife was used to make a small inclination in the direction of the flow (out of the die) and samples were broken along this cut. Pictures were taken with a digital camera (Nikon DS).

2.2.6   Confocal laser scanning microscopy

The microstructure of the samples was visualized with a confocal laser scanning microscope (CLSM). Frozen extrudates were cut into samples of approximately 5 x 10 x 10 mm. Subsequently, slices with a thickness of 60 μm were prepared at -20 °C with a cryo-microtome (Micron CR50-H, ADAMAS-Instruments Corp., Rhenen, The Netherlands). Next, the samples were colored with a 0.2 mg/mL Rhodamine B solution (Sigma-Aldrich GmbH, Steinheim, Germany). The samples were analyzed with a CLSM type 510 (Carl Zeiss AG, Oberkochen, Germany) using a 543 nm HeNe laser and a 405 nm Blue/Violet diode laser. An EC Plan-Neofluar 20x/0.5 lens was attached. Images were analyzed with ZEN v3.4, blue edition (Carl Zeiss AG).

2.2.7 Anisotropy index

The anisotropy index of the samples is measured to compare the degree of fiber formation in the die. A simple way to measure anisotropy is with an optical fiber method, based on the continuous time random walk (CTRW) theory. The CTRW theory has been successfully applied to measure the anisotropy of samples made with HME (Ranasinghesagara et al., 2006). Samples were cut into squares of 2 x 2 cm and placed in a sample holder. A red LED (λ = 660 nm) coupled to an optical fiber (diameter = 400 μm) was directed at the sample in a 45° angle. A digital camera (Nikon DS) was placed above the sample to image the light reflectance by the sample. The anisotropy index was calculated by image analysis using a Matlab script, which was kindly provided by Professor G. Yao (Ranasinghesagara et al., 2006). This parameter indicates the deviation from a circular reflection pattern. For an isotropic sample, the anisotropy index is expected to be 1, meaning the light reflectance was a perfect circle. When the sample is highly anisotropic, the probability that the light scatters along the direction of the fibers is larger than the probability that it scatters in the direction perpendicular to the fibers. This results in an oval reflectance shape and thus a higher anisotropy index. Of each extrudate, three samples were prepared and each sample was imaged 4 times and averaged.

2.2.8 Texture profile analysis

Texture profile analysis (TPA) was performed using a TA-XT2 texture analyzer (Stable Micro Systems, Surrey, UK) equipped with a 30 kg load cell. The larger samples were cut into cylinders of 20 mm in diameter and a height of 1 cm. Subsequently, samples were compressed twice with a P10 probe to 30% of original height with a test speed of 1 mm/s and a waiting time in between the two compressions of 5 s. For each treatment, 9 samples were measured and averaged. The peak maximum force at first compression was taken as the hardness (Meulleneti, 1998).

2.2.9 Statistical analysis

Statistical analysis was performed with R. Normality was tested with descriptive statistics. When the data was normally distributed, a one-way analysis of variance (ANOVA) was done to test if the observed differences between samples were significant. Multiple comparison Tukey tests were done to indicate which treatments were significantly different from each other.

2.3 Results and Discussion

An extruder equipped with the rotating die was used to produce anisotropic products using pea protein isolate (PPI), soy protein concentrate (SPC), vital wheat gluten (VWG) and blends of PPI/SPC with VWG. It was possible to produce layered products when using single ingredients and with blends of those ingredients. These products exited the die as a hollow tube and had a 1 cm thickness. The product was then cut into rectangular samples (Figure 2.4).

2.3.1 Process parameters

During the HME experiments, process parameters were measured and compared. For all products, the specific mechanical energy (SME) was recorded, as well as the pressure and temperature in the last section of the extruder barrel (Table 2.1). We did not observe instabilities or shoot outs during the processing of the different ingredients. Values were recorded for 1 h and a range was obtained, since some variation in the parameters was expected due to the incomplete filling of the extruder barrel. The highest SME and pressure was recorded for SPC, which also had the broadest range of values measured. The total residence time was measured by adding a colorant. However, the color did not exit the die homogeneously. Therefore the residence time had a range of between 6.45 min (first moment color was observed) and 16.27 min (last moment color was observed). When calculating the residence time in the rotating die with Equation 2.1 we obtained a residence time of 10 min. When we assume a residence time in the extruder barrel of around 1 min, this would mean that some material only stayed 5 min in the rotating die, while other material stayed 15 min in the die. There seems to be some preferred faster routes for the material, which can be explained with the velocity gradient due to laminar flow and the temperature gradient. Indeed, we assumed the maximum velocity to be twice the average velocity (Equation 2.6).

Table 2.1: Range of specific mechanical energy (SME), pressure and temperature at the last section of the extruder barrel for pea protein isolate (PPI), soy protein concentrate (SPC) and vital wheat gluten (VWG). Values were recorded for 1 h and averaged, letters indicate significant differences between the ingredients.

Ingredient	SME (kJ/kg)	Pressure (bar)	Temperature (°C)
PPI	184 – 239 [b]	4.16 – 6.90 [c]	110 - 124 [b]
SPC	213 – 468 [a]	13.5 – 20.8 [a]	103 - 126 [a]
VWG	158 – 257 [b]	10.5 – 14.5 [b]	115 - 127 [a]

Figure 2.4: Example of an extrudate obtained with SPC using the rotating die

2.3.2   Processing single ingredients

We tested the rotating die in its ability to produce fibrous textures from PPI, SPC and VWG respectively. Different textures were obtained from PPI after HME when the rotational speed of the die was changed (Table 2.2). At a rotational speed of 45 min^{-1} a parabolic pattern with an angle of around 45° was observed when samples were broken to observe the inner structure. When rotational speed was increased to 75 and 105 min^{-1}, the angle decreased. The decrease of the angle will influence the texture of the product probably, but it is still unclear how this angle correlates with the texture of the final product exactly.
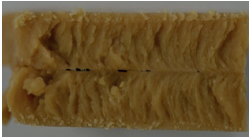
The decrease in the orientation angle was also observed in the SPC samples. Interestingly, the SPC sample produced at low rotational speed (45 min^{-1}) seemed most fibrous. In contrast, the fibrousness of the VWG products slightly increased when rotational speed was increased (Table 2.2).

The microstructure of the PPI, SPC and VWG samples was analyzed with CLSM after coloring the samples with Rhodamine B (Table 2.3). Three colors can be differentiated: red, dark grey and light grey. The red color indicates material that has been colored by Rhodamine B, thus a protein-rich phase. Dark grey indicates material that was not colored, thus non-protein material such as carbohydrates or fibers. Finally, light grey is the background color, thus either air or water. When a rotational speed of 45 min^{-1} was applied, SPC and VWG samples became compact. When the rotational speed was increased to 75 min^{-1}, two phases became visible for all samples. The phases were red or dark grey, which suggested a protein-rich and

a protein-poor phase. The lighter grey areas on the pictures probably represented air between the breaking planes of the product. For PPI samples, there was no dark grey material visible. At a rotational speed of 105 min^{-1}, the orientation of the phases for the PPI samples changed from diagonal to horizontal. Interestingly, the SPC samples also had diagonal orientation at a rotational speed of 75 min^{-1} and more horizontal orientation at 105 min^{-1}. The VWG samples had phases that were orientated slightly diagonally at a rotational speed of 45 min^{-1}, and horizontal phases at 75 and 105 min^{-1}. Furthermore, the VWG products appear to be slightly more compact at higher rotational speed.

The anisotropy indexes of the samples were measured with the optic fiber method (Figure 2.5). With this method, an index between 1 (isotropic) and 2 (anisotropic) is obtained. A very fibrous product thus has a higher anisotropy index than a product that is not fibrous. Therefore, a high anisotropy index can be interpreted as a more fibrous texture of the product. However, fibers in both directions or shorter fibers might influence the anisotropy index of a meat analogue, as was the case with PPI blends (Schreuders et al., 2022). Anisotropy indexes of 1.14-1.63 were reported for extrudates made from soy protein isolate/VWG/starch mixtures, dependent on process temperature and moisture content (Ranasinghesagara et al., 2006). The values found in this study were in the same range (1.14-1.35). VWG samples had the highest anisotropy index, followed by SPC and PPI. Anisotropy indexes of the PPI and VWG samples were significantly different at all rotational speeds tested. The anisotropy indexes of SPC and PPI first decreased when the rotational speed was increased from 45 min^{-1} to 75 min^{-1}, and then increased when the rotational speed was further increased to 105 min^{-1}. For SPC, the anisotropy indexes at 45 and 105 min^{-1} were not significantly different, but for PPI the anisotropy index increased significantly. The hardness of the samples was analysed with TPA (Figure 2.6). Other parameters obtained with TPA, such as chewiness and springiness, are reported in the appendix including their correlations the hardness (Appendix A). Extrudates with PPI significantly had the highest hardness, followed by SPC and VWG. The effect of increasing the rotational speed was small on the hardness, except for VWG. Those products were significantly softer at a rotational speed of 45 min^{-1}. The small differences in hardness indicated that increasing the rotational speed did not have large effects on the hardness of the extrudates formed. Interestingly, a significant negative correlation was found between hardness and the anisotropy index for all raw materials and processing conditions (-0.6). This correlation was positive for PPI (0.7) and VWG (0.8), but negative for SPC (-0.8, Appendix B). This indicates that there could be a relation between the anisotropy of a sample and the hardness, but that this relation is specific for the ingredient tested.

Table 2.2: *Visual observations of structures obtained with different rotational speeds in the first section of the rotating die for samples made from PPI, SPC, VWG and blends of PPI/SPC with VWG at a total dry matter content of 40 wt%. Samples were cut and broken to show the inner texture.*

Ingredient	Rotational speed (min⁻¹)		
	45	75	105
PPI			
SPC			
VWG			
PPI/VWG 28:12			
PPI/VWG 20:20			
PPI/VWG 12:28			
SPC/VWG 28:12			

2
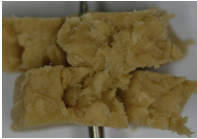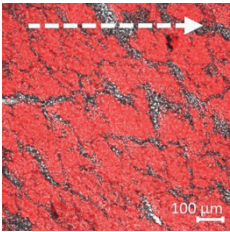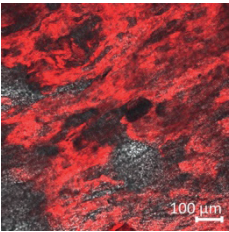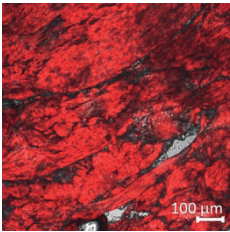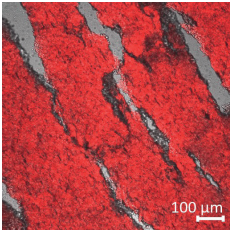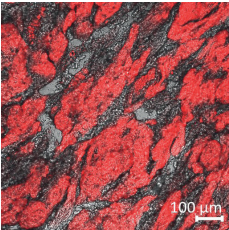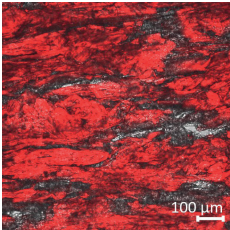
Ingredient	Rotational speed (min^-1)		
	45	75	105
SPC/VWG 20:20			
SPC/VWG 12:28			

Table 2.3: CLSM images of the PPI, SPC and VWG samples produced with a rotational speed in the first section of the die of 45, 75 and 105 min^-1, stained with Rhodamine B. The red color corresponds to a protein-rich phase and the grey color to a protein-poor phase. White dashed arrow indicates the direction of the shear induced by the rotation of the inner cylinder.

Rotational speed (min^-1)	Sample		
	PPI	SPC	VWG
45			
75			

Rotational speed (min⁻¹)	Sample		
	PPI	SPC	VWG
105			

2.3.3 Processing ingredient blends

The rotating die was also tested with blends of SPC or PPI with VWG, since these blends are commonly used in high moisture extrusion (Table 2.2). A higher VWG content seemed to result in more fibrous textures and the fibers again showed a specific angle. This was confirmed by the anisotropy index of the products, which increased with increasing VWG content. VWG had the highest anisotropy index when used as a single ingredient (Figure 2.5), which explains this increase of anisotropy index for the blends. The VWG blends behaved differently at various rotational speeds, but for the PPI/VWG blend, we found a maximum at a rotational speed of 105 min^{-1} when the ratio of PPI:VWG was 20:20 and 12:28 (Figure 2.7a). However, at a ratio of 28:12 the optimum was seen at 45 min^{-1}. These observations do not completely align with the visual observed fibrousness of PPI/VWG blends, where an optimum is seen at 75 min^{-1} at a ratio of 20:20 (Table 2.2). The lack of coherence in fibrousness and measured anisotropy has been previously observed in PPI blends with cellulose and pectin, and seems specific for blends containing PPI (Schreuders et al., 2022).

For the SPC/VWG samples, the highest anisotropy index was found at a rotational speed of 75 min^{-1} for products with a VWG:SPC ratio of 20:20 and 12:28 (Figure 2.7b). An increase in anisotropy index of samples with increasing VWG content has also been shown for rapeseed and soy meat analogues produced with the shear cell (Jia et al., 2021). Cornet et al. stated that fibrous structures can be formed from any leguminous protein, as long as at least 50% of VWG is added to the dry mixture (2021). Our research seems to be in-line with this hypothesis, when considering the anisotropy index as a measure for fibrousness.

In contrast to the anisotropy index, the hardness decreased with increasing VWG content (Figure 2.8), which in turn is in line with the hardness of VWG as a single ingredient (Figure 2.6). Again, correlations between the two parameters were tested and a negative correlation was found (-0.4, Appendix B). However, for the separate blends, only a significant relation was found for 20:20 VWG:SPC (-0.5). When the dataset was divided

for rotational speeds, correlation was significant for 45 and 75 min⁻¹ (-0.3 and -0.5), hinting that the VWG content determined the correlation mostly. For SPC, the products became harder when VWG:SPC ratio was 12:28 compared to 0:40 (Figure 2.8b). This aligned with previous research in which 40% VWG was added to soy protein isolate/corn starch extrudates (Samard et al., 2019). However, we observed that more VWG decreased the hardness of the products. For PPI, no initial increase in hardness was observed (Figure 2.8a). Instead, the hardness seemed to decrease linearly with higher VWG content. The effect of rotational speed on the hardness of the blends was small, and thus similar to its effect when extruding single ingredients. These results show that depending on the ingredients, a change in rotational speed can be used to create different structures with similar hardness. Therefore, these results confirm that the use of the rotating die gives more processing freedom and the structure could be changed directly in the extruder die.
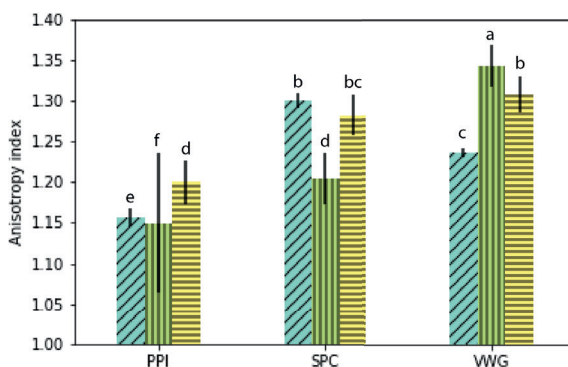
Figure 2.5: Anisotropy indexes for PPI, SPC and VWG samples extrudated with a rotational speed of 45 min⁻¹ (blue, diagonal stripes), 75 min⁻¹ (green, vertical stripes) and 105 min⁻¹ (yellow, horizontal stripes). Rotational speed is the applied rotational speed in the first section of the rotating die, n = 12.
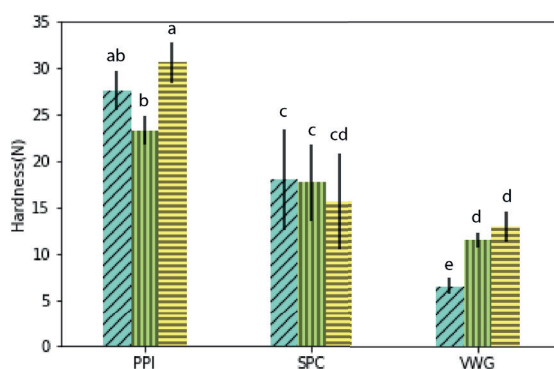
Figure 2.6: Hardness as measured with TPA for PPI, SPC and VWG samples extrudated with a rotational speed of 45 min⁻¹(blue, diagonal stripes), 75 min⁻¹(green, vertical stripes) and 105 min⁻¹(yellow, horizontal stripes). rotational speed is the applied rotational speed in the first section of the rotating die, n = 9.
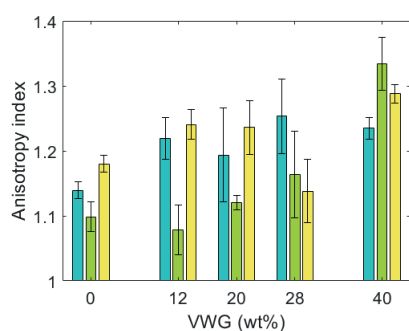
(a) PPI
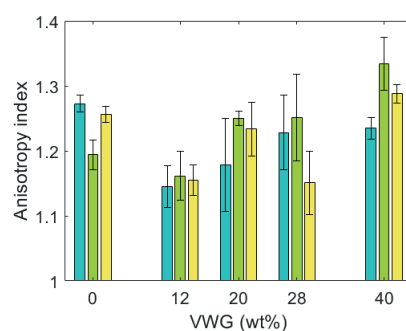
(b) SPC

Figure 2.7: Anisotropy indexes of samples extrudated with a rotational speed of 45 min⁻¹ (blue), 75 min⁻¹(green) and 105 min⁻¹(yellow). On the left (a): PPI with VWG blends and on the right (b): SPC with VWG blends at a total dry matter content of 40 wt%, n = 12.

(a) PPI   (b) SPC
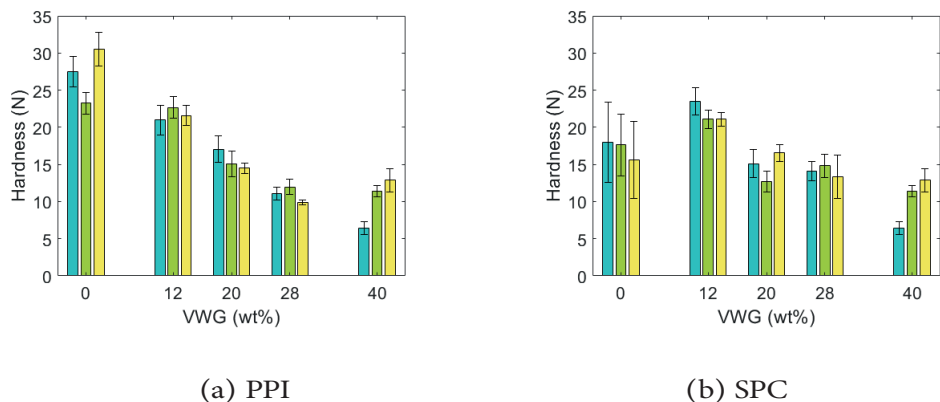
Figure 2.8: Hardness of samples as measured with TPA, extrudated with a rotational speed of 45 min^{-1}(blue), 75 min^{-1}(green) and 105 min^{-1}(yellow). On the left (a): PPI with VWG blends and on the right (b): SPC with VWG blends at a total dry matter content of 40 wt%, n = 9.

2.3.4   Comparison with existing technologies

The use of an extruder equipped with a rotating die could be seen as a combination of HME and a shear cell. We will therefore compare these processes with this new extrusion process in terms of shear rates, pressure, SME and textures obtained. The shear rate in a conventional cooling die depends on the throughput. When comparing shear and throughput in cooling dies from literature, an exponential relationship was observed (Cornet, Snel, et al., 2021). Shear rates reported ranged from 1 to 45 s^{-1} in HME cooling dies. Shear rates in the shear cell can range from 7-1050 s^{-1}, but 39 s^{-1} is most often the condition (Dekkers et al., 2018). The shear rates we tested with the rotating die were mainly dependent on the rotational speed, which was 45, 75 and 105 min^{-1}. This resulted in apparent shear rates of 31, 51 and 71 s^{-1}, but lower or higher shear rates are possible with the new die. This makes the rotating die unique in combination with an extruder since the shear rate can be increased without adjusting the throughput. The total residence time for a throughput of 15 kg/h was between 6.45 and 16.27 min. This is comparable to the shear cell, (15 min), but long compared to HME with a static die (2-5 min) (Cheftel et al., 1992). Direct comparison of process pressures and SME is not straightforward, since these values depend strongly on the extruder conditions, the process parameters and the ingredients used (Alam et al., 2016). Moreover, these values are often not reported. However, the recorded pressures in this study were in the lower range of those reported for HME with rectangular slit dies. For meat analogues produced with SPC and a slit cooling die, a pressure of 2.4 MPa (24 bar) was reported at similar extruder conditions (screw speed of 180 rpm, throughput of 15 kg/h and melt temperature of 140 °C) (Pietsch et al., 2019). This is higher than the highest pressure we measured (20.8 bar, Table 2.1). In another study from the same author with VWG, pressures ranged between 1.2 - 5.1 MPa (12 - 51 bar, screw speed = 300 rpm, throughput = 10 kg/h and melt temperature = 145 °C)

(Pietsch et al., 2017). The SME in these studies was up to 350 kJ/kg and 206 kJ/kg for SPC and VWG respectively, which is similar to our findings (Table 2.1). For the larger prototype of the shear cell, the Couette cell, the pressure is kept below 7 bar and measured SME values were at maximum 63 kJ/kg (Krintiras et al., 2016).

Extrudates produced with HME coupled with a static die have a rectangular shape and a parabolic flow pattern (Osen et al., 2014). They are limited in their width, due to limitations in heat transfer and pressure release. Larger products can be obtained with the Couette cell, which makes these samples more comparable to our samples. Products produced with the Couette cell showed a parabolic pattern which was directly related to the shear gradient in the samples (Krintiras et al., 2016). This parabolic pattern was also observed for PPI samples produced at a rotational speed of 45 min^{-1} (Table 2.2). Interestingly, we observed a change in the angle of the fibers formed dependent on the shear applied in the rotational direction. Different mechanisms could take place in the rotation die that could lead to this change in flow pattern. The increase in rotational shear could lead to a difference in the direction of the vector shear (Equation 2.8), although this difference is expected to be minimal in the conditions used in this study. Alternatively, the shear thinning behavior of the plant proteins could explain the observed patterns, since at a higher rotational speed, a higher rotation shear would lead to a lower viscosity of the melt. Other mechanisms that could change the flow profile are wall slip and temperature gradients in the products.

Due to the relatively larger cross sectional surface area of a cylindrical die, and thus lower resistance, the maximum throughput is expected to be larger than those for HME with a static die, while it can still be operated as a continuous process.

2.4   Conclusion

We developed a new cooling die with a rotating inner cylinder. Changing the speed of rotation of the cylinder enabled us to change the shear rate as an independent and additional parameter. It was possible to make layered and fibrous products using ingredients commonly used in meat analog applications, which were PPI, SPC, VWG and blends of PPI/SPC with VWG. The application of different apparent shear rates resulted in differences in micro- and macro-texture and anisotropy. The effect of the change in shear rate was different for the different ingredients. Apart from the ability to adjust the apparent shear rate, the cylindrical design also resulted in larger product sizes compared to those produced with a static die, which opens numerous new application possibilities. A further advantage is that meat analogue manufacturers already use HME and can thus simply attach the new die to their current extruder.

Appendix A. TPA parameters and their correlation with hardness

(a)

(b)

(c)

(d)
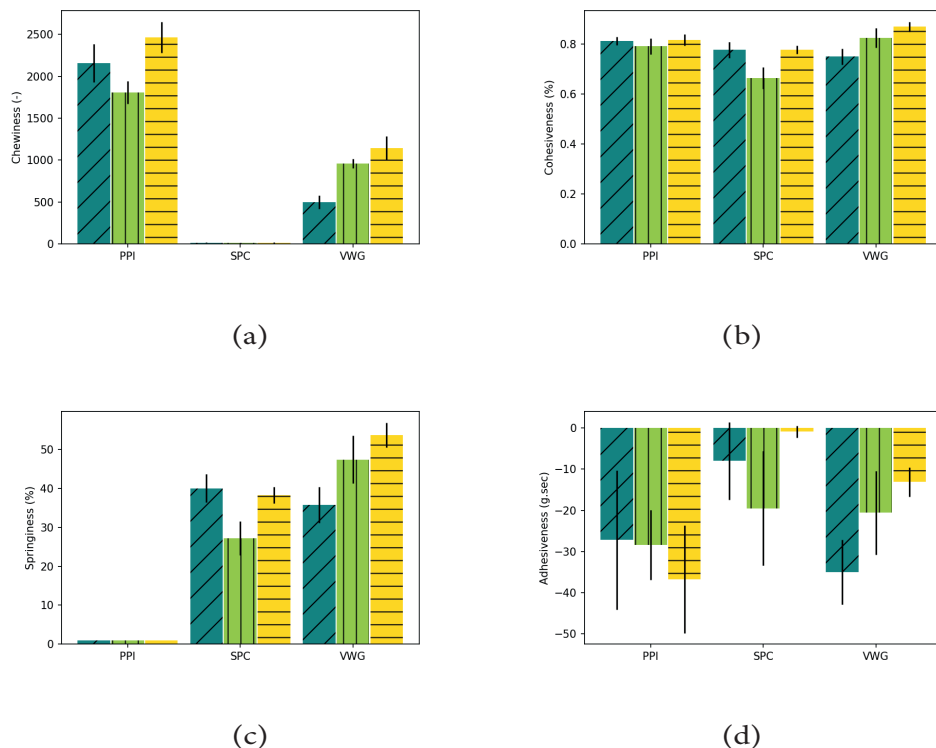
Figure A.9: Chewiness (a), cohesiveness (b), springiness (c) and adhesiveness (d) of samples as measured with TPA, extruded with a rotational speed of 45 min−1 (blue), 75 min−1 (green) and 105 min−1 (yellow) for PPI, SPC and VWG at a total dry matter content of 40 wt%, n = 9.

TPA parameters were tested on their correlation with R (Table A.4). Program: R, function 'cor', and 'cor.test (method = 'pearson'). The correlation with hardness was significant for springiness, cohesiveness and chewiness with p-values of 3.9E-05, 4.0E-03 and 2.2E-16 (Pearson test, a=0.05).

Table A.4: Correlation coefficients of TPA parameters

	Hardness	Adhesiveness	Springiness	Cohesiveness	Chewiness
Hardness	1	-0.11	-0.25	-0.17	0.47
Adhesiveness	-0.11	1	0.51	-0.07	-0.48
Springiness	-0.25	0.51	1	-0.03	-0.87
Cohesiveness	-0.17	-0.07	-0.03	1	0.25
Chewiness	0.47	-0.48	-0.87	0.25	1

Appendix B. Correlation hardness and anisotropy index

Correlation between hardness and anisotropy index were tested with R. Program: R, function 'cor', and 'cor.test (method = 'pearson'). Significant correlations can be found in Table B.5.

Table B.5: Correlation coefficients of hardness and anisotropic index, for different subsets of the dataset

VWG	PPI	SPC	RPM	Cor	P-value
All	All	All	All	-0.4	1.6×10^{-9}
100%	-	-	All	0.8	1.4×10^{-6}
-	100%	-	All	0.7	8.2×10^{-5}
-	-	100%	All	-0.8	2.4×10^{-6}
100%	100%	100%	All	-0.6	4.8×10^{-10}
100%	100%	100%	45	-0.5	8.0×10^{-3}
100%	100%	100%	75	-0.7	2.7×10^{-5}
100%	100%	100%	105	-0.8	1.1×10^{-8}
50%	50%	-	All	-0.5	9.2×10^{-3}
All	All	All	45	-0.3	2.1×10^{-3}
All	All	All	75	-0.5	6.2×10^{-7}

2

References

Aiking, H., & de Boer, J. (2018). The next protein transition. *Trends in Food Science and Technology*, *May*, 0–1. https://doi.org/10.1016/j.tifs.2018.07.008

Akdogan, H. (1999). High moisture food extrusion. *International Journal of Food Science and Technology*, *34*(3), 195–207. https://doi.org/10.1046/j.1365-2621.1999.00256.x

Alam, M. S., Kaur, J., Khaira, H., & Gupta, K. (2016). Extrusion and Extruded Products: Changes in Quality Attributes as Affected by Extrusion Process Parameters: A Review. *Critical Reviews in Food Science and Nutrition*, *56*(3), 445–473. https://doi.org/10.1080/10408398.2013.779568

Beyrer, M., Cachelin, C., & Rapillard, L. (2022). *Nozzle for extruding a material rich in protein and water, as well as an extrusion machine comprising such a nozzle* (Patent No. WO2022018084). Clextral. https://register.epo.org/application?number=EP21742446

Chaudhary, A., Gustafson, D., & Mathys, A. (2018). Multi-indicator sustainability assessment of global food systems. *Nature Communications*, *9*(1). https://doi.org/10.1038/s41467-018-03308-7

Cheftel, J. C., Kitagawa, M., & Queguiner, C. (1992). New Protein Texturization Processes by Extrusion Cooking at High Moisture Levels. *Food Reviews International*, *8*(2), 235–275. https://doi.org/10.1080/87559129209540940

Cornet, S. H. V., Bühler, J. M., Gonçalves, R., Bruins, M. E., van der Sman, R. G. M., & van der Goot, A. (2021). Apparent universality of leguminous proteins in swelling and fibre formation when mixed with gluten. *Food Hydrocolloids*, *120*. https://doi.org/10.1016/j.foodhyd.2021.106788

Cornet, S. H. V., Snel, S. J. E., Schreuders, F. K. G., Van der Sman, R. G. M., Beyrer, M., & Van der Goot, A. J. (2021). Thermo-mechanical processing of plant proteins using shear cell and high-moisture extrusion cooking. *Critical Reviews in Food Science and Nutrition*, *0*(0), 1–18. https://doi.org/10.1080/10408398.2020.1864618

Dekkers, B. L., Boom, R. M., & van der Goot, A. J. (2018). Structuring processes for meat analogues. *Trends in Food Science and Technology*, *81*, 25–36. https://doi.org/10.1016/j.tifs.2018.08.011

Dekkers, B. L., Hamoen, R., Boom, R. M., & van der Goot, A. J. (2018). Understanding fiber formation in a concentrated soy protein isolate - Pectin blend. *Journal of Food Engineering*, *222*, 84–92. https://doi.org/10.1016/j.jfoodeng.2017.11.014

Dinani Taghian, S., Van der Harst, J. P., Boom, R., & Van der Goot, A. J. (2022). Effect of l-cysteine and l-ascorbic acid addition on properties of meat analogues. *Food Hydrocolloids Submitted*, *108059*(ISSN 0268-005X). https://doi.org/10.1016/j.foodhyd.2022.108059

Emin, M. A., & Schuchmann, H. P. (2017). A mechanistic approach to analyze extrusion processing of biopolymers by numerical, rheological, and optical methods. *Trends in Food Science and Technology*, *60*, 88–95. https://doi.org/10.1016/j.tifs.2016.10.003

FAO. (2017). The future of food and agriculture: trends and challenges. In *The future of food and agriculture: trends and challenges* (Vol. 4, Issue 4). www.fao.org/publications%0Ahttp://www.fao.org/3/a-i6583e.pdf%0Ahttp://siteresources.worldbank.org/INTARD/825826-1111044795683/20424536/Ag_ed_Africa.pdf%0Awww.fao.org/cfs%0Ahttp://www.jstor.org/stable/4356839%0Ahttps://ediss.uni-goettingen.de/bitstream/han

González, A. D., Frostell, B., & Carlsson-Kanyama, A. (2011). Protein efficiency per unit energy and per unit greenhouse gas emissions: Potential contribution of diet choices to climate change mitigation. *Food Policy*, *36*(5), 562–570. https://doi.org/10.1016/j.foodpol.2011.07.003

Jia, W., Curubeto, N., Rodríguez-Alonso, E., Keppler, J. K., & van der Goot, A. J. (2021). Rapeseed protein concentrate as a potential ingredient for meat analogues. *Innovative Food Science and Emerging Technologies*, *72*(May), 102758. https://doi.org/10.1016/j.ifset.2021.102758

Krintiras, G. A., Gadea Diaz, J., Van Der Goot, A. J., Stankiewicz, A. I., & Stefanidis, G. D. (2016). On the use of the Couette Cell technology for large scale production of textured soy-based meat replacers. *Journal of Food Engineering*, *169*, 205–213. https://doi.org/10.1016/j.jfoodeng.2015.08.021

Kyriakopoulou, K., Dekkers, B., & van der Goot, A. J. (2019). Plant-Based Meat Analogues. In *Sustainable Meat Production and Processing*. Elsevier Inc. https://doi.org/10.1016/B978-0-12-814874-7.00006-7

Meulleneti, J. (1998). Relationship between sensory. *Journal of Sensory Studies*, *13*(1998), 77–93.

Michel, F., Hartmann, C., & Siegrist, M. (2021). Consumers' associations, perceptions and acceptance of meat and plant-based meat alternatives. *Food Quality and Preference*, *87*(August 2020), 104063. https://doi.org/10.1016/j.foodqual.2020.104063

Osen, R., Toelstede, S., Wild, F., Eisner, P., & Schweiggert-Weisz, U. (2014). High moisture extrusion cooking of pea protein isolates: Raw material characteristics, extruder responses, and texture properties. *Journal of Food Engineering*, *127*, 67–74. https://doi.org/10.1016/j.jfoodeng.2013.11.023

Pietsch, V. L., Bühler, J. M., Karbstein, H. P., & Emin, M. A. (2019). High moisture extrusion of soy protein concentrate: Influence of thermomechanical treatment on protein-protein interactions and rheological properties. *Journal of Food Engineering*, *251*(August 2018), 11–18. https://doi.org/10.1016/j.jfoodeng.2019.01.001

Pietsch, V. L., Emin, M. A., & Schuchmann, H. P. (2017). Process conditions influencing wheat gluten polymerization during high moisture extrusion of meat analog products. *Journal of Food Engineering*, *198*, 28–35. https://doi.org/10.1016/j.jfoodeng.2016.10.027

Pimentel, D., & Pimentel, M. (2003). Sustainability of meat-based and plant-based diets and the environment. *American Journal of Clinical Nutrition*, *78*(3 SUPPL.). https://doi.org/10.1093/ajcn/78.3.660s

Ranasinghesagara, J., Hsieh, F., & Yao, G. (2006). A photon migration method for characterizing fiber formation in meat analogs. *Journal of Food Science*, *71*(5). https://doi.org/10.1111/j.1750-3841.2006.00038.x

Samard, S., Gu, B. Y., & Ryu, G. H. (2019). Effects of extrusion types, screw speed and addition of wheat gluten on physicochemical characteristics and cooking stability of meat analogues. *Journal of the Science of Food and Agriculture*, *99*(11), 4922–4931. https://doi.org/10.1002/jsfa.9722

Scarborough, P., Allender, S., Clarke, D., Wickramasinghe, K., & Rayner, M. (2012). Modelling the health impact of environmentally sustainable dietary scenarios in the UK. *European Journal of Clinical Nutrition*, *66*(6), 710–715. https://doi.org/10.1038/ejcn.2012.34

Schreuders, F. K. G., Schlangen, M., Bodnár, I., Erni, P., Boom, R. M., & van der Goot, A. J. (2022). Structure formation and non-linear rheology of blends of plant proteins with pectin and cellulose. *Food Hydrocolloids*, *124*(October 2021). https://doi.org/10.1016/j.foodhyd.2021.107327

Stehfest, E., Bouwman, L., Van Vuuren, D. P., Den Elzen, M. G. J., Eickhout, B., & Kabat, P. (2009). Climate benefits of changing diet. *Climatic Change*, *95*(1–2), 83–102. https://doi.org/10.1007/s10584-008-9534-6

Steinfeld, H., Gerber, P., Wassenaar, T., Castel, V., Rosales, M., Rosales, M., & de Haan, C. (2006). *Livestock's long shadow: environmental issues and options* (Food & Agriculture Org., Ed.).

2

Chapter 3

Rework Potential of Soy and Pea Protein Isolates in High-Moisture Extrusion

Abstract

High-moisture extrusion (HME) is an effective process to make fibrous products that can be used as meat analogues. In this study, the effect of extrusion of already extruded products (i.e., re-extrusion) was tested with the aim to explore the potential of rework in HME. The rework of material is important because it is a route to reduce waste, which is always produced, for example during the start or at the end of a production run. Pea and soy protein isolates (PPI and SPI) were first extruded, then freeze-dried and ground, and extruded again. The visual and textural properties of the fibrous products were evaluated. Also, the rheological properties, solubility, and water-holding capacity (WHC) of the ingredients and the products after the first and second extrusion were quantified. The obtained freeze-dried powders after the first HME cycle had a reduction in solubility of 15% for PPI and 74% for SPI. Furthermore, WHC was reduced by 65% and 17% for PPI and SPI, respectively. After the second HME cycle, the reduction in solubility and WHC was augmented to 22% and 90% for PPI, and 79% and 63% for SPI. No effect on stock and loss moduli after heating and cooling were found, even after two HME cycles. SPI fibrous products did not differ in cutting strength, anisotropy index, or visual appearance after re-extrusion. Only, a decrease in hardness was detected, from 62.0 N to 51.1 N. For PPI, re-extrusion did reduce the cutting force and hardness but not the anisotropy index. It was concluded that even though HME induces a loss of solubility and WHC, this did not affect the fibrous texture formation of the protein. This means that the texture formed during HME does not depend on the process history and that rework is thus possible for fibrous products.

3.1   Introduction

High-moisture extrusion (HME) is a common method that has been used for several decades to produce fibrous products that can be used as meat analogues (Cheftel et al., 1992). Soy and pea protein are often used ingredients in high-moisture extrusion to make fibrous products (Osen et al., 2014; Pietsch et al., 2019). The HME process could generate waste streams during the start or end of the extrusion run. Waste produced during processing is one of the main factors that contribute to global food loss (Ishangulyyev et al., 2019). It is thus of importance to find solutions to reduce losses, for example, by reworking waste streams. HME consists of a mixing and hydration step, a thermomechanical processing step, and finally a cooling step (S. H. V. Cornet, Snel, Schreuders, et al., 2021). Most proposed mechanisms behind texture formation consider the deformation of a flow in the extruder cooling die, being either laminar flow (Akdogan, 1999), phase deformation (Tolstoguzov, 1993), or elongational flow (Wittek, Ellwanger, et al., 2021). Apart from the mechanisms considering deformation, some authors have discussed the importance of protein-protein interactions and shown that aggregates had formed after extrusion of pea and soy (Fang et al., 2014; Osen et al., 2015a). With dead-stop HME, Liu & Hsieh (2008) showed that covalent binding took place in the extruder barrel before entering the cooling die. These protein-protein interactions could reduce the solubility of the protein, as has been shown for pea and soy (K. Liu & Hsieh, 2008; Osen et al., 2015b). However, van der Sman & van der Goot (2023) argued that the high temperatures and high shear stresses during HME induce a transient protein network and that instead of measuring relative contributions of the different bonds, rheology is a more accurate method to characterize the protein melt. A closed cavity rheometer (CCR) was recently introduced to mimic extrusion-like conditions and to quantify the effects of processing on ingredient properties (Emin et al., 2017). The CCR is able to quantify rheological properties of dense protein dispersions at high temperature and pressure through oscillatory deformation. It has been further suggested that large amplitude oscillatory shear (LAOS) in combination with Lissajous curves could reveal relevant information on the melt properties (Schreuders et al., 2021b). With the use of LAOS and the dissipation ratio, it was found that the elasticity of pea protein isolate (PPI) and soy protein isolate (SPI) increased after a heat treatment (Schreuders et al., 2019).

Noguchi (1989) reported that it was possible to extrude soy protein in three to four steps by grinding the extrudate and feeding it again to the extruder, and a similar fibrous product was obtained. It was concluded that the extrudate was little affected by multiple extrusion steps, as no visual effects were observed. Furthermore, it was proposed that in HME 'reaction' and 'texture formation' should be considered independently (Noguchi, 1989). In addition, the protein-protein reactions are expected to take place at a much smaller length scale compared to the formation of the fibrous texture (van der Sman & van der Goot, 2023). This would mean that denaturation of the plant protein is less important during HME and not likely to be important for fibrous texture formation.

We hypothesize that extrusion changes protein properties, for example, the solubility and water-holding capacity, and this could impact its rework potential. Therefore, this study aims to report how important these changes are for the rework ability of soy and pea by extruding them in a second step and to compare the product properties in terms of anisotropy, hardness, and cutting strength. Furthermore, the dry protein powders after the first and second steps of extrusion were compared to the isolates in terms of rheological properties and solubility and water-holding capacity.

3.2 Methods and Materials

3.2.1 Materials
Pea protein isolate (PPI, NUTRALYS® F85M) was obtained from Roquette Frères S.A. (Lestrem, France). Soy protein isolate (SPI, SUPRO 500E A®8) was obtained from Solae (St. Louis, MO, USA). PPI contained at least 83 wt% protein, and SPI 90% (N x 6.25, indicated by supplier). Powders were sieved to obtain a particle size of <400 µm (PowCN-Sif X600, CapsulCN, Ruian, China) to exclude size effects when compared with the freeze-dried powder.

3.2.2 Design of Experiments
Figure 3.1 shows an overview of the performed experimental steps. First, PPI and SPI were textured into fibrous products with HME (PPI-E1, SPI-E2). The obtained extrudates were freeze-dried, ground, and used again as starting material for HME. The obtained fibrous products (PPI-E2, SPI-E2) were compared to the PPI-E1 and SPI-E1 fibrous products in terms of visual appearance and texture properties. The solubility, water-holding capacity (WHC), and rheological properties of the protein isolates and freeze-dried powders were measured. All analyses are discussed in detail in the following sections.

3.2.3 High Moisture Extrusion
Protein isolates and freeze-dried extrudates (Figure 3.1) were extruded with an Evolum 25 twin-screw extruder (Clextral, Firminy, France). The screw diameter was 25 mm and the length/diameter ratio was 40. The extruder barrel consisted of 10 sections, which were heated to 30, 50, 70, 90, 100, 120, 130, 145, 145, and 125 °C, respectively. The rotational speed of the screws was set to 300 rpm. A rotating cooling die was attached that consists of a rotating inner cylinder and a thermo-regulated, static outer cylinder (Snel et al., 2022). The cylinder can be further divided into two sections that can differ in their rotating speed. The rotation speed of the inner cylinder was set at 75 rpm in the first section, while the second section was kept at 0.5 rpm. The temperature of the cooling die was 85 °C. A breaker plate was placed between the extruder barrel and rotating die, which had 31 holes with a diameter of 3 mm. A twin-screw gravimetric feeder type KCM (K-Tron, Niederlenz, Switzerland) was used to feed the dry ingredients into the extruder,

and water was injected in the second section with a water pump (DKM). The dry feed rate and water rate were adjusted according to the moisture content of the isolates to obtain samples with a moisture content of 58% for PPI and 62% for SPI. Throughput was 18 kg h^{-1} for all conditions.
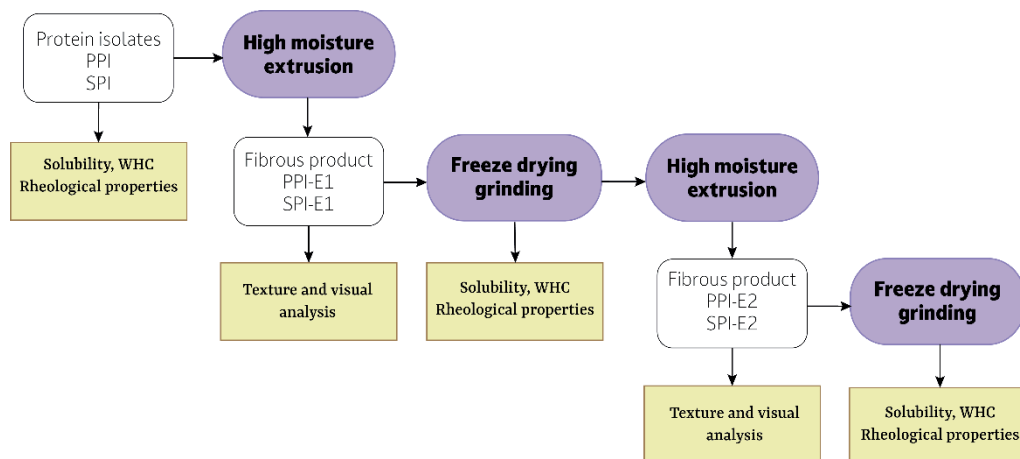
Figure 3.1: Schematic overview of the experimental design of experiments. PPI = pea protein isolate, SPI = soy protein isolate, WHC = water holding capacity.

3.2.4 Freeze-Drying of the Extrudates

Extrudates were freeze-dried and milled to facilitate feeding of those extrudates to the extruder. Freeze-drying was chosen for technical reasons and since it has limited effects on protein solubility and gelling capacity compared to other drying techniques such as oven and spray drying (Brishti et al., 2020). Extrudates were cut and collected in a sealed plastic bag. Packed extrudates were then frozen to -20 °C with a blast freezer (Electrolux, Stockholm, Sweden). Samples were then taken out of the plastic bag and transferred to a vacuum freeze-dryer (Sublimater, Zirbus, Bad Grund, Germany). The temperature of the samples was followed with temperature probes, one for each tray of samples. First, temperature was lowered to -30 °C for 3 h followed by a drying step under vacuum (0.1 mbar) for 34 h. After the samples were dehydrated, temperature and pressure were increased to 20 °C and 10 mbar. Dried samples were collected and ground with a hammer mill (Pulverizer MP, Hosokawa Alpine, Augsburg, Germany) and sieved with a vibrating sieve to obtain a particle size of <400 µm (PowCN-Sif X600, Capsulcn, Ruian, China).

3.2.5 Texture Analysis

Extrudates obtained from SPI and PPI were compared to extrudates made from freeze-dried extrudate powders of SPI and PPI. For simplicity, we will call the former SPI-E1 and PPI-E1, and the latter SPI-E2 and PPI-E1 (Figure 3.1). To prevent any other parameters

from influencing the extrudates, all samples were prepared on the same day. Samples were defrosted overnight and compared visually by making a small inclination to aid in breaking the sample. Samples were opened in both parallel and perpendicular directions and photographed. Texture profile analysis and cutting tests were performed with a TA-XT2 texture analyzer and the Exponent Connect software (Stable Micro Systems, Surrey, UK). The texture analyzer was equipped with a 50 kg load cell and calibrated with a 1 kg weight.

3.2.6 Texture Profile Analysis

The larger extrudates were cut into cylinders of 20 mm in diameter and a height of 10 mm. Samples were compressed twice with a 60 mm aluminum cylinder probe to 30% of original height with a test speed of 1 mm/s and a waiting time in between the two compressions of 5 s. Samples were measured in triplicate. The peak maximum force at first compression was taken as the hardness (Meulleneti, 1998).

3.2.6.1 Cutting Test

Cutting tests were performed in both parallel and perpendicular directions to the rotational shear flow. First, samples were cut in squares of 20 x 20 mm. Height was again 10 mm. Samples were cut up to 90% of their initial height with a Warner-Bratzler blade at a speed of 1 mm/s. Anisotropy was calculated as the ratio between cutting force in parallel and perpendicular directions:

$$AI_F = \frac{F_\parallel}{F_\perp} \qquad\qquad 3.1$$

3.2.6.2 Solubility and Water-Holding Capacity

The moisture contents of the powders were measured with a moisture analyzer (Mettler Toledo, Columbus, OH, USA). Solubility and water holding capacity (WHC) of the protein isolates and freeze-dried powders was measured in triplicate with a method reported by (Bühler et al., 2020). with some minor alterations. A dispersion of 0.0125 g/g protein isolate in demineralized water was prepared and shaken overnight at 300 rpm at room temperature. Subsequently, the dispersions were centrifuged at 10,000 x g at 21 °C for 20 min. The weight of the pellet was recorded and dried at 100 °C for at least 10 h. The solubility and WHC were calculated as follows:

$$Solubility = \frac{M_{drypowder} - M_{drypellet}}{M_{drypowder}} \qquad\qquad 3.2$$

$$WHC = \frac{M_{wetpellet} - M_{drypellet}}{M_{drypowder}} \qquad\qquad 3.3$$

in which $M_{drypowder}$ is the overall weight of the isolate, and $M_{wetpellet}$ and $M_{drypellet}$ are the weights of the pellet before and after drying.

3.2.7   Rheological Properties

Strain amplitude sweeps were performed with a CCR (RPA elite, TA instruments, New Castle, DE, USA). The geometry in the CCR has a radius of 2.25 mm, a maximum height of 4 mm, and a biconical opening with an angle of 3.35 ° to ensure homogeneous transmission of the shear stress applied. The top and bottom cones have grooves to prevent slip. The upper cone remains stationary while the lower cone oscillates. First, powders were mixed with demineralized water to obtain the same moisture content as in extrusion: 58% for PPI and 62% for SPI, calculated with the relative dry matter content of the powders. Next, approximately 5 g of the sample was placed between two plastic films in the CCR. The cavity was then sealed with a pressure of 4 bar to prevent evaporation. Samples were then heated to 30 or 145 °C for 2 min without shear. Three measuring conditions were tested: 30 °C, 145 °C, or cooled from 145 °C to 30 °C. The latter could reflect the behavior during a HME cycle, in terms of temperature profile. An amplitude strain sweep was performed from 0.1 to 1000% at 1 Hz. The yield stress and strain at the end of the linear viscoelastic (LVE) regime were defined as the point where G' differs more than 5% from its value in the LVE regime. The flow stress and strain were defined at the crossover point, where G' (stock modulus) is equal to G'' (loss modulus). These values were used to define if the materials were mushy (low stress and low strain), brittle (low strain and high stress), rubbery (high strain and low stress), or tough (high strain and high stress) (Schreuders et al., 2021a)).

3.2.8   Lissajous Plots

The data obtained with the strain amplitude sweeps were further analyzed with the MITlaos software (version 2.1 beta, freeware distributed from MITlaos@mit.edu). With this software, Lissajous plots were made to visualize the response of the material to the oscillatory strain for both the elastic and viscous stress. Furthermore, the dissipation ratio was calculated (Schreuders et al., 2021a). The energy dissipated per unit volume in a single cycle as a function of the first-order viscous Fourier coefficient G''_1 was calculated as:

$$E_d = G''_1 \gamma_0^2 \qquad\qquad 3.4$$

in which E_d is the energy dissipated and γ_0 the strain amplitude. For a perfect plastic material the energy dissipated is equal to:

$$E_d^{pp} = 4\gamma_0 \sigma_{max} \qquad\qquad 3.5$$

in which σ_{max} is the maximum stress. The ratio between the actual energy dissipated and the energy dissipated by a perfect plastic then gives the energy dissipation ratio ϕ (Ewoldt et al., 2010):

$$\phi = \frac{E_d}{E_d^{pp}} = \frac{\pi G''_1 \gamma_0}{4\sigma_{max}} \qquad\qquad 3.6$$

For a perfect plastic material, this ratio would be 1. An elastic material would have a dissipation ratio of 0, and a purely viscous material a ratio of 0.8.

3.2.9 Standardization of Results

The relative difference between the extruded powder and extrudates was illustrated by calculating a ratio for each parameter measured. For each parameter, the obtained value was divided by the obtained value of their corresponding isolate, so SPI or PPI, or their corresponding extrudate, SPI-E1 or PPI-E1. For the corresponding sample, the value was thus taken as 1.

3.2.10 Statistical Analysis

Statistical analysis was performed with R prior to standardization of the results. It was assumed that the different factors tested in this study (protein type, processing, and temperature in the case of the rheological properties) did not interact. To confirm this, a two-way analysis of variance (ANOVA) or three-way ANOVA in the case of rheological properties was performed. First, normality and equal variance were tested with descriptive statistics. If the data were normally distributed, a two- or three-way ANOVA was performed to test if the observed differences between samples were significant (α = 0.05). Multiple comparison Tukey tests were performed to indicate which treatments were significantly different from each other (α = 0.05). If the data was not normally distributed, Welch's ANOVA and Dunn's tests were performed. All tests in this study were performed in triplicate.

3.3 Results and Discussion

3.3.1 Extrudate Properties after Second Step HME

Extrudates were made with HME from protein isolates (PPI-E1, SPI-E1) and freeze-dried powders of the extrudates (PPI-E2, SPI-E2). The visual appearance, hardness, cutting strength, and anisotropy of cutting strength were compared.

The samples prepared from protein isolates and freeze-dried powders of the extrudates did not differ in their visual appearance for both SPI and PPI (Figure 3.2). In general, it was noted that SPI samples looked more inhomogeneous when broken in the parallel direction, while for PPI no clear difference was observed between the parallel and perpendicular direction of breaking. This observation was made for products obtained after the first and second extrusion steps.

Extrudate	Direction	
	Parallel	Perpendicular
PPI-E1		
PPI-E2		
SPI-E1		
SPI-E2		

Figure 3.2: Visual appearance of extrudates from PPI (58% MC) and SPI (62%). A small inclination was made to allow breaking of the extrudates in parallel and perpendicular direction to the shear flow in the rotating cooling die. Samples -E1 were made from the isolates (PPI, SPI), and samples -E2 were made from the freeze-dried and ground -E1 extrudates.

The hardness, cutting force in both parallel and perpendicular directions, and the calculated anisotropy index were set to 1 for the PPI-E1 and SPI-E1 extrudates (Table 3.1). Then, the obtained values of the PPI-E2, and SPI-E2 samples were divided by the values obtained for PPI-E1, and SPI-E1, to show their relative difference (Figure 3.3). For PPI, cutting force decreased in both parallel and perpendicular directions after the second HME step, and a similar anisotropy index was thus found (Figure 3.3c). The cutting force in both directions was not altered for SPI after a second HME step, resulting in a similar anisotropy index. It can further be observed that the hardness of the PPI-E2 and SPI-E2 samples was slightly lower compared to PPI-E1 and SPI-E1 (Figure 3.3).

Table 3.1:Hardness (N), cutting force (N) in both parallel (par) and perpendicular (per) direction, and the anisotropy index calculated as the ratio between the two cutting forces for PPI-E1 (58% MC) and SPI-E1 (62% MC) extrudates, letters indicate significant groups, n = 3.

Extrudate	Hardness (N)	Cutting Force Par (N)	Cutting Force per (N)	AI (-)
PPI-E1	116 ± 3.5 [a]	14.3 ± 0.2 [a]	15.1 ± 0.3 [b]	1.1± 0.03 [b]
SPI-E1	62.0 ± 2.5 [b]	13.6 ± 0.8 [a]	22.1 ± 0.4 [a]	1.6± 0.1 [a]
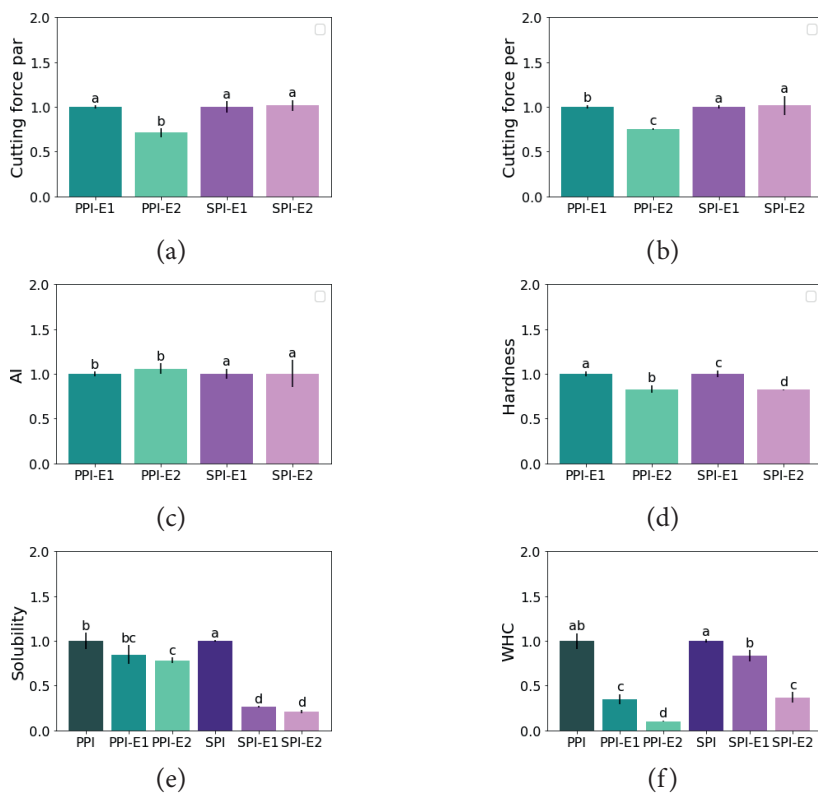
Figure 3.3: Relative change of extrudate parameters obtained from a cutting test (a–c), texture profile analysis (d), and relative solubility (e) and WHC (f) of the powders after HME after a first (-E1) and second (-E2) HME step as compared to PPI and SPI (Table 2). Values are reported as averages with standard deviations (black bars); letters indicate significant groups; n = 3. A relation was found between HME cycle and protein type for cutting force in both par and per direction, solubility, and WHC (α < 0.05).

3.3.2 Effect of HME on Protein Properties

Apart from the comparison between extrudates after a second HME step, the obtained freeze-dried powders were also analyzed. Extrudates obtained after the first (called -E1) and second (-E2) HME were freeze-dried, ground, and sieved, and their properties were compared to the protein isolates (PPI, SPI) in terms of solubility, WHC (Table 3.2, Figure 3.3f), and rheological properties (Table 3.3, Figures 3.4-3.7).

Table 3.2: Solubility, and WHC for PPI and SPI before and after extrusion. After extrusion, extru- dates were freeze-dried, ground, and sieved (-E), this powder was extruded, freeze-dried, ground, and sieved again (-E2). Values are averages ± standard deviation, and letters indicate significant groups, n = 3.

Powder	Solubility (g g^{-1})	WHC (g g^{-1})
PPI	0.30 ± 0.03 [b]	9.6 ± 0.8 [ab]
SPI	0.47 ± 0.00 [a]	11 ± 0.2 [a]

Solubility and WHC of PPI were slightly lower than the solubility and WHC of SPI (Table 3.2). The obtained powders from freeze-dried extrudates, PPI-E1 and SPI-E1, had a lower solubility compared to PPI and SPI (Figure 3.3e). For PPI, this reduction was not significant. The powders obtained from the second-step extrudates, PPI-E2 and SPI-E2 had again a lower solubility, but this additional decrease was not significantly different from the PPI-E1 and SPI-E1 samples. The WHC of the PPI-E1 and SPI-E1 samples was significantly lower compared to PPI and SPI (Figure 3.3f). The second HME step significantly reduced the WHC further. Overall, the effect of HME on solubility and WHC was similar for both PPI and SPI, although the solubility was more drastically reduced for SPI and the WHC for PPI. It seems that HME leads to additional cross-links which impact the powder properties. With the use of cross-linking and reducing agents, it was found that more cross-links lead to lower WHC for whey protein (Peters et al., 2015). The WHC could be used to predict the maximum moisture content during HME. For example, PPI-E1 had a WHC of 3.3 ± 0.4 g g^{-1}, and extrudates had a dry matter content of 42%. The 42 g PPI-E1 could thus hold 140 g water, which translates to a maximum moisture content of 77%, which is still higher than the 58% in the extrudate. However, PPI-E2 had a WHC of 1.0 ± 0.1 g g^{-1}, which would result in a maximum moisture content of 50%. Therefore, extruding PPI-E2 in a third HME cycle might become problematic.

Rheological properties were examined with a strain amplitude sweep at 30 °C, 145 °C, and heating to 145 °C followed by cooling to 30 °C (Figures 3.4 and 3.5). The measured *G'* and *G''* at 145 °C were found to be close to or even below the torque limits of the CCR, and thus it was not possible to determine the LVE-regime, yielding, and cross-over point for the measurements at this temperature. From the other strain amplitude sweeps, *G'* and *G''* in the LVE-regime, yield strain and stress, and flow strain and stress were determined (Table 3.3). The strain and stress at the yield and flow point give an indication of the texture of the material, being either mushy, rubbery, tough, or brittle (Schreuders et al., 2021a).

The alterations of these parameters after the first and second HME steps were again calculated relative to PPI and SPI (Figure 3.6). It can be seen that the HME step increased the G' and G'' measured at 30 °C for both PPI and SPI, and this remained constant after the second step. After heating to 145 °C and cooling to 30 °C, no significant changes were found for both PPI and SPI, although G' and G'' decreased slightly with each step.

Table 3.3: Storage modulus (G'), loss modulus (G''), yield strain (γ_y), yield stress (σ_y), flow strain (γ_{co}), and flow stress (σ_{co}) for PPI and SPI before and after extrusion. After extrusion, extrudates were freeze-dried, ground, and sieved (-E1), this powder was extruded, freeze-dried, ground, and sieved again (-E2). G', γ_y, and γ_{co} were determined from strain amplitude sweeps. Values are averages ± standard deviation, and letters indicate significant groups, n = 3.

Powder	T (°C)	G' $(10^2$ kPa)	G'' $(10^2$ kPa)	γ_y (%)	σ_y (kPa)	γ_{co} (%)	σ_{co} (kPa)
PPI	30	1.4 ± 0.3 [b]	0.3 ± 0.0 [a]	4.8 ± 0.5 [bc]	6.9 ± 0.5 [b]	137 ± 19 [b]	48 ± 5.1 [b]
	145-30	2.2 ± 0.4 [ab]	0.5 ± 0.1 [a]	3.3 ± 0.6 [c]	7.1 ± 1.0 [b]	173 ± 24 [ab]	62 ± 5.9 [b]
SPI	30	1.7 ± 0.3 [ab]	0.3 ± 0.1 [a]	8.0 ± 0.0 [a]	14 ± 2.1 [ab]	200 ± 0.0 [a]	75 ± 11 [ab]
	145-30	2.5 ± 0.4 [a]	0.5 ± 0.1 [a]	6.5 ± 1.2 [b]	16 ± 1.1 [a]	200 ± 0.0 [a]	105 ± 13 [a]

The lower yield stress and strain of PPI samples compared to SPI, indicated a more mushy material for PPI compared to the brittle SPI (Table 3.3). Both the yield strain and flow strain decreased significantly for both PPI and SPI measured at 30 °C (Figure 3.6a,c). In other words, after an HME step, the isolates will yield and flow at a lower strain, and this might affect the flow behavior in the extruder barrel. After heating to 145 °C and cooling to 30 °C, PPI samples were less affected, and yield strain and stress even increased after the first HME step (Figure 3.6b). SPI became slightly more brittle after the first HME cycle, seen by the lower yield strain, but after the second cycle, a similar stress and strain value was found as for the non-extruded SPI (Figure 3.6d). So, breakdown of the network structure seems to take place, but it can (partly) recover.

The flow stress and strain were determined at the cross-over point of the amplitude sweeps. Again, a lower flow strain and stress were observed for PPI compared to SPI, indicating that SPI is a more tough material (Table 3.3). The first HME step reduced the flow strain and stress for both PPI and SPI, indicating a more mushy or brittle material (Figure 3.6a,c). After the second HME step, the strain and stress were not reduced further. After heating to 145 °C and cooling to 30 °C, both the flow strain and stress were less affected, but still, a reduction was observed for PPI samples (Figure 3.6b,d). Interestingly, the cross-over stress and strain of SPI were not changed after two cycles of extrusion after heating and cooling, indicating that the SPI samples remained tough.

(a) PPI

(b) PPI

(c) PPI

(d) PPI-E1

(e) PPI-E1

(f) PPI-E1

(g) PPI-E2
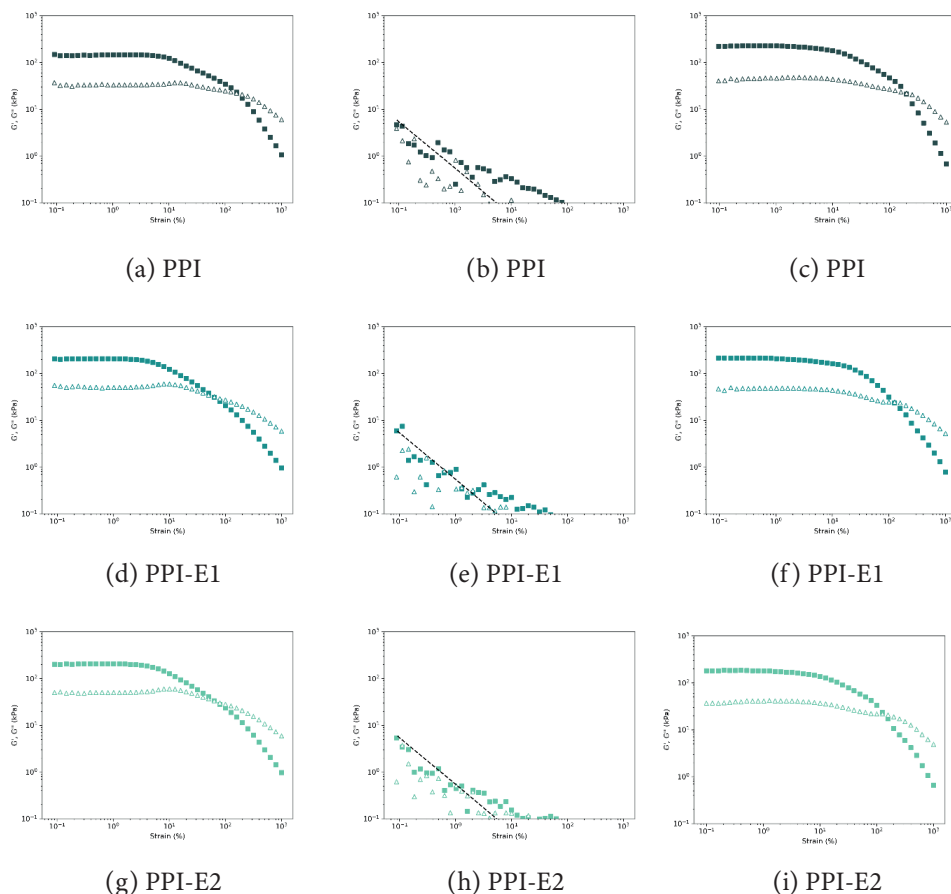
(h) PPI-E2

(i) PPI-E2

Figure 3.4: Strain sweeps (f = 1 Hz) of PPI (a–c), PPI-E1 (d–f), and PPI-E2 (g–i) at 30 ℃ (a,d,g), at 145 ℃ (b,e,h), and heated to 145 ℃ and cooled to 30 ℃ (c,f,i). G′: closed symbols and G″: open symbols. The black dotted line in the measurement at 145 ℃ represents the torque limits of the CCR.

Figure 3.5: Strain sweeps (f = 1 Hz) of SPI (**a**–**c**), SPI-E1 (**d**–**f**), and SPI-E2 (**g**–**i**) at 30 °C (a,d,g), at 145 °C (b,e,h), and heated to 145 °C and cooled to 30 °C (c,f,i). G': closed symbols and G'': open symbols. The black dotted line in the measurement at 145 °C represents the torque limits of the CCR.
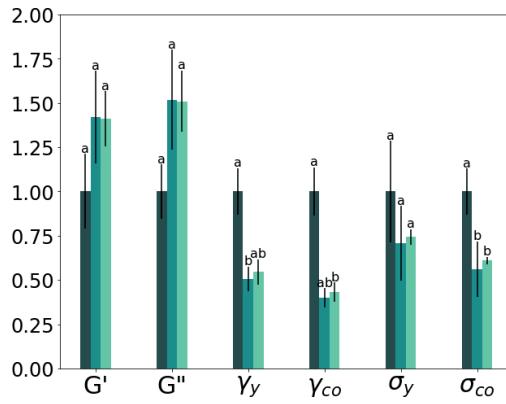
(a) PPI - 30 °C
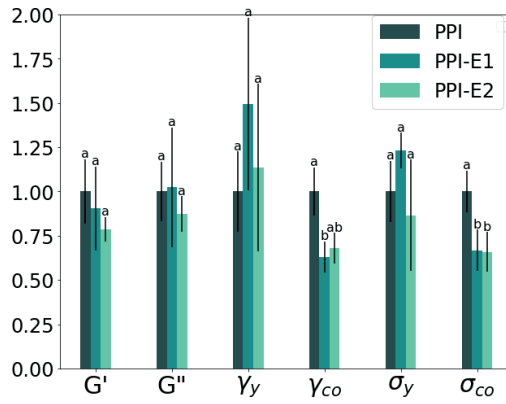
(b) PPI - 145 °C
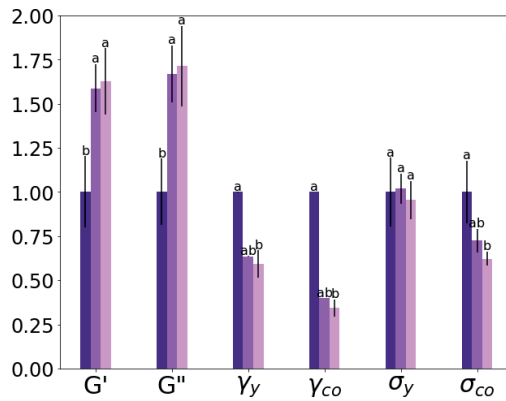
(c) SPI - 30 °C

Figure 3.6 (continued)
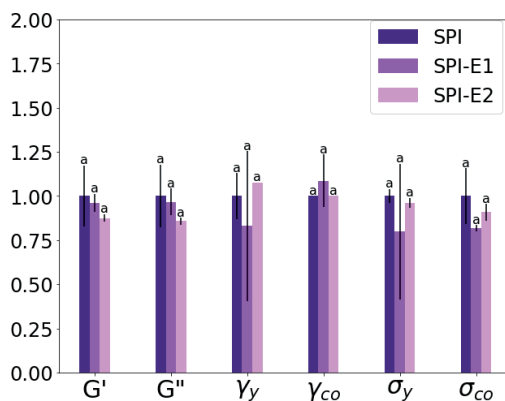
(d) SPI - 145 °C

Figure 3.6: Relative change of rheological parameters obtained from a strain sweep after a first (-E1) and second (-E2) HME step as compared to PPI (a,b) and SPI (c,d) (Table 3). The strain sweeps were performed at 30 °C (a,c) and after heating to 145 °C and cooling to 30 °C (c,d). Values are reported as averages with standard deviations (black bars); letters indicate significant groups per variable; n = 3.

Lissajous curves were made from the strain amplitude sweeps (Appendix A), and dissipation ratios were calculated (Figure 3.7). At 30 °C, all samples were in the elastic regime at low strain amplitude and became more viscous with increasing strain amplitude. For both PPI and SPI, the point where the samples became viscous was at a lower strain amplitude after the first HME cycle. A second HME cycle did not seem to affect this further. When the samples were first heated to 145 °C and then cooled again to 30 °C, both PPI and SPI remained elastic at higher strain amplitudes compared to the unheated samples. This increase in elasticity has been found before for both pea and soy (Schreuders et al., 2021a). The first and second HME cycles made the PPI samples slightly more viscous at higher shear, but almost no difference was observed for the SPI samples.

(a)
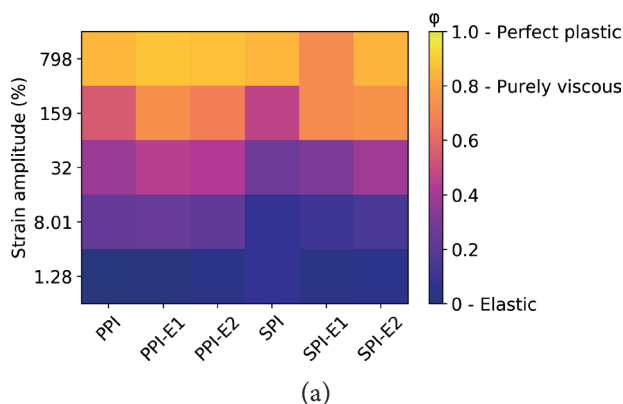
Figure 3.7 (continued)

(b)
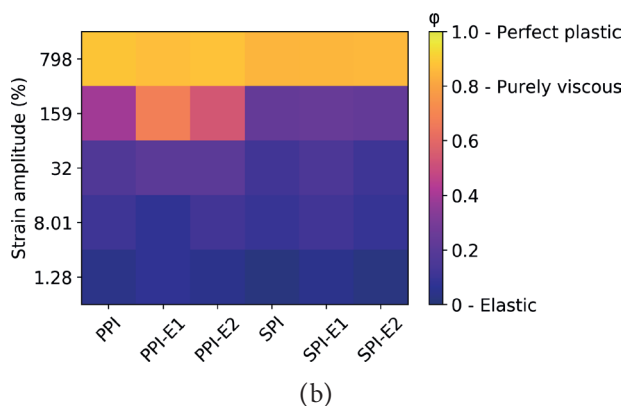
Figure 3.7. Heat map of the dissipation ratio φ at different strain amplitudes for the powders before (SPI, PPI) and after one (-E1) and two (-E2) HME cycles, measured at 30 °C, (a) and after heating to 145 °C followed by cooling to 30 °C (b).

3.4 Discussion

In this study, the rework potential of fibrous products was tested by repetitive extrusion of protein isolates. This was accomplished by comparing the relative change of the obtained fibrous products in terms of hardness, cutting strength, and anisotropy. For improved comparability, extrudates were freeze-dried and ground before the second HME step. The properties of the obtained powder after the first and second HME steps were compared to the untreated protein isolate in terms of solubility, WHC, and rheological properties.

The effect of repetitive extrusion on the extrudate properties was small, especially for SPI. Visually, no differences were found between samples after the first and second HME steps. For soy protein, this was observed before, as no visual difference was reported for defatted soy protein after three HME steps (Isobe & Noguchi, 1987). PPI extrudates had a lower anisotropy index compared to SPI, which has been observed previously (Snel et al., 2022). For SPI samples the cutting force and anisotropy indexes were not affected by the second HME step. Only the hardness was slightly decreased. For PPI, the cutting force and hardness were decreased, however, the anisotropy index remained the same. This then confirms that soy can be extruded in several cycles without altering product properties, as was suggested before (Isobe & Noguchi, 1987). The ability to extrude SPI and PPI in several HME cycles is remarkable, as we see that ingredient properties (solubility, WHC) changed. This could be explained because some changes are less relevant; for example, the WHC was still sufficient, and other changes were partly reversible through heating. The changes in rheological properties became smaller after heating, suggesting the breaking and reforming of bonds upon heating. The hydrophobic bonds in proteins are broken at temperatures of 130-140 °C (Tolstoguzov, 1993). Furthermore, the high shear rates in the extruder barrel could lower the activation energy for breaking the disulfide bonds (Pommet et al., 2003).

Each HME cycle reduced the solubility and the WHC of both PPI and SPI, even if the reduction in solubility was only significant after two HME cycles for PPI. The decrease in solubility after HME has been reported previously for both PPI (Osen et al., 2015a) and SPI (K. Liu & Hsieh, 2008), although both studies used reducing buffers to break specific bonds between the proteins. Isobe & Noguchi (1987) also found a reduction of soy protein solubility after each HME step. The reduced solubility and WHC were probably caused by the formation of insoluble aggregates during HME. Fang et al. (2014) performed sodium dodecyl sulfate-polyacrylamide gel electrophoresis (SDS-PAGE) before and after extruding SPI and observed a reduction in the intensity of specific bands, which they attributed to aggregate formation. Similarly, Osen et al. (2015a) saw a reduction of specific bands in SDS-PAGE after HME of PPI and came to a similar conclusion. The decrease in WHC could also reflect a higher density of cross-links (Peters et al., 2015)

The formation of aggregates could also explain observed changes in rheological properties when measured at 30 °C. Remarkably, these changes became smaller after heat treatment was performed. Possibly, the heating and cooling step allowed the proteins to rearrange in a more optimal way. For pea protein, it has been found previously that a low cooling rate allowed pea vicilin to make more optimal interactions (O'Kane et al., 2004). O'Kane et al. (2004) showed that the elastic modulus of soy protein gels followed the same trajectory during reheating and subsequent cooling between 85 and 25 °C, even at a higher cooling rate. This further confirms the found reversibility of soy during extrusion (Noguchi, 1989).

In this study, rework was tested by freeze-drying the extrudates and feeding them as a powder to the extruder. We are confident that rework is also possible using other mild drying techniques. In the case rework is combined with native ingredients, it might be possible to add the rework without a drying step. The latter has been proven for extrudates made from soy flour (Isobe & Noguchi, 1987).

3.5   Conclusion

SPI and PPI were extruded twice to test rework potential. First, extrudates for both protein isolates were obtained with HME and subsequently, these extrudates were freeze-dried and ground for a next HME cycle. HME led to a reduction of solubility and WHC of proteins, probably caused by protein-protein interactions and aggregate formation. A second HME cycle reduced solubility and WHC further. However, after heating, the rheological properties were not significantly different after HME. This was explained by the weakening of protein-protein interactions upon temperatures of 145 °C. In HME, the weakening of the bonds will be further achieved by the high shear stresses. We, therefore, hypothesize that protein aggregates can be formed and aligned in a repetitive, reversible manner, and fibrous textures can be formed again. This hypothesis was confirmed by the similarity in structural and textural properties of the fibrous products of the first and second HME cycle.

For both PPI and SPI, the visual appearance of the extrudates was not altered. Even though the hardness and cutting strength of PPI were slightly reduced, visual aspects and anisotropy of PPI fibrous products remained similar after the second HME step. It is concluded that the reactions taking place in HME can be viewed as separate from the texture formation. SPI could be seen as a thermoplastic reversible material, and even PPI was not affected largely by HME. This thus concludes that rework is possible for both PPI and SPI.

3

Appendix A

Figure A1. Elastic Lissajous curves of the stress versus strain amplitude at 30 °C. Solid lines represent normalized stress and dashed lines the elastic stress.

Figure A2. Elastic Lissajous curves of the stress versus strain amplitude of samples heated to 145 °C and cooled to 30 °C. Solid lines represent normalized stress and dashed lines represent the elastic stress.
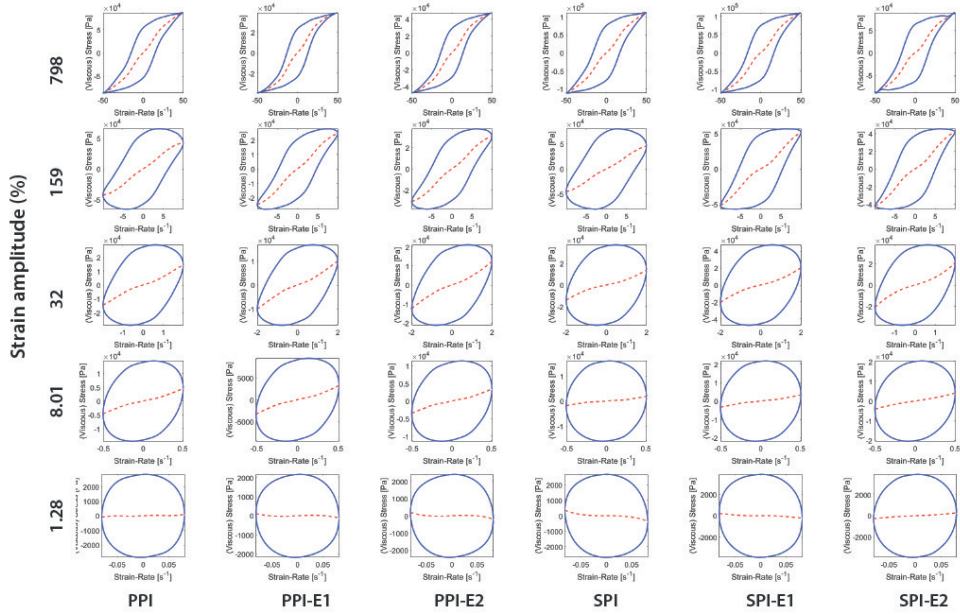
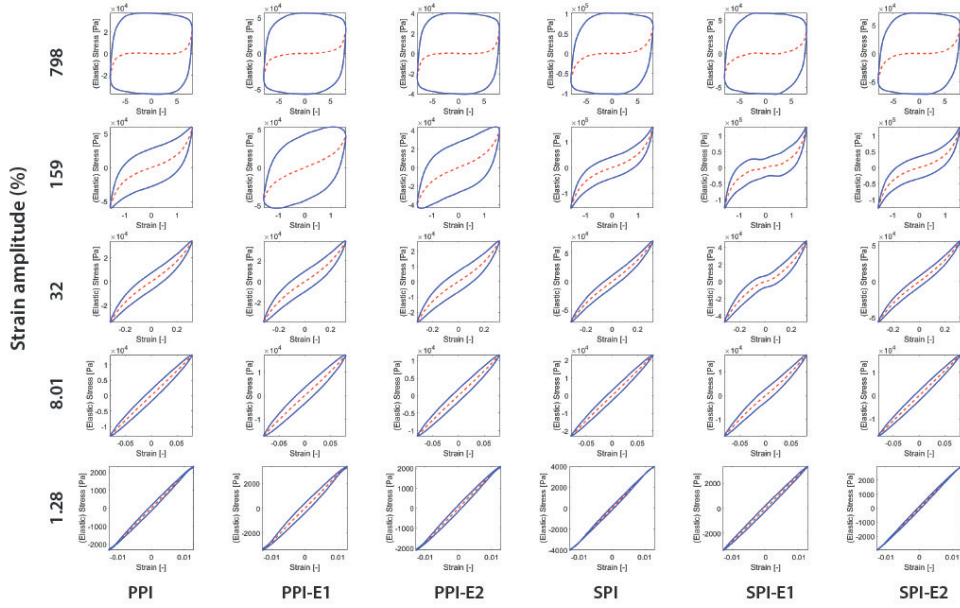*Figure A3. Viscous Lissajous curves of the stress versus strain amplitude at 30 °C. Solid lines represent normalized stress and dashed lines represent the elastic stress.*
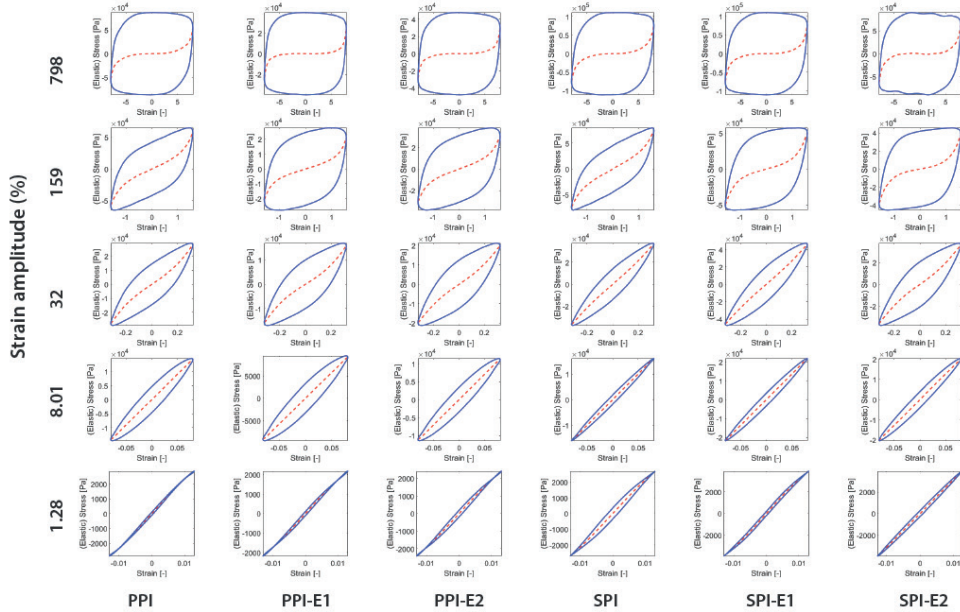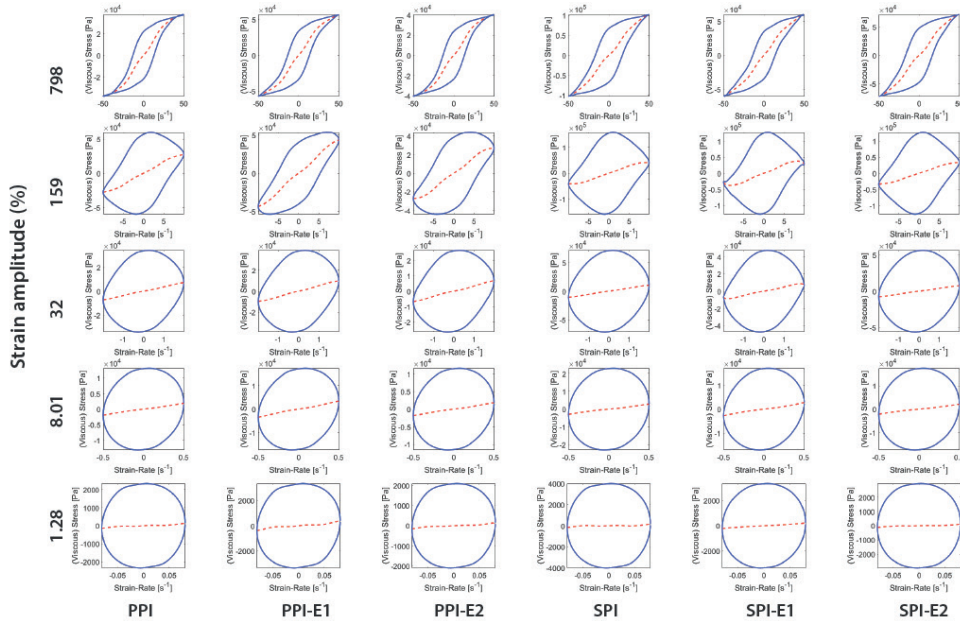

Figure A4. Viscous lissajous curves of the stress versus strain amplitude of samples heated to 145 °C and cooled to 30 °C. Solid lines represent normalized stress and dashed lines the elastic stress.

References

Akdogan, H. (1999). High moisture food extrusion. *International Journal of Food Science and Technology*, *34*(3), 195–207. https://doi.org/10.1046/j.1365-2621.1999.00256.x

Brishti, F. H., Chay, S. Y., Muhammad, K., Ismail-Fitry, M. R., Zarei, M., Karthikeyan, S., & Saari, N. (2020). Effects of drying techniques on the physicochemical, functional, thermal, structural and rheological properties of mung bean (Vigna radiata) protein isolate powder. *Food Research International*, *138*(PB), 109783. https://doi.org/10.1016/j.foodres.2020.109783

Bühler, J. M., Dekkers, B. L., Bruins, M. E., & Goot, A. J. Van Der. (2020). *Modifying Faba Bean Protein Concentrate Using Dry Heat to Increase Water Holding Capacity*. 1–16. https://doi.org/10.3390/foods9081077

Cheftel, J. C., Kitagawa, M., & Queguiner, C. (1992). New Protein Texturization Processes by Extrusion Cooking at High Moisture Levels. *Food Reviews International*, *8*(2), 235–275. https://doi.org/10.1080/87559129209540940

Cornet, S. H. V., Snel, S. J. E., Schreuders, F. K. G., Van der Sman, R. G. M., Beyrer, M., & Van der Goot, A. J. (2021). Thermo-mechanical processing of plant proteins using shear cell and high-moisture extrusion cooking. *Critical Reviews in Food Science and Nutrition*, *0*(0), 1–18. https://doi.org/10.1080/10408398.2020.1864618

Emin, M. A., Quevedo, M., Wilhelm, M., & Karbstein, H. P. (2017). Analysis of the reaction behavior of highly concentrated plant proteins in extrusion-like conditions. *Innovative Food Science and Emerging Technologies*, *44*, 15–20. https://doi.org/10.1016/j.ifset.2017.09.013

Ewoldt, R. H., Winter, P., Maxey, J., & McKinley, G. H. (2010). Large amplitude oscillatory shear of pseudoplastic and elastoviscoplastic materials. *Rheologica Acta*, *49*(2), 191–212. https://doi.org/10.1007/s00397-009-0403-7

Fang, Y., Zhang, B., & Wei, Y. (2014). Effects of the specific mechanical energy on the physicochemical properties of texturized soy protein during high-moisture extrusion cooking. *Journal of Food Engineering*, *121*(1), 32–38. https://doi.org/10.1016/j.jfoodeng.2013.08.002

Ishangulyyev, R., Kim, S., & Lee, S. H. (2019). Understanding food loss and waste-why are we losing and wasting food? *Foods*, *8*(8). https://doi.org/10.3390/foods8080297

ISOBE, S., & NOGUCHI, A. (1987). High moisture extrusion with twin screw extruder - Fate of soy protein during the repetition of extrusion cooking. In *Nippon Shokuhin Kogyo Gakkaishi* (Vol. 34, Issue 7, pp. 456–461). https://doi.org/10.3136/nskkk1962.34.7_456

Liu, K., & Hsieh, F. H. (2008). Protein-protein interactions during high-moisture extrusion for fibrous meat analogues and comparison of protein solubility methods using different solvent systems. *Journal of Agricultural and Food Chemistry*, *56*(8), 2681–2687. https://doi.org/10.1021/jf073343q

Meulleneti, J. (1998). Relationship between sensory. *Journal of Sensory Studies*, *13*(1998), 77–93.

Noguchi, A. (1989). Extrusion Cooking of High-Moisture Protein foods. In C. Mercier, P. Linko, & J. M. Harper (Eds.), *Extrusion Cooking* (1st ed., pp. 343–370). American Association of Cereal Chemists. https://wur.on.worldcat.org/oclc/19418265

O'Kane, F. E., Happe, R. P., Vereijken, J. M., Gruppen, H., & Van Boekel, M. A. J. S. (2004). Heat-induced gelation of pea legumin: Comparison with soybean glycinin. *Journal of Agricultural and Food Chemistry*, *52*(16), 5071–5078. https://doi.org/10.1021/jf035215h

Osen, R., Toelstede, S., Eisner, P., & Schweiggert-Weisz, U. (2015a). Effect of high moisture extrusion cooking on protein-protein interactions of pea (Pisum sativum L.) protein isolates. *International Journal of Food Science and Technology*, *50*(6), 1390–1396. https://doi.org/10.1111/ijfs.12783

Osen, R., Toelstede, S., Eisner, P., & Schweiggert-Weisz, U. (2015b). Effect of high moisture extrusion cooking on protein-protein interactions of pea (Pisum sativum L.) protein isolates. *International Journal of Food Science and Technology*, *50*(6), 1390–1396. https://doi.org/10.1111/ijfs.12783

Osen, R., Toelstede, S., Wild, F., Eisner, P., & Schweiggert-Weisz, U. (2014). High moisture extrusion cooking of pea protein isolates: Raw material characteristics, extruder responses, and texture properties. *Journal of Food Engineering*, *127*, 67–74. https://doi.org/10.1016/j.jfoodeng.2013.11.023

Peters, J. P. C. M., Luyten, H., Alting, A. C., Boom, R. M., & Van der Goot, A. J. (2015). Effect of crosslink density on the water-binding capacity of whey protein microparticles. *Food Hydrocolloids*, *44*, 277–284. https://doi.org/10.1016/j.foodhyd.2014.09.030

Pietsch, V. L., Bühler, J. M., Karbstein, H. P., & Emin, M. A. (2019). High moisture extrusion of soy protein concentrate: Influence of thermomechanical treatment on protein-protein interactions and rheological properties. *Journal of Food Engineering*, *251*(August 2018), 11–18. https://doi.org/10.1016/j.jfoodeng.2019.01.001

Pommet, M., Redl, A., Helene, M., Morel, M. H., Domenek, S., & Guilbert, S. (2003). Thermoplastic processing of protein-based bioplastics : chemical engineering aspects of mixing, extrusion and hot molding Thermoplastic processing of protein-based bioplastics : chemical engineering aspects of mixing, extru-sion and hot molding. *Macromolecular Symposia*, *197*. https://doi.org/10.1002/masy.200350719ï

Schreuders, F. K. G., Dekkers, B. L., Bodnár, I., Erni, P., Boom, R. M., & van der Goot, A. J. (2019). Comparing structuring potential of pea and soy protein with gluten for meat analogue preparation. *Journal of Food Engineering*, *261*(May), 32–39. https://doi.org/10.1016/j.jfoodeng.2019.04.022

Schreuders, F. K. G., Sagis, L. M. C., Bodnár, I., Erni, P., Boom, R. M., & van der Goot, A. J. (2021a). Mapping the texture of plant protein blends for meat analogues. *Food Hydrocolloids*, *118*(February). https://doi.org/10.1016/j.foodhyd.2021.106753

Schreuders, F. K. G., Sagis, L. M. C., Bodnár, I., Erni, P., Boom, R. M., & van der Goot, A. J. (2021b). Small and large oscillatory shear properties of concentrated proteins. *Food Hydrocolloids*, *110*. https://doi.org/10.1016/j.foodhyd.2020.106172

Snel, S. J. E., Bellwald, Y., van der Goot, A. J., & Beyrer, M. (2022). Novel rotating die coupled to a twin-screw extruder as a new route to produce meat analogues with soy, pea and gluten. *Innovative Food Science & Emerging Technologies*, *81*(August), 103152. https://doi.org/10.1016/j.ifset.2022.103152

Tolstoguzov, V. B. (1993). *Thermoplastic Extrusion-the Mechanism of the Formation of Extrudate Structure and Properties I.*

van der Sman, R. G. M., & van der Goot, A. J. (2023). Hypotheses concerning structuring of extruded meat analogs. In *Current Research in Food Science* (Vol. 6). Elsevier B.V. https://doi.org/10.1016/j.crfs.2023.100510

Wittek, P., Ellwanger, F., Karbstein, H. P., & Emin, M. A. (2021). Morphology development and flow characteristics during high moisture extrusion of a plant-based meat analogue. *Foods*, *10*(8). https://doi.org/10.3390/foods10081753

3

Chapter 4

Type of pectin determines structuring potential of soy proteins into meat analogue applications

Abstract

The addition of pectin to soy protein isolate (SPI) is a route to create fibrous products using shear cell technology. In this study, we investigated pectins derived from soybean, sugar beets, and citrus (two variants) that vary in sugar composition, degree of methylation and acetylation. The objective was to examine how these different pectins impact the functional properties of the SPI dispersions. The SPI-pectin blends were shear structured and their visual appearance, microstructural, rheological, and mechanical properties were analyzed. The addition of pectins from citrus (the highly methyl-esterified form) and soybean resulted in fibrous products when mixed with SPI. The addition of the low methyl-esterified pectin derived from citrus led to less pronounced fibrous product, and pectin from sugar beet did not lead to fibrous products. To explain the effect, several properties of the blends and products were tested. It was found that the fibrous products contained more air (i.e. higher void fraction) than products that were not fibrous, and that air bubbles were deformed in the shear direction. The rheological measurements of the blends revealed that the pectins lowered the yield and flow point of SPI, and the flow transition index. The blend with the highest elasticity after heating also had the highest deformation of air bubbles. Based on all results it was concluded that pectin influenced the structure formation in two ways: 1) affecting the ability to facilitate air inclusion and 2) influencing the storage modulus and elasticity of the matrix.

4.1   Introduction

The reduction of animal products in our diet would help to lower the environmental impact of food production (González et al., 2011). To ease the transition, animal products, such as meat, could be replaced by plant-based products, such as meat analogues (Smetana et al., 2023). Meat analogues are often made from soy protein concentrate or isolate (Kyriakopoulou et al., 2021). Thermo-mechanical processing is needed to structure soy protein into meat analogues (S. H. V. Cornet, Snel, Schreuders, et al., 2021).

Shear cell technology is a technique that applies defined shear deformation at elevated temperatures to structure plant proteins, such as soy, into fibrous products (Grabowska et al., 2014). It has been shown before that the addition of a dispersed phase to soy protein isolate (SPI) induces fibrous structure formation (Dekkers et al., 2016). High methyl-esterified citrus pectin was previously tested for this purpose in different concentrations and it was found that 2.2% pectin addition led to products with the highest anisotropy index and visual fibrous structure (Dekkers et al., 2016). Cellulose was also tested in combination with SPI but did not result in fibrous products (Schreuders et al., 2022). Dekkers et al. (2016) hypothesized that the pectin droplets form a deformed phase in the SPI matrix and that this creates the fibrous structure. They further hypothesized that this mechanism takes place when texturizing soy protein concentrate as well, since soybean pectin is naturally present (Dekkers et al., 2016). To allow deformation of the dispersed phase, a certain viscosity ratio between the dispersed and continuous phase is required (Tolstoguzov et al., 1974). Apart from forming an elongated dispersed phase, pectin may hold air in the protein blends, as has been shown for maltodextrin in calcium caseinate (Z. Wang, Dekkers, et al., 2019). It was shown that maltodextrin assembles around the air bubbles in the sample, stabilizing the foam, which was thought to result in fibrous products (Z. Wang, Dekkers, et al., 2019). This finding explains our interest to further explore pectins in more detail because certain pectins have been shown to improve the foam stability of napin, a protein extracted from rape meal (Schmidt et al., 2010). The importance of air in fibrous products is further illustrated by a recent invention of a novel technology to include gas during high moisture extrusion (Weinberger et al., 2021).

Pectin is a polysaccharide consisting of a linear to branched region, composed of mainly homogalacturonan and rhamnogalacturonan I and II respectively (Voragen et al., 2009). Depending on the degree of methyl-esterification, pectins can be classified as either high methyl-esterified or low methyl-esterified pectin (Einhorn-Stoll et al., 2021). Pectins differ not only in their degree of methyl esterification, but also in the linear and branched ratio, the degree of acetylation, molecular weight, and size distribution (Einhorn-Stoll et al., 2021). So far, high methyl-esterified citrus pectin induced fibrous structure formation in both SPI and pea protein isolate (Schreuders et al., 2022). Low methyl-esterified pectin did not result in fibrous structures in combination with pea protein isolate and gluten (Taghian Dinani et al., 2023). Apart from their application in fibrous products, the interactions between SPI and pectins have been studied for their application as coacervates (Lam et al., 2008; Mendanha

et al., 2009). The interaction with pectin was described to improve the functional properties of proteins, such as interfacial properties in foams and emulsions (Einhorn-Stoll et al., 2021). SPI was able to form coacervates with both high methyl-esterified and low methyl-esterified citrus pectin at pH conditions around the isoelectric point of SPI (Lam et al., 2008; Mendanha et al., 2009). Other pectins with a variation of degree of methyl-esterification were tested for interactions with pea protein and less coacervates were formed for low methyl-esterified pectins such as sugarbeet pectin and low methyl-esterified citrus pectin (Warnakulasuriya et al., 2018). It can therefore be concluded that pectins can help to improve the functional properties of protein dispersions by forming coacervates, but the exact effect depends both on the type of pectin and protein used.

In this study, four different pectins were compared on their ability to induce fibrous structure formation in SPI blends structured with the shear cell. The selected pectins were high- and low methyl-esterified citrus pectin, soybean pectin, and sugarbeet pectin. The pectins were compared on their chemical composition, foaming capacity, solubility, and water-holding capacity. The visual appearance, microstructure, tensile strength, and air inclusion of the SPI-pectin fibrous products were evaluated. Furthermore, the rheological properties of the SPI-pectin blends were analyzed. We hypothesize that the ability of pectin to induce fibrous structures in SPI fibrous products depends on their ability to hold air in the fibrous product, as well as on the rheological properties of the blend.

4.2   Methods and Materials

4.2.1   Materials
Soy protein isolate (SPI, SUPRO 500E A® 8) was obtained from Solae (St. Louis, MO, USA). SPI contained at least 90 g protein per 100 g dry matter (N x 6.25, indicated by supplier), and had a dry matter content of 93.2 ± 0.1 g/100 g (n=3). Citrus pectins in low and high methyl-esterified forms (HMC and LMC) were obtained from CP Kelco (Lille Skensved, Denmark). Pectin from soybean was obtained from Fuji Oil (Osaka, Japan) (SYB). Pectin from sugarbeet was obtained from CP Kelco (Lille Skensved, Denmark) (SGB). The dry matter content of HMC, LMC, SYB, and SGB was respectively 89.3 ± 0.2, 88.4 ± 0.1, 87.9 ± 0.1, and 88.4 ± 0.1 g/100 g. Sodium chloride (NaCl) and Rhodamine B were obtained from Sigma Aldrich (Zwijndrecht, the Netherlands).

4.2.2   Sugar composition
The sugar composition of the pectins was measured by gas chromatography (GC) after pre-treatment with 72% H_2SO_4 (1h, 30 °C) followed by acid hydrolysis with 1M H_2SO_4 and derivatization of neutral sugars to alditol acetates (Jermendi et al., 2022). Galacturonic acid conent was determined by the automated colorimetric m-hydroxydiphenyl method (Jermendi et al., 2022). Methyl ester content and level of acetylation was measured after saponification using high-performance liquid chromatography (HPLC) (Voragen et al.,

1986). All measurements were performed in duplicate and the standard deviation was within a 2% window.

4.2.3   Particle size distribution

The particle size distribution of the pectins was measured with a Mastersizer 3000 equipped with a Scirocco 2000 dry dispersion unit (Worcestershire, UK) and a pressure of 2 bar. Particle size was measured in duplicate and the $d_{4,3}$ was determined, assuming that the particles are spherical and using the Fraunhofer method.

4.2.4   Solubility and water holding capacity

Solubility and water holding capacity (WHC) of the pectins was measured in triplicate with a method reported by (Bühler et al., 2020) with some minor adaptations. A dispersion of 0.0125 g/g pectin in demineralized water was prepared and shaken overnight at 300 rpm at room temperature. Subsequently, the dispersions were centrifuged at 10,000 g at 21 °C for 20 min. The weight of the pellet was recorded and the pellet was dried at 100 °C for 15 h. The solubility and WHC were calculated as follows:

$$Solubility = \frac{M_{drypowder} - M_{drypellet}}{M_{drypowder}} \qquad 4.1$$

$$WHC = \frac{M_{wetpellet} - M_{drypellet}}{M_{drypowder}} \qquad 4.2$$

in which $M_{drypowder}$ is the overall weight of the isolate after correcting for the initial dry weight of the powder, and $M_{wetpellet}$ and $M_{drypellet}$ are the weights of the pellet before and after drying.

4.2.5   Foaming capacity

The ability to hold air during the production of the fibrous product is hypothesized to be an important property for the formation of a fibrous structure (Z. Wang, Tian, et al., 2019). Therefore, foaming capacity (FC) experiments were performed on SPI and SPI + pectin dispersions based on an overrun method (Lie-Piang et al., 2023). The SPI was dispersed in demineralized water at 0.1 g/kg (corrected for dry matter content). In the case of SPI + pectins, SPI was dispersed at 0.95 g/kg and the pectins at 0.05 g/kg, to reach similar SPI:pectin ratios as in the fibrous products. The dispersions were mixed with a magnetic stirrer at 500 rpm for 30 min. Then, 10 mL of the dispersion was placed in a plastic tube with a diameter of 33.5 mm. Next, a froth (Aerolatte, United Kingdom) attached to a Vortex was used to implement air in the dispersion at a speed of 2000 rpm for 2 min. A picture was taken of the foam and the foam height was analyzed with ImageJ (version 1.54d). The foaming capacity was calculated as:

$$FC = \frac{V_{in} + V_{foam}}{V_{in}} * 100 \qquad 4.3$$

in which V_{in} and V_{foam} are the volume of the initial dispersion and the volume of the foam,

respectively. The V_{foam} was calculated as:

$$V_{foam} = \pi r^2 h \tag{4.4}$$

in which r is the radius of the tube (16.75 mm) and h was the height of the foam. To compare the foaming capacity of the SPI-pectin blends with SPI, the foaming capacity of SPI was subtracted from the foaming capacity of SPI, resulting in a parameter for additional FC.

4.2.6   Preparation of SPI-pectin blends

SPI-pectin blends were prepared for the measurements in the shear cell and closed cavity rheometer. SPI blends were prepared with a total dry matter content of 45 g/100 g, which consisted of 44 g/100 g SPI, and 1 g/100 g NaCl. For SPI-pectin blends, SPI content was adjusted to 41.8 g/100 g and pectin content was 2.2 g/100 g. SPI blends with a dry matter content of 41.8 g/100 g without pectin added were prepared as a control. Blends were prepared by first dissolving NaCl in demineralized water and subsequently, the SPI was added. The blend was manually stirred with a spatula for 3 min. A hydration step was included at room temperature for 30 min. After hydration, pectin was added and the blend was mixed with a spatula for 3 min.

4.2.7   Shear structuring

Fibrous products were prepared using the in-house developed shear cell (SC, Wageningen University, the Netherlands). The SC consists of an upper static cone and a lower rotating cone, which are both thermo-regulated with circulating oil. The cones are sealed with pressurized air at a pressure of 6.5 bar. %The rotational speed and temperature were controlled with Haake Polylab drive (Haake Polylab QC drive, Germany).

The SPI and SPI-pectin blends were transferred to the pre-heated SC and processed at 140 °C with a rotational speed 19.5 or 39 s^{-1} for 15 min. Then, the blends were cooled down to 50 °C at 0 s^{-1} for 10 min. The obtained fibrous products were transferred into an airtight bag and left to cool at room temperature for 1 h. Approximately 1 x 5 cm of the fibrous products was frozen (-18 °C) before further analyses with the confocal laser scanning microscopy (CLSM) and X-ray microtomography (XRT). These cuts were taken from the outer part of the fibrous product. The remaining fibrous product was used for visual analysis and tensile tests on the day of preparation. Fibrous products produced at 39 s^{-1} were prepared in triplicate, and at 19.5 s^{-1} in duplicate. The inner structure of the fibrous products was observed by folding the fibrous product parallel to the direction of the shear.

4.2.8   Tensile test

Tensile tests were performed with a TA.XT texture analyzer (Stable Micro Systems Ltd., Surrey, United Kingdom) using a static load cell of 5 kg to analyze the tensile strength of the fibrous products both parallel and perpendicular to the shear direction. A bowtie-shaped mold with a length of 53 mm, exterior width of 10 mm, and interior width of 3.4 mm was

used to cut samples in the outer ring of the fibrous product in both directions, as described by Schreuders et al. (2022) Each fibrous product was produced in triplicate or duplicate with the shear cell, and of each repetition, triplicates were sampled in both parallel and perpendicular directions. The width and thickness of the sample were recorded. Samples were placed between the upper and lower clamps of the texture analyzer. The sample height used for the analysis was 15.5 mm. The tensile test was performed in uniaxial mode with a displacement of 1 mm/s until the fracture point. Young's modulus was derived from the initial, linear part of the stress-strain curve. The tensile strain and stress were calculated with equation 4.5 and 4.6 and the fracture point was defined as the point where the stress was maximum and the corresponding strain.

$$\gamma_h = ln\frac{h\left(t\right)}{h_0} \qquad\qquad 4.5$$

$$\sigma\left(t\right) = \frac{F\left(t\right)}{A\left(t\right)} \qquad\qquad 4.6$$

in which h_0 is the initial height of the sample, $h(t)$ is the height of the sample at time t, $F(t)$ is the force at time t, and $A(t)$ the surface area of the sample at time t, calculated as:

$$A\left(t\right) = \frac{h_0}{h\left(t\right)} * A_0 \qquad\qquad 4.7$$

in which A_0 is the initial surface area of the sample.

The anisotropy index of the strain and stress in parallel and perpendicular directions was calculated as:

$$AI_\gamma = \frac{\gamma_\parallel}{\gamma_\perp} \qquad\qquad 4.8$$

$$AI_\sigma = \frac{\sigma_\parallel}{\sigma_\perp} \qquad\qquad 4.9$$

4.2.9   CLSM

Microstructures of the samples were visualized with confocal laser scanning microscopy (CLSM). Frozen shear cell samples were cut into specimen of approximately 5 x 10 x 10 mm. Subsequently, slices with a thickness of 60 μmwere prepared at -16 °C with a cryomicrotome (Micron CR50-H, ADAMAS-Instruments Corp., Rhenen, The Netherlands). Next, the specimen was colored with a 2 μg/mL Rhodamine B solution. The excess solution was removed after at least 1 h. The speciment were analyzed with a CLSM type 510 (Carl Zeiss AG, Oberkochen, Germany) using a 543 nm HeNe laser and a 405 nm Blue/Violet diode laser. An EC Plan-Neofluar 20x/0.5 lens was attached. Images were analyzed with ZEN v3.4, blue edition (Carl Zeiss AG).

4.2.10 XRT

The void fractions and the elongation of air bubbles in the products were analyzed with a GE Phoenix X-ray microtomography (v|tome|z, General Electric, Wunstorf, Germany). Defrosted shear cell samples were cut into specimen with a dimension of 3 x 4 x 20 mm and placed in an eppendorf tube. The tube was placed at a distance of 28.55 mm from the X-ray source, resulting in a spatial resolution of 7 μm. X-rays were produced with a voltage of 80 kV and a current of 90 μA. Images were recorded with a GE DXR detector array (2024 x 2024 pixels, pixel size =200 μm). The detector was placed at a distance of 815 mm from the X-ray source. A full scan consisting of 1500 projections over an angle of 360 °, step ratio of 0.24 ° was performed, excluding the first image. Three images over 250 ms were averaged into one projection and the 3D structure was calculated using GE reconstruction software (Wunstorf, Germany). The void fraction, the length of deformed air bubbles in the shear direction, and the width of the bubble in the velocity gradient direction were obtained using the Avizo imaging software (version 9.X.0). The air void fraction was calculated as the volume of air divided by the total volume. The deformation of the air bubbles was calculated as the length divided by the width of the air bubbles. All the bubbles in the sample were analyzed, and the median of bubble deformation in one sample was obtained. Furthermore, air bubbles were divided into four volume classes: <0.001, 0.001-0.01. 0.01-0.1, and >0.1 mm^3, and the number of air bubbles in each volume class was summed. The analysis was performed in duplicate and averaged.

4.2.11 Rheological properties

Strain sweeps were performed with a CCR (RPA elite, TA instruments, New Castle, Delaware, USA). The geometry in the CCR has a radius of 2.25 mm, a maximum height of 4 mm, and a biconical opening with an angle of 3.35 ° to ensure homogeneous transmission of the shear stress applied. The top and bottom cones have grooves to prevent slip. The upper cone remains stationary while the lower cone oscillates. Approximately 5 g of the SPI or SPI-pectin blends were placed between two plastic films in the pre-heated CCR. The cavity was then sealed with a pressure of 4 bar to prevent moisture evaporation. Samples were then heated to 30 or 140 °C without shear for 2 min. Three measuring conditions were used: 30 °C, 140 °C, or heated to 140 °C and cooled to 30 °C. The latter imitates the temperature during the shear cell process. An amplitude strain sweep was performed from 0.1 to 1000% at 1hz. The yield stress and strain at the end of the linear viscoelastic (LVE) regime were defined as the point where *G'* differs more than 5% from its value in the LVE regime. The flow stress and strain were defined at the crossover point, which was identified as the last point before *G'* (storage modulus) was smaller than the G» (loss modulus). Furthermore, the flow transition index was calculated as the stress at flow point (σ_{co}) divided by the stress at yield point (σ_y) (Nair & Roy Choudhury, 2020).

4.2.12 Lissajous plots

The data obtained with the strain amplitude sweeps were further analyzed with the MITlaos

software (version 2.1 beta, freeware distributed from MITlaos@mit.edu). With this software, Lissajous plots were made, comparing the response of the material to the oscillatory strain for both the elastic and viscous stress. Furthermore, the dissipation ratio was calculated (Schreuders et al., 2021a). The energy dissipated per unit volume in a single cycle as a function of the first-order viscous Fourier coefficient (G_1'') was calculated as:

$$E_d = G_1'' \gamma_0^2 \qquad\qquad 4.10$$

in which E_d is the energy dissipated and γ_0 the strain amplitude. For a perfect plastic material the energy dissipated is equal to:

$$E_d^{pp} = 4\gamma_0 \sigma_{max} \qquad\qquad 4.11$$

in which σ_{max} is the maximum stress. The ratio between the actual energy dissipated and the energy dissipated by a perfect plastic then gives the energy dissipation ratio ϕ (Ewoldt et al., 2010):

$$\phi = \frac{E_d}{E_d^{pp}} = \frac{\pi G_1'' \gamma_0}{4\sigma_{max}} \qquad\qquad 4.12$$

For a perfect plastic material, this ratio would be 1. An elastic material would have a dissipation ratio of 0, and a purely viscous material a ratio of 0.8.

4.2.13   Standardization of results
The relative contribution of pectin to SPI was illustrated by calculating a ratio for the parameters measured with the tensile test and strain sweeps. Each parameter for the different SPI-pectin samples was divided by the values obtained for the SPI sample at 45 g per 100 g, resulting in a relative change parameter (R). Thus, SPI samples had a value of 1. This allowed for easier comparison between the samples.

4.2.14   Statistical analysis
Statistical analysis was performed with R. First, normality was tested with a Shapiro-Wilk test ($\alpha = 0.05$). If the data were normally distributed, multiple comparison Tukey tests were done to indicate which treatments were significantly different from each other ($\alpha = 0.05$). If the data was not normally distributed, a Dunn's test was performed. All tests in this study were performed in triplicate unless indicated otherwise.

4.3   Results

4.3.1   Pectin chemical composition and properties
The chemical composition and functional properties of the pectins were determined and presented in Table 4.1. The sugar composition of HMC and LMC were similar. These pectins differed mainly in the degree of methyl esterification. The sugar composition of SYB and SGB

pectins differed from HMC and LMC. SYB had a lower galacturonic acid content compared to the other pectins. Since galacturonic acid is the main component of the pectin backbone, a lower content of galacturonic acid reflects a more branched structure for SYB pectin (Voragen et al., 2009). The branched structure is further confirmed with the higher arabinose, galactose, and xylose content of SYB, which are mainly found in the Rhamnogalacturonan I (Voragen et al., 2009). SGB also had a lower galacturonic acid content and higher side-chain sugar contents than HMC and LMC pectin. SYB pectin had the smallest mean particle size ($d_{4,3}$). SGB had a slightly larger particle size, followed by LMC and HMC. The difference between the particle size might reflect differences in drying technique (Brishti et al., 2020). All tested pectins had high solubility in water (Table 4.1). SYB was completely soluble. The solubility of HMC was slightly lower, followed by LMC, and lastly SGB pectin. SGB had the highest WHC, followed by LMC, HMC, and SYB pectin. To test the effect of pectin addition on the foaming capacity of SPI, pectins were added to SPI dispersions. All pectins improved the initial foaming capacity of SPI (50.9 ± 0.1 %, Table 4.1). SPI-LMC had significantly the highest FC, followed by SPI-HMC, SPI-SGB, and SPI-SYB.

In summary, HMC and LMC pectins differ in their degree of methyl esterification and foaming capacity. Both SGB and SYB are more branched than HMC and LMC pectins and were acetylated. SYB had the most branched structure, smallest particle size, highest solubility, and lowest WHC. SGB had the highest degree of acetylation and lowest solubility.

Table 4.1: Sugar composition, degree of methyl esterification and acetylation, particle size, solubility, water holding capacity (WHC), and foaming capacity (FC) of high methyl-esterified citrus pectin (HMC), low methyl-esterified citrus pectin (LMC), soy pectin (SYB), and sugarbeet pectin (SGB). Foaming capacity was measured in combination with SPI and represented as the additional FC, compared to the FC of 50.9 % ± 0.1 of SPI at 1 g/100 g. Particle size was measured in duplicate, and all other parameters were measured in triplicate. Values are averages ± standard deviation, with letters indicating significant groups.

	SGB	LMC	SYB	HMC
Sugars (mol %)				
Arabinose	7	0	25	4
Fucose	0	0	3	0
Galactose	11	4	41	6
Galacturonic acid	73	94	17	88
Glucose	0	1	4	1
Mannose	2	0	0	1
Rhamnose	5	1	4	1

	SGB	LMC	SYB	HMC
Xylose	1	0	5	0
Degree of methyl esterification	58	31	1	67
Degree of acetylation	15	0	5	0
Particle size $d_{4,3}$(µm)	80.4 ± 0.5 [bc]	97.9 ± 21 [ab]	49.5 ± 0.4 [c]	135 ± 4.2 [a]
Solubility (g/g)	0.83 ± 0.07 [b]	0.95 ± 0.02 [ab]	1.01 ± 0.00 [a]	0.98 ± 0.01 [ab]
WHC (g/g)	6.7 ± 0.4 [a]	4.6 ± 0.5 [b]	1.6 ± 0.2 [c]	4.3 ± 0.3 [b]
$FC_{SPI+pectin}$ – FC_{SPI} (%)	4.5 ± 0.9 [bc]	15 ± 3.8 [a]	3.4 ± 0.1 [bc]	7.9 ± 1.0 [b]

4.3.2 SPI-pectin fibrous products

4.3.2.1 Macro- and micro-structure

Fibrous products were prepared from SPI and the SPI-pectin blends using shear rates of 19.5 and 39 s^{-1}, temperatures of 140 °C, and a shear time of 15 min (Table 4.2). The visual appearance differed slightly between the fibrous products prepared at the two rotational speeds. At 39 s^{-1}, samples seemed more fibrous, except for SPI-HMC, which appeared slightly more fibrous at 19.5 s^{-1}. Previously, SPI-HMC samples had the highest visual fibrousness at 26 and 39 s^{-1}, while samples prepared with shear rates of 0 and 13 s^{-1} were less fibrous (Dekkers, Hamoen, et al., 2018b). Shear structuring of SPI alone did not result in clear fibrous structures, which was in line with previous findings (Dekkers et al., 2016). SPI-SGB had a weak anisotropic structure, which showed some fibrils at 19.5 s^{-1}. SPI-LMC had some fibrils, although not very pronounced. Both SPI-SYB and SPI-HMC did show a fibrous inner structure.

Table 4.2: Visual observations of soy protein isolate (SPI) and SPI-pectin fibrous products after folding in parallel direction of applied shear. SPI was replaced by pectin in 2.2 g/100 g. SPI with alower dry matter content was included as a control, where pectin was replaced with demineralized water. Apart from SPI or pectin, 1 g salt was added to 100 g samples. Dry matter content (DM) is included in the table as the DM of SPI and of the pectin. SGB = sugarbeet pectin, LMC = low methyl-esterified citrus pectin, SYB = soybean pectin, and HMC = high methyl-esterified citrus pectin. The picture of the SPI-SYB sample produced at 19.5 s^{-1} was color adjusted to correct for different light settings when taking the picture.

Sample	DM	Shear rate (s[-1])	
	(g/100 g)	19.5	39
SPI	44		

Sample	DM	Shear rate (s⁻¹)	
	(g/100 g)	19.5	39
SPI	41.8		
SPI-SGB	41.8 - 2.2		
SPI-LMC	41.8 - 2.2		
SPI-SYB	41.8 - 2.2		
SPI-HMC	41.8 - 2.2		

Table 4.3 shows the CLSM and XRT images of fibrous products produced at 39 s⁻¹. The microstructure of products consisting of SPI only was rather homogeneous, with some small non-protein regions, indicated as uncolored regions, of approximately 0.5-3 µm. SPI-SGB samples included some larger non-protein regions of 40-80 µm. Non-protein regions in SPI-LMC and SPI-SYB samples were elongated with a length of approximately 200 µmand width of approximately 20-70 µm, while SPI-HMC had long non-protein regions larger than 400 µmand width of 10-30 µm.

From the 3D images, it was observed that SPI and SPI-SGB samples included large fracture planes. This might be caused by the freezing of the samples. SPI-LMC, SPI-SYB, and SPI-HMC had more homogeneously distributed air bubbles. In SPI-LMC, SPI-SYB, and SPI-HMC the median air bubble width was between 30-50 µm, compared to 18 µmin SPI and SPI-SGB. For SPI-SYB and SPI-HMC these bubbles had a larger length than width, reflecting elongation.

Table 4.3: CLSM images and 3D images of the microstructure of SPI and SPI-pectin fibrous products. Protein was colored with Rhodamine B (2e-6 g L^{-1}) prior to CLSM analysis. SGB = sugarbeet pectin, LMC = low methyl-esterified citrus pectin, SYB = soybean pectin, and HMC = high methyl-esterified citrus pectin. The white bar in the CLSM picture represents a distance of 100 μm, scales in XRT images are 11 by 11 mm.

	SPI	SPI-LMC	SPI-SYB	SPI-HMC
CLSM				
Solid				
Air				
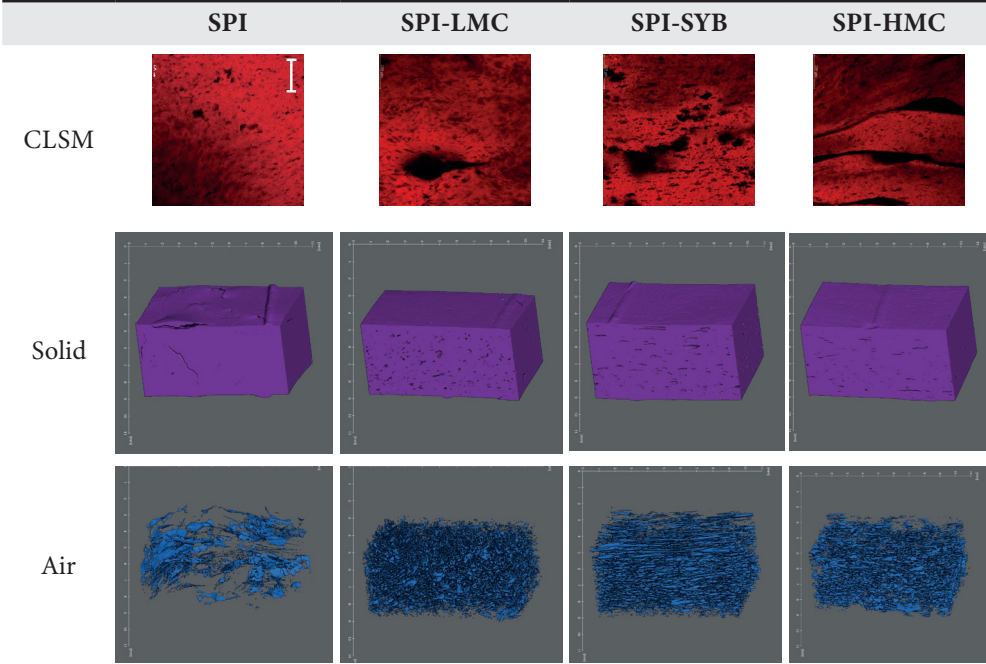
Figure 4.1 represents the results on void fraction and deformation of air bubbles. The colors represent the visual fibrousness of the samples, with red being not fibrous and dark blue being very fibrous. The SPI and SPI-SGB fibrous products had a more compact structure, with a low void fraction of 1% (Figure 4.1a). The SPI-LMC, SPI-SYB, and SPI-HMC fibrous products had a significantly larger void fraction. As these products were fibrous on a macro scale, we suspect a relation between higher air inclusion levels (thus larger void fractions) and the fibrousness of the product. However, the difference in foaming capacity of the SPI-pectin dispersions could not explain the increased void fraction (Table 4.1). Possibly, the foaming capacity in the fibrous products is different from an SPI-pectin dispersion at lower dry matter content and lower temperature, implying that other mechanisms such as stabilization of the air bubbles are of higher importance. Apart from the void fraction, the degree of deformation of the air bubbles was analyzed with XRT (Figure 4.1b). Most air bubbles had a small volume (0.001 mm³), but SPI-LMC, SPI-SYB, and SPI-HMC also had large numbers of bubbles with volumes of 0.01, and 0.1 mm³. At the volume classes of 0.001, 0.01, and 0.1, SPI-SYB and SPI-HMC had higher bubble deformation compared to SPI, SPI-SGB, and SPI-LMC. SPI-SYB samples had highly deformed large air bubbles of 0.1 and 1 mm³.

Even though SPI-LMC samples contained a higher void fraction and a higher number of air bubbles, the bubbles were not deformed in the direction of shear. It can thus be seen that the most fibrous products also had the highest degree of deformed air bubbles with different volumes.

(a)

(b)
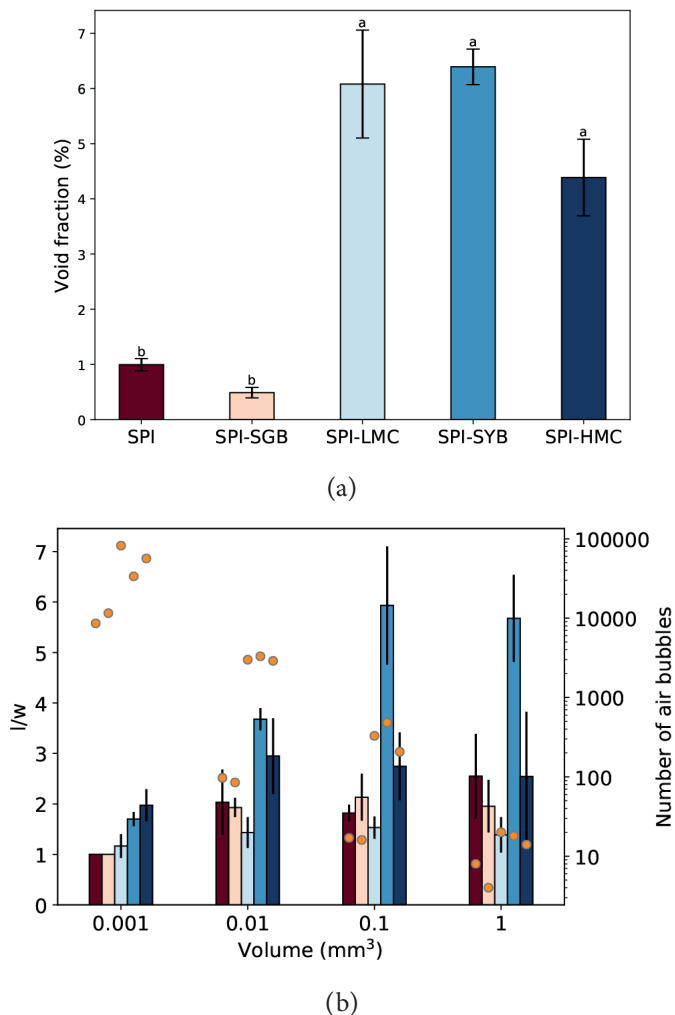
Figure 4.1: The void fraction (a), deformation of the air bubbles (b, primary y-axis, bars), and the number of air bubbles (b, secondary y-axis, orange circles) as a function of volume in soy protein isolate (SPI, dark red) and SPI-pectin fibrous products produced with shear structuring at 39 s^{-1}. Pectins added to SPI were sugarbeet pectin (SGB, pink), low methyl-esterified citrus pectin (LMC, light blue), soybean pectin (SYB, blue), and high methyl-esterified citrus pectin (HMC, dark blue). The colors of the samples represent fibrous structure, with dark red = not fibrous, and dark blue = very fibrous. Values are either the average (a) or median (b) with standard deviation (bar), and letters indicate significant groups (p ≤ 0.05, n=3).

4.3.2.2 Mechanical strength in extension

The mechanical strength of the fibrous products was tested with a tensile test. The obtained stress and strain at the fracture point when measured in parallel direction to the shear rate and the anisotropy indices of the stress and strain were plotted as a relative value compared to the SPI fibrous product (Figure 4.2). The measured values for the SPI product can be found in Appendix A.1, and the fracture stress and strain in perpendicular direction in Appendix A.2. The fracture point of SPI fibrous products in parallel and perpendicular directions was very similar, and thus their anisotropy index was around 1, meaning that a non-fibrous product was formed (Figure 4.2b, d). At a lower dry matter content of SPI, fracture stress and strain and Young's modulus were lower than expected. When SYB or HMC pectin was added, the fracture stress and strain lowered in the perpendicular direction (Appendix A.2), while fracture stress and strain in the parallel direction remained similar. This resulted in high anisotropy indices for these samples. The addition of LMC and SGB pectin resulted in lower fracture stress and strain in both parallel and perpendicular directions, leading to an anisotropy index only slightly larger than 1. The apparent relationship between anisotropy strain and anisotropy stress was due to a similar Young's modulus of all samples. This means that small deformation hardly differed between the samples, but the fracture point, or large deformation, differed depending on the pectin and parallel or perpendicular direction.

In summary, the fracture stress and strain parallel to the shear of SPI-SYB and SPI-HMC samples remained similar to SPI, resulting in a high mechanical anisotropy in these fibrous products. SPI-SGB and SPI-LMC did not have clear fibrous structures, mechanical anisotropy, or deformed air bubbles.

4

(a)

(b)

(c)

(d)
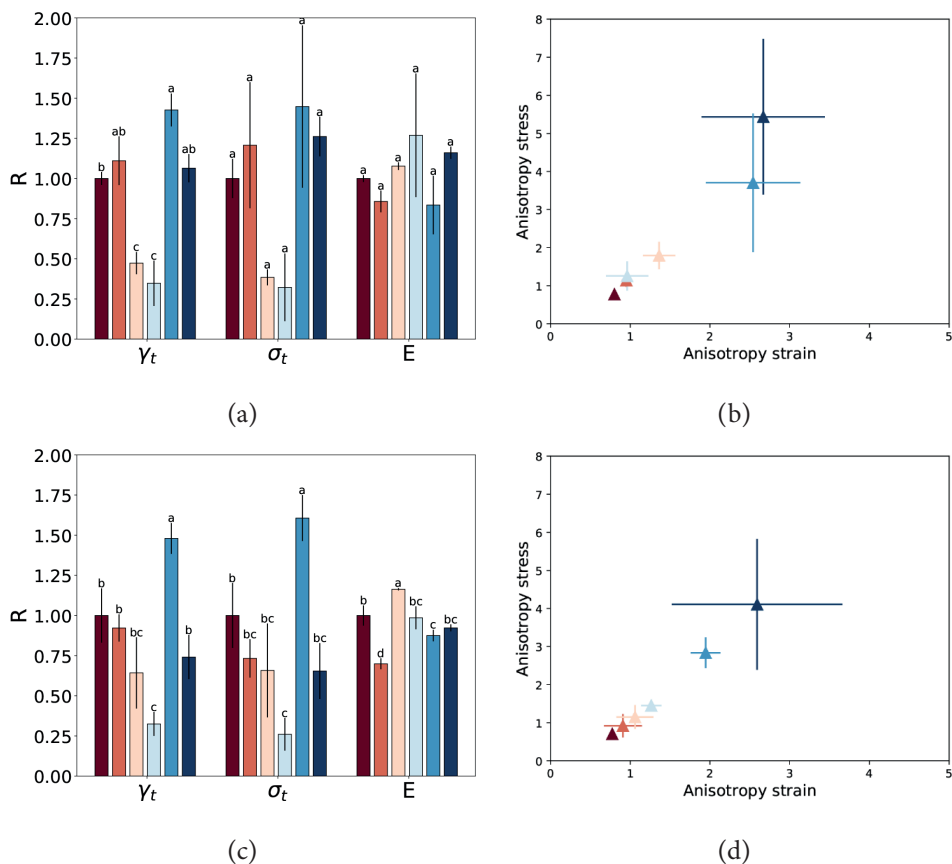
Figure 4.2: Relative change (R) in fracture strain (γ_t), fracture stress (σ_t) and youngs modulus (E) when pectin was added to a soy protein isolate (SPI) fibrous product measured in parallel direction to the shear stress (a, c) and the anisotropy stress versus anisotropy strain (b, d) of SPI fibrous products produced with shear structuring at 19.5 s^{-1} (a,b) and 39 s^{-1} (c,d). The γ_t, σ_t, and E of the SPI sample at 45% DM were taken as 1 (dark purple). Samples were made from SPI at 45% DM (dark red), SPI at 42.8 % (orange), SPI-SGB (sugarbeet pectin, pink), SPI-LMC (low methyl-esterified citrus pectin, light blue), SPI-SYB (soybean pectin, blue), and SPI-HMC (high methyl-esterified citrus pectin, dark blue). The colors of the samples represent fibrous structure, with dark red = not fibrous, and dark blue = very fibrous. Values are averages with standard deviation (bars), letters indicate significant groups (p ≤ 0.05), n=2 (a,b), and n=3 (c,d).

4.3.3   Rheological properties SPI-pectin blends

Strain sweeps of SPI and SPI-pectin blends were performed at 30 °C, 140 °C, and after heating to 140 °C followed by cooling to 30 °C (Appendix A.4). From the strain sweeps, the yield stress and strain at the end of the LVE regime, and the flow stress and strain at the cross-over point were determined and compared to SPI (Figure 4.3). The measured values for SPI can be found in Appendix A.1. Since the strain sweeps performed at 140 °C were too close to the torque limits of the measuring device, their values were not considered.
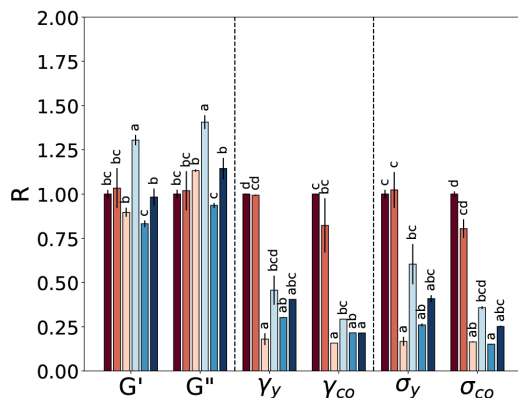
(a)
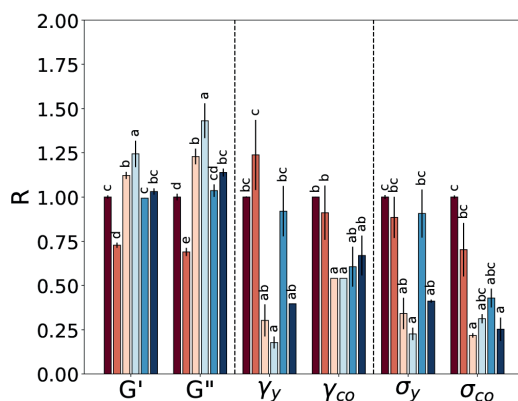
(b)

Figure 4.3: Relative change (R) in storage (G') and loss (G″) moduli, yield strain and stress (γ_{co} and σ_{co}), and flow strain and stress (γ_y and σ_y) derived from a strain sweep performed at 30 °C (a) and after heating to 140 °C and cooling to 30 °C(b). The relative change was calculated compared to soy protein isolate (SPI) at 45% dm, which was taken as 1 (dark red). Compared samples were SPI at 42.8% DM (orange), SPI-SGB (sugarbeet pectin, pink), SPI-LMC (low methyl-esterified citrus pectin, light blue), SPI-SYB (soybean pectin, blue), and SPI-HMC (high methyl-esterified citrus pectin, dark blue). The colors of the samples represent fibrous structure, with dark red = not fibrous, and dark blue = very fibrous. Values are averages with standard deviation (bars), and letters indicate significant groups (p ≤0.05, n=3).
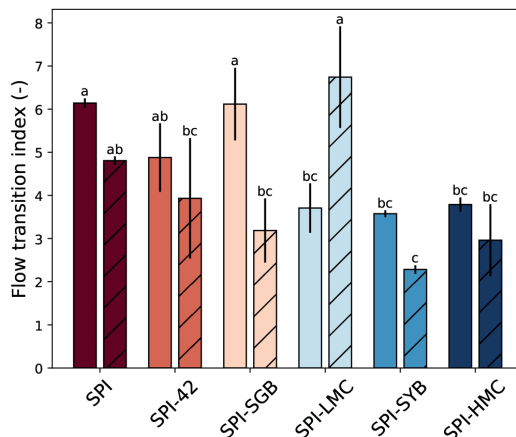
Figure 4.4: Flow transition index (σ_{co}/σ_y) of the SPI-pectin samples derived from a strain sweep performed at 30 °C (no stripes) and after heating to 140 °C and cooling to 30 °C (diagonal stripes). Values are averaged with standard deviation (bars) and significantly different groups across all samples are indicated with letters (n=3, α = 0.05). SPI = soy protein isolate, SGB = sugarbeet pectin, LMC = low methyl-esterified citrus pectin, SYB = soybean pectin, and HMC = high methyl-esterified citrus pectin.

The *G'* and *G''* upon pectin addition were affected both at 30 °C and after heating to 140 °C and cooling to 30 °C, with the highest *G'* and *G''* for SPI-LMC samples. The addition of pectins to SPI decreased both the yield and flow stress and strain when measured at 30 °C and after heating to 140 °C and cooling to 30 °C. After the heating and cooling step, the yield stress and strain of SPI-SYB samples were most similar to SPI samples. The transition of the material from the yield point to the flow point can be further analyzed by calculating the flow transition index (σ_{co}/σ_y, Figure 4.4). A flow transition index approaching 1 reflects brittle fracturing or fast breakdown of the material (Nair & Roy Choudhury, 2020). All samples had values higher than 1, thus a more ductile degradation or slow breakdown of the material. At 30 °C the flow transition index of SPI-LMC, SPI-SYB, and SPI-HMC was significantly lower than SPI, reflecting the degradation of the material becoming less ductile and more brittle by the addition of pectin. After heating to 140 °C and cooling to 30 °C, values were lower compared to 30 °C, indicating that the material had more brittle fracturing. Interestingly, SPI-LMC showed an opposite trend, with a significantly increased flow transition index after heating. SPI-SGB, SPI-SYB, and SPI-HMC had lower transition indices than SPI, although this effect was only significant for SPI-SYB.

The energy dissipated per cycle at different strain amplitudes (E_d) was calculated as the area between the curves of Lissajous plots (Equation 10, Appendix). From these plots, the energy dissipation ratios (ϕ) were calculated and plotted (Equation 4.12, Figure 4.5). SPI samples remained elastic until a higher strain amplitude compared to the SPI-pectin samples at 30 °C. The SPI-SGB blend showed the most viscous behavior from a strain amplitude of 5.44

% compared to the other SPI-pectin blends. After heating to 140 °C and cooling to 30 °C, the energy dissipation ratio of SPI-SGB and SPI-LMC samples was higher compared to SPI, especially upon higher strain amplitudes, indicating less elastic behavior. The SPI-SYB samples resembled SPI the most, with elastic behavior at higher strain amplitudes.
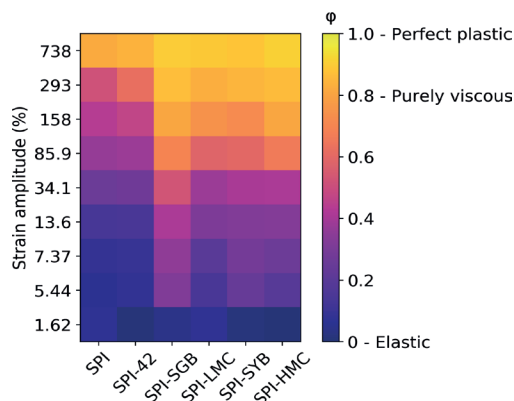
(a)
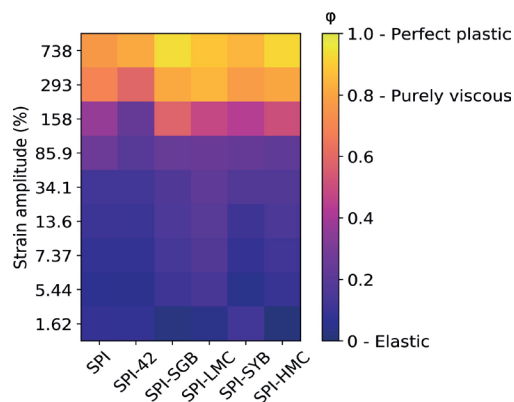
(b)

Figure 4.5: Heat map of the dissipation ratio ϕ at different strain amplitudes for the soy protein isolate (SPI) and pectin blends measured at 30 °C (a), and heated to 140 °C followed by cooling to 30 °C (b). SPI-42 reflects the SPI sample with a dry matter content of 41.8, SGB = sugarbeet pectin, LMC = low methyl-esterified citrus pectin, SYB = soybean pectin, HMC = high methyl-esterified citrus pectin.

4.4   Discussion

Four different pectins were compared in their ability to induce fibrous structure formation in SPI fibrous products produced with a shear cell at two different rotational speeds. Different structures were obtained for each pectin, with an increase in fibrous structure from SPI < SPI-SGB < SPI-LMC < SPI-SYB < SPI-HMC. A similar order was obtained when analyzing the anisotropy indices from tensile tests at fracture point. Furthermore, positive correlations were found between air bubble deformation in the samples, visual fibrousness, and mechanical anisotropy.

The addition of SYB and HMC pectin to SPI induced a fibrous structure. The ability of HMC to induce a fibrous structure has been found for SPI before (Dekkers et al., 2016). SPC, naturally having soybean pectin in its composition, also obtains a fibrous structure after shear structuring, while SPI alone does not (Grabowska et al., 2016). The difference in structure formation between SPI and SPC could thus be linked to SYB. Dekkers et al. (2016) proposed the formation of a dispersed pectin phase which elongated within a continuous SPI phase upon shear. The CLSM images showed larger non-protein areas upon pectin addition. For HMC, these non-protein areas were stretched. These stretched areas could be either elongated pectins or elongated air bubbles in the sample. From XRT, it became indeed clear that the air bubbles were in a similar size range as the observed non-protein areas in CLSM.

The anisotropy indices obtained at fracture point of a tensile test were in line with the visual fibrousness of the samples, where SPI-SYB and SPI-HMC had the highest mechanical anisotropy. The anisotropy arose from a similar parallel fracture stress and strain of these samples compared to SPI, while the perpendicular fracture stress and strain was lower than the perpendicular fracture stress and strain of SPI only. For SPI-SGB and SPI-LMC, strain and stress decreased in both parallel and perpendicular directions. Remarkably, the impact of SGB and LMC pectin on fracture stress and strain was larger than the impact of water. This could indicate that pectin is hindering SPI to form a stronger network by forming a second dispersed phase. The volume fraction of this phase is small (0.05), but pectin could take up more water than SPI, resulting in a relatively larger volume fraction (Dekkers, Boom, et al., 2018b). Furthermore, Dekkers, Hamoen, et al. (2018b) showed that assuming a volume fraction of 0.15 for pectin could explain differences observed in mechanical anisotropy. The deformed air bubbles in the SPI-SYB and SPI-HMC samples might have strengthened the network in parallel direction. The stress arising from small cracks formed during deformation can be distributed over the complete area of the air bubble, which results in lower stress and a stronger material (Andersons et al., 2015). Although SPI-LMC did include a higher void fraction compared to SPI, the lower deformation and relatively higher fraction of larger air bubbles probably made the material weaker.

The link between anisotropy and air inclusion and bubble deformation has been studied in depth for calcium caseinate with maltodextrin samples (Z. Wang, Dekkers, et al., 2019). In that study, CLSM pictures revealed that maltodextrin grouped around an air bubble before

shearing, and after shearing maltodextrin was distributed throughout the sample (Z. Wang, Dekkers, et al., 2019) This mechanism seems applicable to SPI-pectin blends as well, with the clear exception of SGB. The higher void fraction of SPI-HMC samples compared to SPI samples has been observed before, and it was found that a high void fraction was already present before shearing (Dekkers, Hamoen, et al., 2018a). This would thus mean that pectin stabilizes the air fraction, rather than increasing the air fraction. For the dispersed air bubble to coalesce and deform, a certain matrix viscosity is required. A higher matrix viscosity will lead to reduced coalescence (Wildes et al., 1999). Apart from the matrix viscosity, the shear rate also affects coalescence and at the mild shear rates tested in this study coalescence is possible (Emin et al., 2012).

Interestingly, after heating, the trends of G' and G'' in the LVE followed exactly the same trend as Young's moduli of fibrous products produced at a shear rate of 39 s^{-1}, with SPI-LMC having the highest G', G'', and E. The increased G', G'', an E of the SPI-LMC sample could explain the reduced coalescence of air bubbles. We hypothesize that the E, G', and G'' of the SPI-pectin samples are linked to both the pH of the blends (Appendix A.3), and water redistribution between pectin and SPI phases. Dekkers et al. (2018) showed that with decreasing pH, the complex modulus G^* increased. SPI-LMC samples had the lowest pH, and highest E, G', and G''. Since LMC is less methylated, this pectin has a higher charge than HMC before processing. The pH of all the SPI-pectin blends reduced after the strain sweep performed at 140 °C. The high temperature and pH > 5.5 possibly induced β-elimination of especially HMC pectin, which resulted in the release of methanol groups, the lowering of the molecular weight, and a lower pH of SPI-HMC and SPI-LMC samples (Voragen et al., 2009). SGB and SYB pectin have some acetyl groups that can be released upon heating, reducing the pH. Apart from the pH effect, it should also be considered that the pectin phase could absorb more water, leading to a higher concentrated SPI phase and thus a higher G' and G'' (Dekkers, Boom, et al., 2018b).

Apart from pH and water redistribution, molecular interactions between pectin and SPI might influence the matrix properties. Pectin can interact with proteins in different manners: electrostatic interactions with the free carboxyl groups, hydrophobic interactions with methoxyl or acetyl groups, and hydrogen bonds with carboxyl groups(Einhorn-Stoll et al., 2021). Electrostatic interactions between the negatively charged pectin and SPI are possible when the pH is lower than the isoelectric point (pI) of SPI. The pI of SPI is around 4 to 5, and it is thus unlikely that these interactions took place in the dispersions used in this study, as has been found for SPI with high methyl-esterified citrus pectin (Jaramillo et al., 2011). In the case of citrus pectin, we assume that both pectin and SPI have a negative charge, and thus repulsion is likely (Fennema, 1996). Hydrophobic interactions between SPI and pectins with a high degree of methyl esterification (HMC) or acetylation (SGB) could take place. It is known that the SGB pectin is less able to form a gel-like structure, due to its high acetylation, feruloylation, and rhamnogalacturonan I branching (B. Liu et al., 2012). The acetylation hinders the capacity to interact through hydrogen bonding. Therefore, SGB pectin might not

be able to form a stable network around the air bubble, and thus did not result in higher void fraction. It should be noted that the interactions between SPI and pectins are mostly studied at low dry matter (<3%) concentrations and a pH of around the pI of SPI (4-5) (Jaramillo et al., 2011; Lam et al., 2008; Mendanha et al., 2009; Warnakulasuriya et al., 2018). It is thus unclear if similar interactions occur in the SPI-pectin blends used in this study. However, it is unlikely that the molecular reactions play a significant role on the concentration SPI-pectin blends.

Inspired by the mechanism behind maltodextrin-caseinate samples (Z. Wang, Dekkers, et al., 2019), we propose a mechanism for fibrous structure formation upon pectin addition (Figure 4.6). The structuring potential of the pectins depends thus on two factors: first, the ability of the pectin to hold air in the blend after mixing, second: the deformation of the air bubbles during shear structuring. The former depends on the stabilization of the air bubbles by pectin, which could be hindered by high acetylation as in the case of SGB. The latter depends on the elasticity of the blend, as a higher elasticity will prevent droplet break-up and will lead to higher deformation instead (Sibillo et al., 2004). The lower elasticity of the SPI-LMC blend after heating might have led to lower elongation or even bubble breakup. SPI-SYB had the highest elastic properties upon high strain, and thus the air bubbles in this sample showed the highest elongation. Apart from droplet breakup, also coalescence could take place. Under shear, a higher viscosity of the matrix reduced coalescence of oil droplets (Emin et al., 2012). It could thus also be possible that the higher G' and G'' of the SPI-LMC blend prevented coalescence of air bubbles. SPI-HMC samples had high mechanical anisotropy, but lower elongation of the air bubbles compared to SPI-SYB. This could be explained by the coalescence and deformation of the pectin droplets, which together with the elongation of air bubbles results in mechanical anisotropy and fibrous structure. The proposed mechanism in Figure 4.6 thus adds to the mechanism proposed by Dekkers et al. (2016). In addition to the elongation of pectin domains, the elongation of air domains is also a route to create fibrous structure formation in fibrous products.
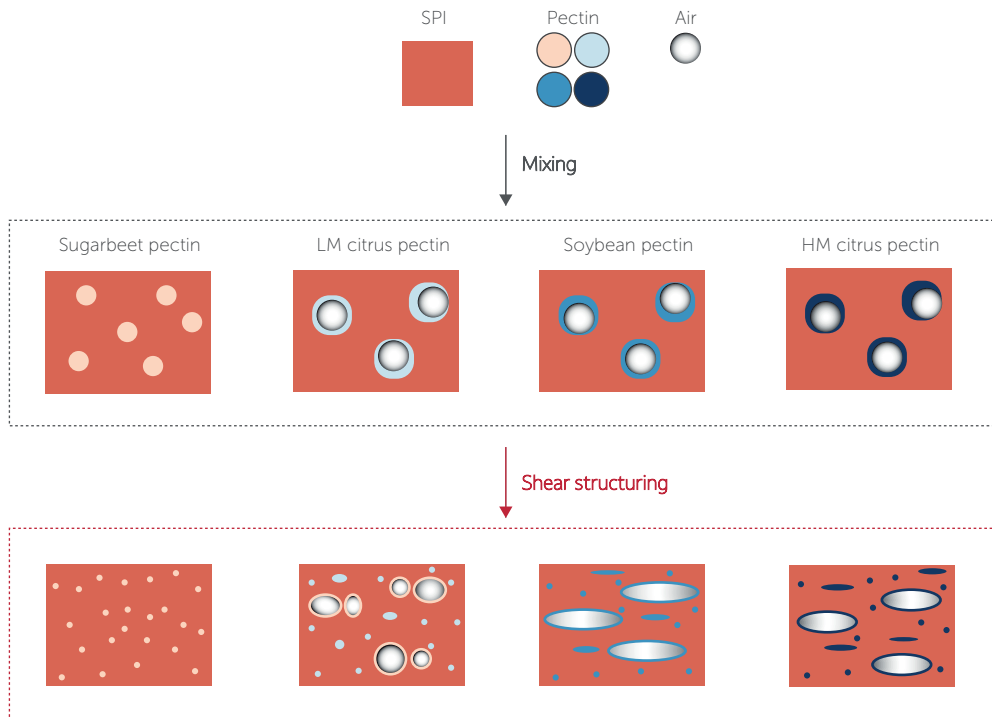
Figure 4.6: Simplified schematic representation of the mechanism behind structuring potential of soy protein isolate (SPI)- pectin blends. LM = low methyl-esterified, HM=high methyl-esterified.

4.5   Conclusion

The addition of pectin to soy protein isolate is a route to create fibrous products. This study revealed which properties of pectin are relevant to induce fibrous structure formation in SPI dispersions. Two out of the four pectins could be used to create fibrous products. In those products, higher levels of air inclusion were found, which confirmed the importance of considering air inclusion when making fibrous products. The addition of soybean pectin not only resulted in high air inclusion, but also deformed bubbles. The formation of deformed air bubbles was attributed to the ability of the SPI-pectin blend to form an elastic matrix as revealed by the rheological measurements. The number and shape of air bubbles was further influenced by pH-changes upon pectin addition and water uptake by the pectins, probably as a result of a change in the G' and G''-values of the blend. A lowered pH of the blend with low methyl-esterified citrus pectin resulted in a higher G', which reduced the deformation of the air bubbles. The lower ability to withstand large deformation of all SPI-pectin blends was attributed to the hindered SPI network.

Based on all results, we hypothesize that the effect of pectin was two-fold. First pectins can form a dispersed phase, which can lead to anisotropy, second pectins can stabilize and deform air bubbles. The latter seems a key aspect when striving for highly fibrous products and a main explanation for the results described in this study.

Appendix A

A.1 Measured values for SPI

Table A1: Measured values for parameters obtained with the tensile test and strain sweep of SPI, that were used as a reference to calculate relative difference. Values are averages ± sd (n=3).

Condition	Parameter	Value (SPI)
19.5 s^{-1} parallel	γ_t (-)	0.81 ± 0.03
	σ_t (kPa)	1291 ± 157
	E (kPa)	1347 ± 28.1
39 s^{-1} parallel	γ_t (-)	0.7 ± 0.1
	σ_t (kPa)	1123 ± 227
	E (kPa)	1560 ± 97
19.5 s^{-1} perpendicular	γ_t (-)	1.01 ± 0.01
	σ_t (kPa)	1663 ± 130
	E (kPa)	1226 ± 31.0
39 s^{-1} perpendicular	γ_t (-)	0.9 ± 0.1
	σ_t (kPa)	1594 ± 291
	E (kPa)	1516 ± 13
30 °C	G' (kPa)	322 ± 7.2
	G'' (kPa)	68.5 ± 1.6
	γ_y (%)	7.4 ± 0.0
	γ_{co} (%)	216 ± 0.1
	σ_y (kPa)	23 ± 0.5
	σ_{co} (kPa)	143 ± 2.1
140-30 °C	G' (kPa)	516 ± 4.7
	G'' (kPa)	102 ± 1.9
	γ_y (%)	7.4 ± 0.0
	γ_{co} (%)	215 ± 0.0
	σ_y (kPa)	36 ± 0.4
	σ_{co} (kPa)	175 ± 1.6

4

A.2 Tensile test in perpendicular direction

(a)   (b)
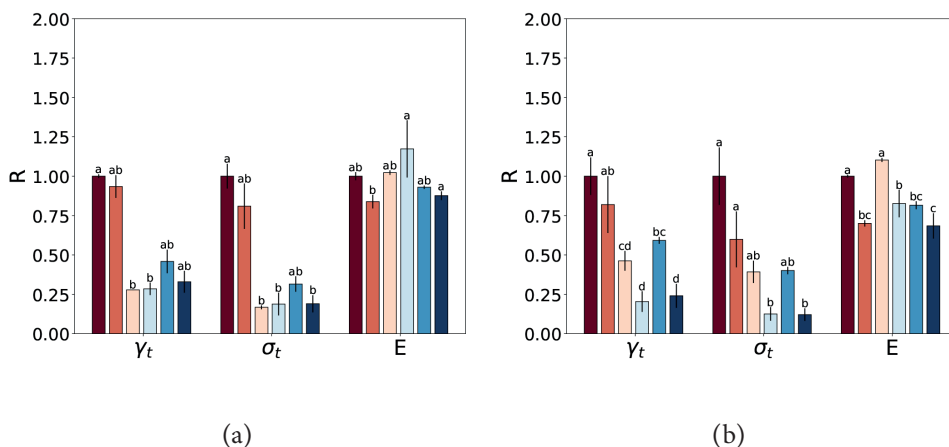
Figure A1: Relative change (R) in tensile strain (γt), tensile stress (σt) and youngs modulus (E) when pectin was added to a soy protein isolate (SPI) fibrous product measured in perpendicular direction to the shear stress of SPI fibrous products produced with shear structuring at 19.5 s^{-1} (a) and 39 s^{-1} (b). The γt, σt, and E of the SPI sample at 45% DM was taken as 1 (dark purple). Samples were made from SPI at 45% DM (dark red), SPI at 42.8 % (orange), SPI-SGB (sugarbeet pectin, pink), SPI-LMC (low methyl-esterified citrus pectin, light blue), SPI-SYB (soybean pectin, blue), and SPI-HMC (high methyl-esterified citrus pectin, dark blue). Colors of the samples represents fibrous structure, with dark red = not fibrous, and dark blue = very fibrous. Values are averages with standard deviation (bars), letters indicate significant groups (p ≤ 0.05), n=2 (a) and n=3 (b)

A.3 pH before and after strain sweep

Table A2: The pH of the SPI and SPI-pectin blends before and after strain sweeps at 140 °C. Values are averages ± standard deviation, n=3.

Blend	pH before strain sweep	pH after strain sweep
SPI	7.0 ± 0.06	7.0 ± 0.08 [a]
SPI-SGB	6.5 ± 0.05 [c]	6.3 ± 0.04 [c]
SPI-LMC	6.2 ± 0.07 [d]	6.1 ± 0.11 [d]
SPI-SYB	6.9 ± 0.02 [a]	6.3 ± 0.05 [c]
SPI-HMC	6.7 ± 0.03 [b]	6.6 ± 0.01 [b]

A.4 Strain sweeps
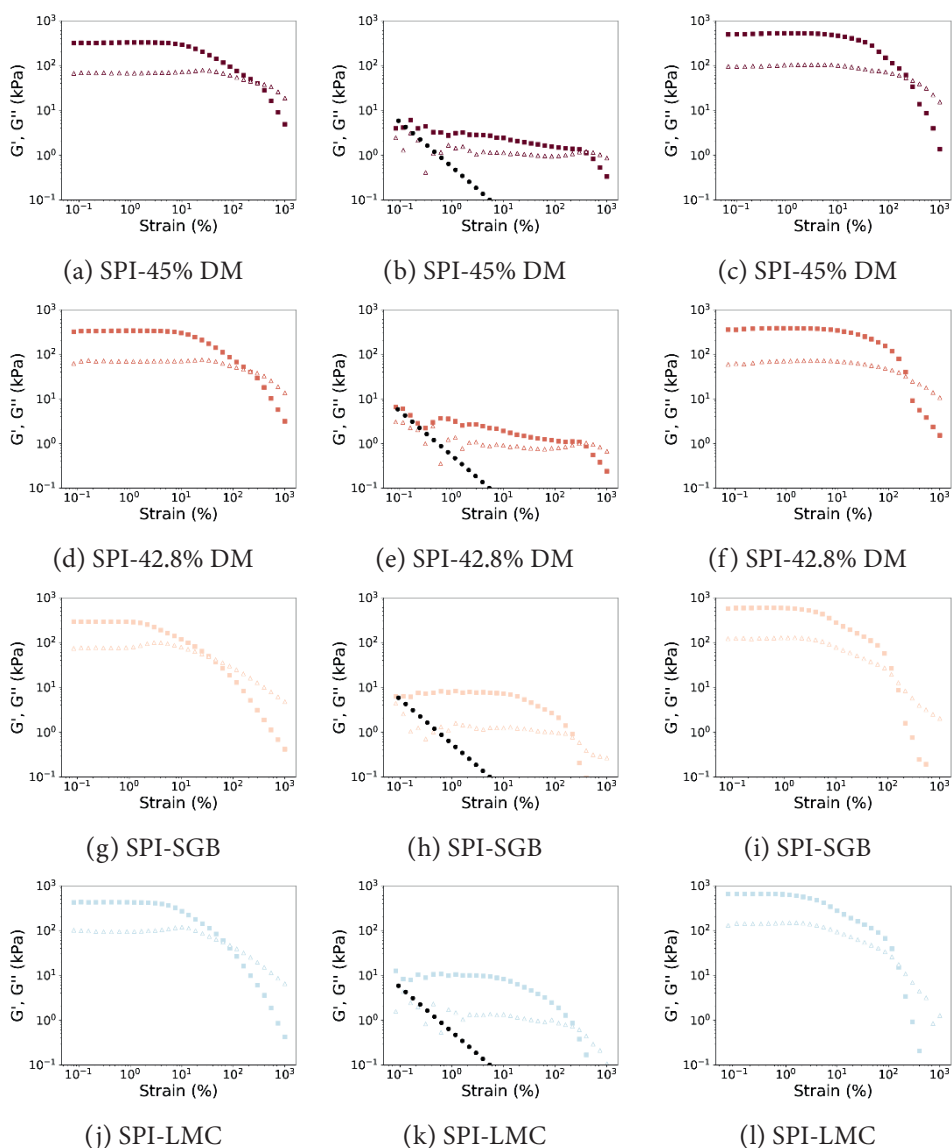
Figure A2: Strain sweeps (f=1 Hz) of soy protein isolate (SPI) and SPI-pectin samples at 30 °C (a, d, g, j, m, p), at 140 °C (b, e, h, k, n, q), and heated to 140 °C and cooled to 30 °C (c, f, i, l, o, r). Samples were SPI at 45% DM (dark red, a, b, c), SPI at 42.8% (orange, d, e, f), SPI-SGB (sugarbeet pectin, pink, g, h, i), SPI-LMC (low methyl-esterified citrus pectin, light blue, j, k, l). G': closed symbols and G'': open symbols. The black dotted line in the measurement at 140 °C represents the torque limits of the CCR. Colors of the samples represents fibrous structure, with dark red = not fibrous, and dark blue = very fibrous.

(m) SPI-SYB (n) SPI-SYB (o) SPI-SYB

(p) SPI-HMC (q) SPI-HMC (r) SPI-HMC
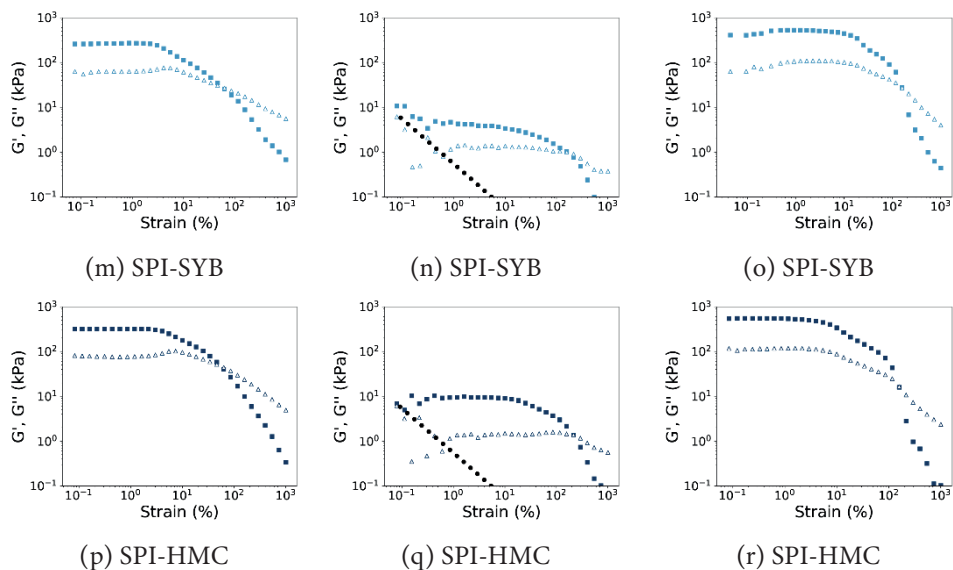
Figure A2 (continued): Strain sweeps (f=1 Hz) of soy protein isolate (SPI) and SPI-pectin samples at 30 °C (a, d, g, j, m, p), at 140 °C (b, e, h, k, n, q), and heated to 140 °C and cooled to 30 °C (c, f, i, l, o, r). Samples were SPI at 45% DM (dark red, a, b, c), SPI at 42.8% (orange, d, e, f), SPI-SGB (sugarbeet pectin, pink, g, h, i), SPI-LMC (low methyl-esterified citrus pectin, light blue, j, k, l), SPI-SYB (soybean pectin, blue, m, n, o), and SPI-HMC (high methyl-esterified citrus pectin, dark blue, p, q, r). G': closed symbols and G'': open symbols. The black dotted line in the measurement at 145 °C represents the torque limits of the CCR. Colors of the samples represents fibrous structure, with dark red = not fibrous, and dark blue = very fibrous.

References

Andersons, J., Kirpluks, M., Stiebra, L., & Cabulis, U. (2015). The effect of a circular hole on the tensile strength of neat and filled rigid PUR foams. *Theoretical and Applied Fracture Mechanics*, *78*, 8–14. https://doi.org/10.1016/j.tafmec.2015.05.001

Brishti, F. H., Chay, S. Y., Muhammad, K., Ismail-Fitry, M. R., Zarei, M., Karthikeyan, S., & Saari, N. (2020). Effects of drying techniques on the physicochemical, functional, thermal, structural and rheological properties of mung bean (Vigna radiata) protein isolate powder. *Food Research International*, *138*(PB), 109783. https://doi.org/10.1016/j.foodres.2020.109783

Bühler, J. M., Dekkers, B. L., Bruins, M. E., & Goot, A. J. Van Der. (2020). *Modifying Faba Bean Protein Concentrate Using Dry Heat to Increase Water Holding Capacity*. 1–16. https://doi.org/10.3390/foods9081077

Cornet, S. H. V., Snel, S. J. E., Schreuders, F. K. G., Van der Sman, R. G. M., Beyrer, M., & Van der Goot, A. J. (2021). Thermo-mechanical processing of plant proteins using shear cell and high-moisture extrusion cooking. *Critical Reviews in Food Science and Nutrition*, *0*(0), 1–18. https://doi.org/10.1080/10408398.2020.1864618

Dekkers, B. L., Boom, R. M., & van der Goot, A. J. (2018). Viscoelastic properties of soy protein isolate - pectin blends: Richer than those of a simple composite material. *Food Research International*, *107*, 281–288. https://doi.org/10.1016/j.foodres.2018.02.037

Dekkers, B. L., Hamoen, R., Boom, R. M., & van der Goot, A. J. (2018a). Understanding fiber formation in a concentrated soy protein isolate - Pectin blend. *Journal of Food Engineering*, *222*, 84–92. https://doi.org/10.1016/j.jfoodeng.2017.11.014

Dekkers, B. L., Hamoen, R., Boom, R. M., & van der Goot, A. J. (2018b). Understanding fiber formation in a concentrated soy protein isolate - Pectin blend. *Journal of Food Engineering*, *222*, 84–92. https://doi.org/10.1016/j.jfoodeng.2017.11.014

Dekkers, B. L., Nikiforidis, C. V., & van der Goot, A. J. (2016). Shear-induced fibrous structure formation from a pectin/SPI blend. *Innovative Food Science and Emerging Technologies*, *36*, 193–200. https://doi.org/10.1016/j.ifset.2016.07.003

Einhorn-Stoll, U., Archut, A., Eichhorn, M., & Kastner, H. (2021). Pectin - Plant protein systems and their application. In *Food Hydrocolloids* (Vol. 118). Elsevier B.V. https://doi.org/10.1016/j.foodhyd.2021.106783

Emin, M. A., Schmidt, U., Van Der Goot, A. J., & Schuchmann, H. P. (2012). Coalescence of oil droplets in plasticized starch matrix in simple shear flow. *Journal of Food Engineering*, *113*(3), 453–460. https://doi.org/10.1016/j.jfoodeng.2012.06.015

Ewoldt, R. H., Winter, P., Maxey, J., & McKinley, G. H. (2010). Large amplitude oscillatory shear of pseudoplastic and elastoviscoplastic materials. *Rheologica Acta*, *49*(2), 191–212. https://doi.org/10.1007/s00397-009-0403-7

Fennema, O. R. (1996). *Food Chemistry* (Vol. 76). CRC Press.

González, A. D., Frostell, B., & Carlsson-Kanyama, A. (2011). Protein efficiency per unit energy and per unit greenhouse gas emissions: Potential contribution of diet choices to climate change mitigation. *Food Policy*, *36*(5), 562–570. https://doi.org/10.1016/j.foodpol.2011.07.003

Grabowska, K. J., Tekidou, S., Boom, R. M., & van der Goot, A. J. (2014). Shear structuring as a new method to make anisotropic structures from soy-gluten blends. *Food Research International*, *64*, 743–751. https://doi.org/10.1016/j.foodres.2014.08.010

Grabowska, K. J., Zhu, S., Dekkers, B. L., De Ruijter, N. C. A., Gieteling, J., & Van Der Goot, A. J. (2016). Shear-induced structuring as a tool to make anisotropic materials using soy protein concentrate. *Journal of Food Engineering*, *188*, 77–86. https://doi.org/10.1016/j.jfoodeng.2016.05.010

Jaramillo, D. P., Roberts, R. F., & Coupland, J. N. (2011). Effect of pH on the properties of soy protein-pectin complexes. *Food Research International*, *44*(4), 911–916. https://doi.org/10.1016/j.foodres.2011.01.057

Jermendi, É., Beukema, M., van den Berg, M. A., de Vos, P., & Schols, H. A. (2022). Revealing methyl-esterification patterns of pectins by enzymatic fingerprinting: Beyond the degree of blockiness. *Carbohydrate Polymers*, *277*. https://doi.org/10.1016/j.carbpol.2021.118813

4

Kyriakopoulou, K., Keppler, J. K., & van der Goot, A. J. (2021). Functionality of ingredients and additives in plant-based meat analogues. *Foods*, *10*(3). https://doi.org/10.3390/foods10030600

Lam, M., Paulsen, P., & Corredig, M. (2008). Interactions of soy protein fractions with high-methoxyl pectin. *Journal of Agricultural and Food Chemistry*, *56*(12), 4726–4735. https://doi.org/10.1021/jf073375d

Lie-Piang, A., Hageman, J., Vreenegoor, I., van der Kolk, K., de Leeuw, S., van der Padt, A., & Boom, R. M. (2023). Quantifying techno-functional properties of ingredients from multiple crops using machine learning. *Submitted*.

Liu, B., Zhang, J., Liu, L., & Hotchkiss, A. T. (2012). Utilization of pectin extracted sugar beet pulp for composite application. *Journal of Biobased Materials and Bioenergy*, *6*(2), 185–192. https://doi.org/10.1166/jbmb.2012.1206

Mendanha, D. V., Molina Ortiz, S. E., Favaro-Trindade, C. S., Mauri, A., Monterrey-Quintero, E. S., & Thomazini, M. (2009). Microencapsulation of casein hydrolysate by complex coacervation with SPI/pectin. *Food Research International*, *42*(8), 1099–1104. https://doi.org/10.1016/j.foodres.2009.05.007

Nair, R., & Roy Choudhury, A. (2020). Synthesis and rheological characterization of a novel shear thinning levan gellan hydrogel. *International Journal of Biological Macromolecules*, *159*, 922–930. https://doi.org/10.1016/j.ijbiomac.2020.05.119

Schmidt, I., Novales, B., Boué, F., & Axelos, M. A. V. (2010). Foaming properties of protein/pectin electrostatic complexes and foam structure at nanoscale. *Journal of Colloid and Interface Science*, *345*(2), 316–324. https://doi.org/10.1016/j.jcis.2010.01.016

Schreuders, F. K. G., Sagis, L. M. C., Bodnár, I., Erni, P., Boom, R. M., & van der Goot, A. J. (2021). Mapping the texture of plant protein blends for meat analogues. *Food Hydrocolloids*, *118*(February). https://doi.org/10.1016/j.foodhyd.2021.106753

Schreuders, F. K. G., Schlangen, M., Bodnár, I., Erni, P., Boom, R. M., & van der Goot, A. J. (2022). Structure formation and non-linear rheology of blends of plant proteins with pectin and cellulose. *Food Hydrocolloids*, *124*(October 2021). https://doi.org/10.1016/j.foodhyd.2021.107327

Sibillo, V., Simeone, M., & Guido, S. (2004). Break-up of a Newtonian drop in a viscoelastic matrix under simple shear flow. *Rheologica Acta*, *43*(5), 449–456. https://doi.org/10.1007/s00397-004-0374-7

Smetana, S., Ristic, D., Pleissner, D., Tuomisto, H. L., Parniakov, O., & Heinz, V. (2023). Meat substitutes: Resource demands and environmental footprints. *Resources, Conservation and Recycling*, *190*(December 2022), 106831. https://doi.org/10.1016/j.resconrec.2022.106831

Taghian Dinani, S., Broekema, N. L., Boom, R., & van der Goot, A. J. (2023). Investigation potential of hydrocolloids in meat analogue preparation. *Food Hydrocolloids*, *135*. https://doi.org/10.1016/j.foodhyd.2022.108199

Tolstoguzov, V. B., Mzhel'sky, A. I., & Gulov, V. Y. (1974). Deformation of emulsion droplets in flow. *Colloid & Polymer Science*, *252*, 124–132. https://link.springer.com/article/10.1007/BF01555536

Voragen, A. G. J., Coenen, G. J., Verhoef, R. P., & Schols, H. A. (2009). Pectin, a versatile polysaccharide present in plant cell walls. *Structural Chemistry*, *20*(2), 263–275. https://doi.org/10.1007/s11224-009-9442-z

Voragen, A. G. J., Schols, H. A., & Pilnik, W. (1986). Determination of the degree of methylation and acetylation of pectins by h.p.l.c. *Topics in Catalysis*, *1*(1), 65–70. https://doi.org/10.1016/S0268-005X(86)80008-X

Wang, Z., Dekkers, B. L., Boom, R., & van der Goot, A. J. (2019). Maltodextrin promotes calcium caseinate fibre formation through air inclusion. *Food Hydrocolloids*, *95*(April), 143–151. https://doi.org/10.1016/j.foodhyd.2019.04.028

Wang, Z., Tian, B., Boom, R., & van der Goot, A. J. (2019). Air bubbles in calcium caseinate fibrous material enhances anisotropy. *Food Hydrocolloids*, *87*(August), 497–505. https://doi.org/10.1016/j.foodhyd.2018.08.037

Warnakulasuriya, S., Pillai, P. K. S., Stone, A. K., & Nickerson, M. T. (2018). Effect of the degree of esterification and blockiness on the complex coacervation of pea protein isolate and commercial pectic polysaccharides. *Food Chemistry*, *264*(May), 180–188. https://doi.org/10.1016/j.foodchem.2018.05.036

Weinberger, M., Stirnemann, E., Schmucki, J., Windhab, E., & Mitra, B. (2021). *WO2021032866A1 Method for the production of protein-containing foods*.

Wildes, G., Keskkula, H., & Paul, D. R. (1999). Coalescence in PC/SAN blends: Effect of reactive compatibilization and matrix phase viscosity. *Polymer*, *40*(20), 5609–5621. https://doi.org/10.1016/S0032-3861(98)00776-9

4

Chapter 5

Flavor-protein interactions for four plant proteins with ketones and esters

Abstract

The interaction between flavors and proteins results in a reduced headspace concentration of the flavor, affecting flavor perception. We analyzed the retention of a series of esters and ketones with different chain lengths (C4, C6, C8, and C10) by protein isolates of yellow pea, soy, fava bean, and chickpea, with whey as a reference. An increase in protein concentration led to a decrease in flavor compound in the headspace as measured with atmospheric pressure chemical ionization time-of-flight mass spectroscopy (APCI-TOF-MS). Flavor retention was described with a flavor-partitioning model. It was found that flavor retention could be well predicted with the octanol-water partitioning coefficient and by fitting the hydrophobic interaction parameter. Hydrophobic interactions were highest for chickpea, followed by pea, fava bean, whey, and soy. However, the obtained predictive model was less appropriate for methyl decanoate, possibly due to its solubility. The obtained models and fitted parameters are relevant when designing flavored products with high protein concentrations.

5.1   Introduction

The replacement of animal products, such as meat and dairy, with plant-based alternatives could help to reduce the impact of diet choices on the environment (Alexander et al., 2017; Kumar et al., 2017; Van Mierlo et al., 2017). Nevertheless, the flavor of these products, such as plant-based meat, is considered less attractive and appealing to consumers who are not vegan or vegetarian (Michel et al., 2021). Flavors are added to improve the hedonistic properties of meat and dairy replacers, by masking off-flavors and improving the overall flavor profile. The addition of flavors might not be straightforward, since these analog products often contain plant-based proteins to which flavors can strongly bind to or interact (Guichard, 2002). Important plant-based proteins for meat, dairy and egg analogs are soy, pea, and fava bean, due to their gelling and emulsifying ability (Kyriakopoulou et al., 2021; McClements & Grossmann, 2021). Protein-flavor interactions are mainly caused by reversible hydrophobic interactions, hydrophilic interactions, Van der Waal's forces, and ionic bonds, but can also be caused by irreversible covalent binding (K. Wang & Arntfield, 2014). The degree of flavor retention depends on the protein source (Viry et al., 2018), the method of protein extraction (K. Wang & Arntfield, 2014), and the chemical class of the flavors (Gremli, 1974; Heng et al., 2004; Viry et al., 2018; K. Wang & Arntfield, 2014). A common approach to study the protein-flavor interaction is to measure equilibrium headspace concentration and to express flavor retention as a percentage of reduced headspace concentration compared to the control (Gremli, 1974; K. Wang & Arntfield, 2015a; Zhou & Cadwallader, 2006). However, this approach is time-consuming and therefore often only a few chemicals are studied, which makes it challenging to offer a mechanism behind the retention.

An alternative method to study protein-flavor interactions is to model experimental data to predict flavor partitioning. Harrison & Hills (1997) developed a mathematical model to predict flavor retention for both hydrophilic and hydrophobic compounds from a liquid containing macromolecules (Harrison & Hills, 1997). This model was applied to predict flavor-retention in casein/whey dispersions with esters, alcohols, and aldehydes (Viry et al., 2018). The study showed that it was sufficient to assume hydrophobic interactions to explain flavor-retention for esters and alcohols (Viry et al., 2018). Recently, partitioning coefficients have been calculated for pea with hexanal and 2-octenal (Bi et al., 2022). However, to our knowledge, no attempt has been made to model flavor partitioning for plant-based proteins so far. A better understanding of the flavor retention in a range of leguminous proteins can help in targeted flavoring of meat analogues. It can be achieved by investigating the applicability of the partitioning model to plant-based proteins.

The aim of this work is, therefore, to apply the flavor partitioning model to different plant-based proteins, important for the production of plant-based substitutes. The proteins studied are pea protein isolate (PPI), soy protein isolate (SPI), chickpea protein isolate (CPPI), and fava bean protein isolate (FBPI). Furthermore, whey protein isolate (WPI) will be included as a control, since the flavor retention to the main protein in whey, β-lactoglobulin, has

been widely studied (Anantharamkrishnan et al., 2020; Anantharamkrishnan & Reineccius, 2020b, 2020a; Kühn et al., 2007). The investigated flavors include a series (C4, C6, C8, C10) of ketones and esters. Ketones and esters are expected to interact non-covalently with proteins, making them suitable for the Harrison and Hills model. Furthermore, they can be added to meat analogues either as flavors or compounds that mask off-flavors. For each protein, 5 concentrations will be prepared and a control. This results in a large dataset of 240 variations in triplicate, which will be used for the model fitting.

5.2   Theory: flavor partitioning models

Harrison & Hills (1997) developed a mathematical model to predict flavor retention in an aqueous solution containing polymers. A system is considered that consists of a water (w) and gas (g) phase, where there is flavor bound to protein (fp), flavor in the water phase (fw), flavor in the gas phase (fg), and total flavor (ft) (Figure 5.1).
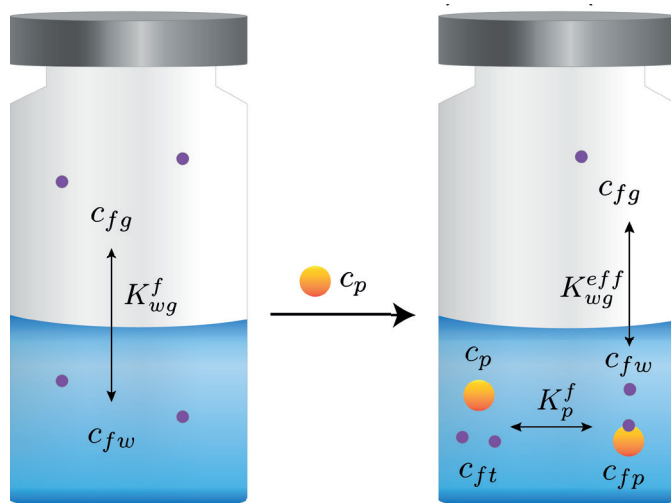
Figure 5.1: Simplified scheme of the flavor-water system (left), and flavored protein dispersion (right): corresponds to concentrations of flavor in water (fw), flavor in the gas phase (fg), flavor bound to protein (fp), total flavor (ft) and protein (p). K_{wg}^f is the partitioning coefficient between gas and water of the flavor, and (K_{wg}^{eff}) is the effective partitioning when protein is added. K_p^f is the interaction constant between protein and flavor. Purple circles represent flavor molecules, and orange circles the protein.

A partition coefficient between flavor in the gas phase and the water phase is considered:

$$K_{wg}^f = \frac{c_{fg}^e}{c_{fw}^e} \qquad\qquad 5.1$$

in which c_{fg}^e and c_{fw}^e are the concentration of flavor in the gas phase and the water phase respectively, at equilibrium conditions. However, some of the flavors in the water phase could interact with the protein. When the reversible first-order reaction is assumed for flavor-

protein interactions, we obtain:

$$PF \rightleftharpoons^{K_p^f} P + F \qquad 5.2$$

in which PF, P, and F represent the flavor retained by protein, protein, and flavor in the aqueous solution respectively. K_p^f is the global interaction constant between protein P and flavor F. At equilibrium condition, K_p^f becomes:

$$K_p^f = \frac{c_{fp}^e}{c_p^e c_{fw}^e} \qquad 5.3$$

in which c_{fp}^e and c_p^e are the concentrations of protein-retained flavor in the dispersion at equilibrium, and protein. When the concentration of free protein exceeds the concentration of protein-flavor complexes largely, c_p can be simply defined as the total protein concentration in the solution.

Now, the effective partition coefficient K_{wg}^{eff} between flavor in the gas phase and the water phase becomes:

$$K_{wg}^{eff} = \frac{c_{fg}^e}{c_{ft}^e} \qquad 5.4$$

in which c_{ft}^e is the total flavor in the water system.

The simplified mass balance derived from eq 5.2 reads:

$$c_{ft} = c_{fp} + c_{fw} \qquad 5.5$$

When no protein is present in the water phase, c_{ft} is equal to c_{fw}. The mass balance (eq 5.5) is altered using eq 5.3 to obtain:

$$c_{ft} = c_{fw}^e + K_p^f c_p^e c_{fw}^e = c_{fw}^e \left(1 + K_p^f c_p^e\right) \qquad 5.6$$

Eq 5.1 can be rewritten as a function of c_{fg} and using eq 5.6 eq 5.4 becomes:

$$K_{wg}^{eff} = \frac{c_{fw}^e K_{wg}^f}{c_{fw}^e \left(1 + K_p^f c_p^e\right)} \qquad 5.7$$

Eq 5.7 leads to:

$$K_{wg}^{eff} = \frac{K_{wg}^f}{1 + K_p^f c_p^e} \qquad 5.8$$

For ketones and esters, the flavor-protein interaction is assumed to be dominated by hydrophobic interactions, the global interaction constant could be approached with (Viry et al., 2018):

$$K_p^f = a_p P_{ow}^f \qquad\qquad 5.9$$

in which a_p and P_{ow}^f are the unknown hydrophobic interaction parameter of the protein and the known octanol-water partition coefficient of the flavor compound.

5.3   Methods and Materials

5.3.1   Materials

Soy protein isolate (SPI, Supro® 500E A) was obtained from Solae (Europe S.A.). Pea protein isolate (PPI, Nutralys® F85M) was obtained from Roquette Frères S.A. (Lestrem, France). Fava bean protein isolate (FBPI, FFBP-90-C-EU) and chickpea protein isolate (CPPI, FCPP-70) were both obtained from AGT Foods (Regina, Canada). Whey protein isolate (WPI, BiPRO) was obtained from Davisco Foods International (Minnesota, USA). The moisture contents of the powders were measured with a moisture analyzer (Mettler Toledo, Ohio, United States). Moisture contents were 8.8± 0.0 g/100 g(SPI), 8.1± 0.0 g/100 g(PPI), 8.0± 0.1 g/100 g(FBPI), 6.6± 0.1 g/100 g(CPPI), and 5.2± 0.1 g/100 g(WPI). Methyl decanoate, 2-hexanone, 2-decanone, and ethanol were purchased from Sigma-Aldrich (St. Louis, USA). The remaining flavors listed in Table 5.1 were provided by Firmenich S.A.

Table 5.1: Flavors studied with their corresponding chemical class, molecular weight (MW), solubility, octanol-water partition coefficient (Log P), and the total concentration in the flavored protein dispersions in this study, corresponding to c_{ft} (ppm)

Name	Class	MW (g mol⁻¹)[1]	Solubility (mg/kg)[1]	Log P[1]	Concentration (mg/kg)
2-Butanone	Ketone	72.11	76100	0.26	5.53
2-Hexanone	Ketone	100.16	7745	1.24	5.84
2-Octanone	Ketone	128.22	884	2.22	0.58
2-Decanone	Ketone	156.27	46.4	3.20	0.55
Methyl butanoate	Ester	102.13	9120	1.36	0.21
Methyl hexanoate	Ester	130.19	926	2.34	0.27
Methyl octanoate	Ester	158.24	102	3.32	0.59
Methyl decanoate	Ester	186.30	8.8	4.30	0.18

[1] *Software EPIWEB v4.1, KOWWIN v1.68*

5.3.2   Protein content and amino acid composition

The crude nitrogen contents of the isolates were determined using the Kjeldahl method in triplicates (AACC, method 46-10). The nitrogen conversion factor was calculated for each isolate with its exact amino composition, which was measured by Triskelion in duplicate (Utrecht, Netherlands). The amino acids were determined with the AOAC 2018.06 method. In this method, samples were first hydrolyzed using hydrochloric acid (HCl). Afterwards, the amino acids were derivatized with phenyl isothiocyanate, and analyzed by high-performance

liquid chromatography (HPLC). HPLC was performed in the reverse phase. The amount of each amino acid is quantified by comparing its peak area to that of a known standard. For each amino acid, the weight of nitrogen per g amino acid was calculated (g/g), by counting the number of nitrogen molecules, calculating the molecular weight, and dividing this by the molecular weight of the amino acid. Then, for each amino acid, the weight per 1 g of protein (g amino acid/g protein) was multiplied by the weight of nitrogen for this amino acid (g nitrogen/g amino acid). Subsequently, the values for each amino acid were summed and 1 g protein was divided by the total nitrogen content to obtain the conversion factor.

5.3.3   Hydrophobic index

By dividing the total hydrophobic content by the total hydrophilic content a hydrophobic:hydrophilic ratio was obtained for each protein. However, the different amino acids differ in degree of hydrophobicity (Monera et al., 1995). Therefore, the hydrophobic index was calculated, using the hydrophobicity scale (Schmidtke & Barril, 2010). The hydrophobic index can give a comprehensive representation of hydrophobicity and allows a good comparison between the different proteins based on their amino acid composition. Hydrophobic amino acids got a positive index (maximum 100), whereas hydrophilic amino acids had a negative index (maximum -100) and neutral ones got an index of 0. Then, the fraction of amino acid (g/g protein) was multiplied with the corresponding hydrophobic score and summed:

$$\sum [F_{Alanine}S_{Alanine} \ldots F_{Valine}S_{Valine}] \qquad 5.10$$

in which F and S correspond to the fraction and score of the amino acid. This resulted in a hydrophobic index for each protein.

5.3.4   Solubility protein isolates

Solubility of the protein isolates was measured in triplicate with a method reported by (Bühler et al., 2020) with some minor alterations. A dispersion of 0.0125 g/g

 protein isolate in demineralized water was prepared and shaken overnight at 300 rpm at room temperature. Subsequently, the dispersions were centrifuged at 10,000 g at 21 °C for 30 min. The weight of the supernatant and pellet were recorded and both were dried at 100 °C for at least 12 h. The solubility was calculated as follows:

$$Solubility = \frac{M_{dry-powder} - M_{dry-pellet}}{M_{dry-powder}} \qquad 5.11$$

in which $M_{dry-powder}$ is the overall weight of the isolate and $M_{dry-pellet}$ is the weight of the pellet after drying.

5.3.5 Preparation flavored protein dispersions

First, a stock solution for each protein isolate was made of 50 g/kgin demineralized water. At this step, the concentration of protein isolate represents total isolate content, not yet corrected for dry matter and protein content. Stock solutions were first stirred at 21 °C for 1 h, then finely dispersed with an Ultra Turrax (T25, IKA) and subsequently left for complete hydration at 5 °C for 24 h. Subsequently, either 0.5, 1, 2, 3, or 5 mL of the stock solution was transferred to crimp vials and demineralized water was added to obtain a total of 5 ml. This resulted in dispersions of 5, 10, 20, 30, and 50 g/kg for each protein isolate. The concentrations were chosen such that flavor retention was expected to occur, but retention was not maximum. The exact amount of protein in each dispersion was then calculated based on the protein content and dry matter content of the protein isolates. Each flavor compound was first diluted in ethanol, to ensure solubility, and then added to the protein dispersion to reach a concentration in a range from 0.1 to 10 mg/kg

(ppm). The concentration used depended on the flavor compound. The final concentrations of each flavor compound in the aqueous phase were chosen such that it was within the range of the calibration curve (Table 5.1). The flavored dispersions were then vortexed for 30 s. The presence of ethanol in the final solution (1 g/kg) was tested and found to not affect the MS signal. The mixture was allowed to reach equilibrium at 21°C for 24 h.

5.3.6 Static headspace measurements

The headspace concentrations were measured at equilibrium as independent triplicates with a G2-XS Q-TOF high-definition mass spectrometer (XEVO, Waters) coupled to a patented Venturi interface (Linforth & Taylor, 1999) An automated PAL system sampled 5 ml of headspace air with a 5 ml headspace syringe and injected this into the mass spectrometer. Mass spectra were collected in centroid mode over the range m/z 20-400 every 1 s. APCI-MS was performed in positive ionization mode with a cone voltage of 4.0 kV, source temperature of 105 °C, heated sample transfer line temperature of 130 °C and auxiliary gas flow of 600 L/h. Lock spray (on-the-fly mass calibration) was used to apply a mass correction to measured m/z values during the analysis. All the signal intensities were corrected for the background addition. The relative headspace concentration (RHC) was calculated as:

$$RHC\% = \frac{Peak\ area_{flavored\ dispersion}}{Peak\ area_{flavor\ in\ water}} * 100 \qquad 5.12$$

5.3.7 Model fitting

The relative headspace concentration can be seen as $\frac{K_{wg}^{eff}}{K_{wg}^{f}}$ since the protein dispersion and water system are directly compared. Therefore, the exact concentration of retained flavor, free flavor, and total flavor are not needed in the model fitting. Eq 5.8 and 5.9 were combined and rewritten to obtain:

$$RHC = \frac{K_{wg}^{eff}}{K_{wg}^f} = \frac{1}{1 + a_p P_{ow}^f c_p} \tag{5.13}$$

For K_{wg}^f we can assume that $c_{ft} = c_{fw}$. Thus, to simplify, $\frac{K_{wg}^{eff}}{K_{wg}^f}$ is interpreted as the concentration in the headspace with and without protein present in the water phase, and eq 5.13 is rewritten to obtain a linear relation:

$$\frac{K_{wg}^f}{K_{wg}^{eff}} = \frac{c_{fg}}{c_{fg}^p} = 1 + a_p P_{ow}^f c_p \tag{5.14}$$

Eq 5.14 was fitted to the experimental results for ketones and esters to obtain the a_p values. The slope of the linear lines is $a_p P_{ow}^f$, and thus a measure of binding. A higher slope means more binding per gram of protein. The calculated octanol-water partition coefficient was obtained from EPIWEB. The c_p was taken as the concentration of protein, thus corrected with the dry matter and protein content for each isolate. The fitting was done with the complete dataset, rather than with the averages. The fitting parameter a_p was fitted per protein for esters and per protein for ketones. Data that did not show a linear relation was excluded from the fits. The fitting was performed with Python and the SciPy package. This resulted in a prediction for a_p and the uncertainty of this prediction.

5.3.8 Statistical analysis

Statistical analysis was performed with R. Normality was tested with descriptive statistics. When the data were normally distributed, a one-way analysis of variance (ANOVA) was done to test if the observed differences between samples were significant. Multiple comparison Tukey tests were done to indicate which treatments were significantly different from each other. A correlation matrix was obtained between measured parameters and fitting results.

5

Table 5.2: Amino acid composition and the obtained nitrogen conversion factor and protein content, pH, and solubility of soy, pea, fava bean, chickpea, and whey protein isolates. Values are means ± standard deviations, letters indicate significant groups. Amino acids were measured in duplicate, and the protein content, pH, and solubility in triplicate. Hydrophobic indexes are a summation of the amino acid fraction multiplied by the hydrophobic score.

Amino acids (mg AA/g protein)		Soy
Hydrophilic	Arginine	78.03 ± 0.31[d]
	Asparagine + Aspartic acid	113.98 ± 0.20[c]
	Glutamine + Glutamic acid	192.06 ± 0.08[a]
	Histidine	27.34 ± 0.12[a]
	Lysine	62.39 ± 0.08[c]
	Serine	51.61 ± 0.17[c]
	Threonine	38.48 ± 0.14[a]
	Tyrosine	40.65 ± 0.04[b]
	Total	604.55 ± 0.58[c]
Hydrophobic	Alanine	39.48 ± 0.02[b]
	Cysteine	12.26 ± 0.12[a]
	Glycine	36.28 ± 0.07[a]
	Isoleucine	46.72 ± 0.09[b]
	Leucine	80.99 ± 0.17[d]
	Methionine	13.39 ± 0.13[b]
	Phenylalanine	54.81 ± 0.10[c]
	Proline	50.18 ± 0.21[a]
	Tryptophan	14.95 ± 0.38[a]
	Valine	46.41 ± 0.60[b]
	Total	395.45 ± 0.58[a]
Ratio hydrophobic : hydrophilic		0.65:1[a]
Hydrophobic index[2]		14.73 ± 0.05[b]
Nitrogen content (g/100 g dw)		14.28 ± 0.48[a]
Protein content (g/100 g dw)		83.25 ± 2.77[a]
pH		7.1 ± 0.01[c]
Solubility g/g		0.59 ± 0.01[b]

[1] *Amino acid composition taken from (Amagliani et al., 2017)*

[2] *Hydrophobic index per amino acid taken from (Monera et al., 1995)*

Yellow pea	Fava bean	Chickpea	Whey[1]
89.24 ± 0.44^c	98.56 ± 0.24^a	93.77 ± 0.06^b	26.2
118.00 ± 0.07^b	114.02 ± 0.75^c	123.27 ± 0.58^a	121
174.31 ± 0.11^c	181.47 ± 0.95^b	173.56 ± 0.25^c	175
26.13 ± 0.07^b	27.44 ± 0.12^a	26.49 ± 0.37^b	19.1
75.80 ± 0.14^a	65.70 ± 0.70^b	64.93 ± 0.35^b	116
51.83 ± 0.10^c	53.96 ± 0.36^b	54.92 ± 0.06^a	41.0
37.19 ± 0.05^b	36.32 ± 0.20^c	34.55 ± 0.14^d	50.9
41.49 ± 0.08^a	40.83 ± 0.29^{ab}	33.17 ± 0.13^c	39.8
613.99 ± 0.41^b	618.29 ± 1.19^a	604.66 ± 0.54^c	589
39.43 ± 0.05^b	38.98 ± 0.16^c	40.19 ± 0.01^a	52.8
10.15 ± 0.35^b	8.39 ± 0.13^c	10.74 ± 0.19^b	32.4
35.87 ± 0.05^a	36.19 ± 0.17^a	34.13 ± 0.06^b	18.5
47.20 ± 0.00^a	47.13 ± 0.17^{ab}	46.78 ± 0.13^{ab}	58.9
84.49 ± 0.27^b	87.83 ± 0.20^a	83.43 ± 0.13^c	132
10.48 ± 0.11^c	8.27 ± 0.07^d	14.21 ± 0.15^a	24.3
57.53 ± 0.17^b	50.85 ± 0.41^d	68.51 ± 0.25^a	38.0
42.08 ± 0.04^d	44.66 ± 0.12^b	43.04 ± 0.09^c	45.6
9.99 ± 0.25^{bc}	10.47 ± 0.09^b	9.23 ± 0.20^c	27.2
48.79 ± 0.08^a	48.94 ± 0.19^a	45.07 ± 0.15^c	50.3
386.01 ± 0.41^b	$381.71 \pm 0.1.19^c$	395.34 ± 0.54^a	480
$0.63:1^b$	$0.62:1^c$	$0.65:1^a$	0.81:1
14.81 ± 0.26^b	14.32 ± 0.12^c	15.23 ± 0.07^a	22.43
13.46 ± 0.05^a	14.18 ± 0.53^a	11.72 ± 0.32^b	
77.11 ± 0.29^b	80.42 ± 2.99^{ab}	67.03 ± 1.83^c	89.7
7.5 ± 0.01^a	6.4 ± 0.02^e	6.6 ± 0.01^d	7.1 ± 0.02^b
0.41 ± 0.03^c	0.12 ± 0.01^d	0.12 ± 0.00^d	1.02 ± 0.00^a

5

5.4   Results

5.4.1   Chemical composition protein isolates

For PPI, SPI, FBPI, and CPPI the amino acid composition was measured (Table 5.2). With the obtained amino acid composition, the nitrogen conversion factor was calculated, and thereafter the protein content for each isolate with the obtained Kjeldahl results. SPI had the highest protein content of the plant proteins (83.25 g/100 g), followed by FBPI (80.42 g/100 g), PPI (77.11 g/100 g), and CPPI (67.03 g/100 g). The plant proteins were very close in their amino acid profile, as has also been observed previously for SPI, PPI, and FBPI (Ma et al., 2022). The amino acid composition of WPI was not measured, but instead, we used values from literature in which a similar WPI was studied (Amagliani et al., 2017). Reference values for WPI showed a clear difference in amino acid composition compared to the plant-based proteins. Subsequently, the hydrophobic:hydrophilic ratio and the hydrophobic index were calculated (eq 5.10). WPI had a higher amount of total hydrophobic amino acids. Furthermore, the hydrophobic:hydrophilic ratio and the hydrophobic index were also higher compared to the plant proteins. Within the plant proteins, CPPI had the highest hydrophobic index (15.23), followed by PPI (14.81), SPI (14.73), and FBPI (14.32). In addition, the pH, and solubility (eq 5.11) of the isolates were measured for each isolate. PPI had the highest pH (7.5), followed by SPI and WPI (7.1), CPPI (6.6), and FBPI (6.4). WPI was completely soluble in water, whereas the plant proteins had a much lower solubility.

5.4.2   Influence of protein concentration on flavor retention

Headspace concentrations of flavor-protein dispersions were measured with APCI-MS. Four different plant proteins, SPI, PPI, FBPI, and CPPI, and WPPI were analyzed in 5 different concentrations (5-50 g/kg). Protein concentrations were corrected with the known protein and moisture content of each protein isolate. This led to protein concentrations of 3.1-4.6 g/kg to 31-46 g/kg, depending on the protein isolate. To the protein dispersions, ketones or esters were added and left to equilibrate. The RHC of ketones and esters was measured as a function of plant-protein and whey protein concentration (Figure 5.2). A decrease in RHC is interpreted as an increase in flavor retention, as described by eq 5.12.

Ketones: The RHC of butanone significantly increased with increasing protein content. This suggests a pushing out effect. The pushing out effect of flavors with a short chain length was reported previously for WPI and caseinate with small (hydrophilic) compounds and was attributed to a size-exclusion effect (Viry et al., 2018). The size-exclusion effect arises due to steric hindrance caused by large proteins, expelling the small flavor compounds from the dispersion and pushing them into the headspace. For hexanone, octanone and decanone a decrease in RHC was observed with increased protein concentration and log P of the ketone. The exact RHC was compared between the proteins, with lower RHC corresponding to higher retention. With this comparison, flavor retention by the proteins followed CPPI (Figure 5.2g) > PPI (Figure 5.2c) > FBPI / WPI (Figure 5.2e,i) > SPI (Figure 5.2a) . A small

part of hexanone was retained and RHCs hardly decreased (from 96 - 100% to 93 - 100%). Octanone was more retained, evidenced by a decrease in RHCs from 90% to 40%. Decanone was the most retained, and RHCs decreased from 4.5-51% to 0.7-9.1% for the proteins tested.

Esters: The RHC of methyl butanoate increased and was significantly higher for the 50 g/kgdispersion compared to the 5 g/kgdispersion for all proteins except SPI (Figure 5.2b). Similar to butanone, this could be caused by a pushing-out effect (Viry et al., 2018). For the other esters, we observed an increase in flavor retention with increased protein content and log P of the esters. Furthermore, RHCs of esters were lower compared to the ketones. The comparison of the exact values of RHC showed that Flavor retention followed CPPI (Figure 5.2h) > PPI (Figure 5.2d) > FBPI /WPI (Figure 5.2f,j) > SPI (Figure 5.2b). RHCs of methyl hexanoate decreased from around 100% to 60%. Methyl octanoate decreased from 40% to 10%. The RHCs of methyl decanoate was very low at 5 g/kgprotein, ranging from 1.0-7.3% and further decreasing to 0.1-1.7% at 50 g/kgisolate dispersion for the different proteins.
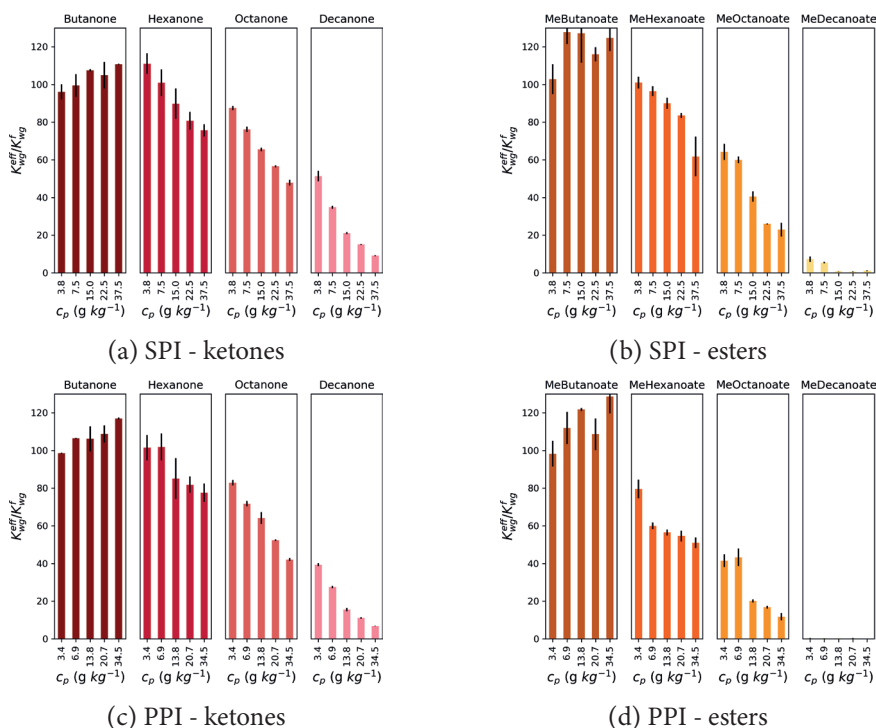
Figure 5.2: K_{wg}^{eff}/K_{wg}^{f} (peak area flavor in dispersion/peak area flavor in water) measured with APCI-TOF-MS of ketones (a, c, e, g, red), and esters (b, d, f, h, orange) as a function of SPI (a, b) and PPI (c, d) concentration. Protein concentration, c_p is the concentration of the isolate corrected for its protein and moisture content. Black bars represent the standard deviation, n = 3.

(e) FBPI - ketones

(f) FBPI - esters

(g) CPPI - ketones

(h) CPPI - esters
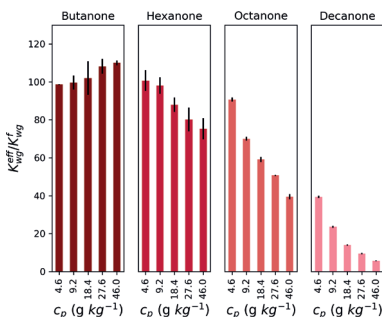
(h) WPI - ketones
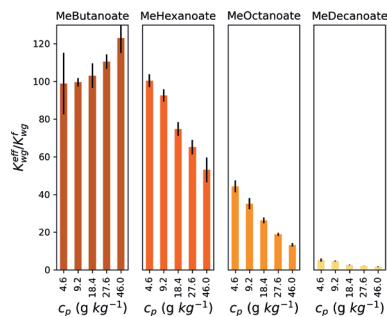
(i) WPI - esters

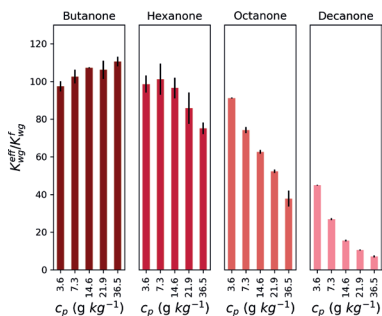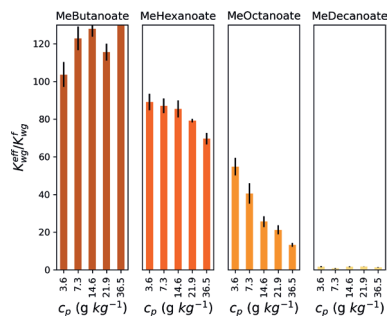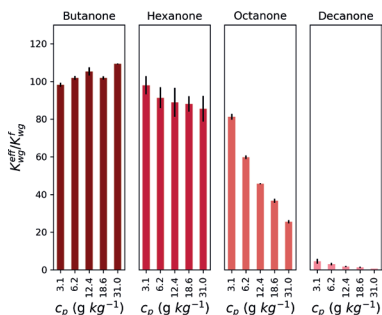*Figure 5.2 (continued): K_{wg}^{eff}/K_{wg}^{f} (peak area flavor in dispersion/peak area flavor in water) measured with APCI-TOF-MS of ketones (a, c, e, g, red), and esters (b, d, f, h, orange) as a function of SPI (a, b), PPI (c, d), FBPI (e, f), CPPI (g,h), and WPI (i,j) concentration. Protein concentration, is the concentration of the isolate corrected for its protein and moisture content. Black bars represent the standard deviation, n = 3.*
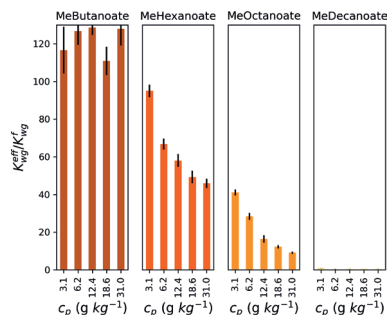
5.4.3   Flavor partitioning models

The experimental data were fitted with flavor partitioning models to describe the protein-flavor interactions. The esters and ketones are expected to have hydrophobic interactions and were fitted with eq 5.14. This resulted in predictions for a_p, used to describe flavor retention of SPI (Figure 5.3a, b), PPI (Figure 5.3c, d), FBPI (Figure 5.3e, f), CPPI (Figure 5.3g, h), and WPI (Figure 5.3i, j). Methyl decanoate did not show a linear relation with protein concentration, and was thus not used for the fitting. For the esters more than 93% of the data was predicted with the model and for ketones more than 97% (Table 5.3). For both esters and ketones, the hydrophobic interaction parameter, a_p, was highest for CPPI, followed by PPI, FBPI, WPI, and SPI. The esters had lower fitted a_p values than the ketones. Interestingly, the a_p of CPPI for ketones was 10x higher than the other protein isolates. The predictions obtained when flavor compounds were fitted separately are presented in the supplementary material. For these fits, only the protein concentration is varied, while in the fits for the complete dataset, the octanol-water partition coefficients are also considered. From these fits it can be observed that octanone and decanone were closer to the combined a_p for ketones than hexanone. The only exception is CPPI, where the a_p for decanone was similar to the combined a_p, which showed that decanone overshadowed the retention of the other ketones. This could also explain the overestimation of hexanone and octanone (Fig 5.3g). For the esters, the combined a_p was closer to individual a_p of methyl hexanoate and methyl octanoate fit values. The poor fit of of methyl decanoate confirmed the non linear behavior, except for WPI, which had an a_p similar to the overall a_p of WPI. Probably, additional effects play a role to explain the very high binding of methyl decanoate. The retention of methyl decanoate was predicted with the obtained fits for (supplementary material). All fits underestimated the observed data points.

The parameters obtained in Table 5.2 were tested for correlation with the a_p of the protein isolates. When excluding WPI, a correlation of 0.74 and 0.71 was obtained between the hydrophobic index and a_p for ketones and esters, respectively. A correlation of -0.68 and -0.56 was found between solubility and a_p (supplementary material).

Table 5.3: Fitting results of ketones and esters for soy, yellow pea, fava bean, chickpea, and whey protein isolates, using the flavor partitioning model and P_{ow}^f. Model parameters are the hydrophobic interaction parameter $a_p \pm$ the linear of the parameter, and the corresponding residuals squared R^2.

Protein source	Ketones		Esters	
	a_p (10^{-5} L/g)	R^2	a_p (10^{-5} L/g)	R^2
Soy	16 ± 0.1	1.00	4.8 ± 0.2	0.93
Yellow pea	25 ± 0.1	1.00	11 ± 0.3	0.96
Fava bean	23 ± 0.2	0.99	8.6 ± 0.2	0.98
Chickpea	290 ± 5.7	0.97	17 ± 0.4	0.97
Whey	22 ± 0.1	1.00	7.2 ± 0.1	0.98
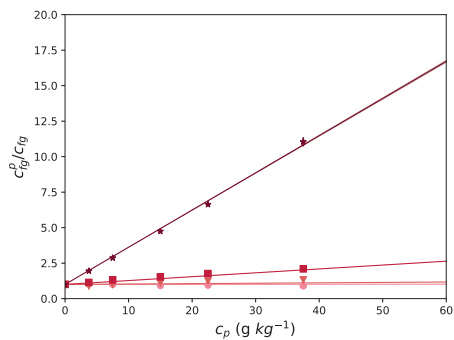
(a) SPI - ketones
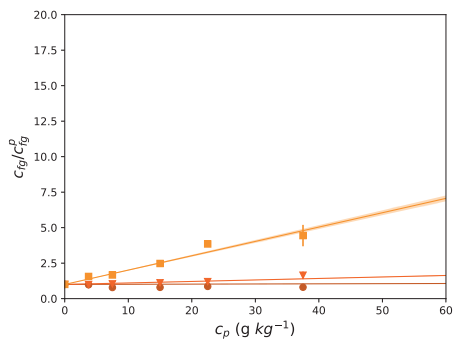
(b) SPI - esters
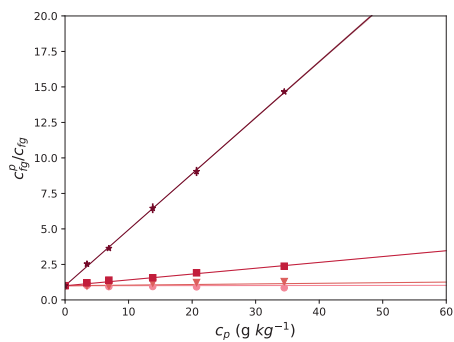
(c) PPI - ketones
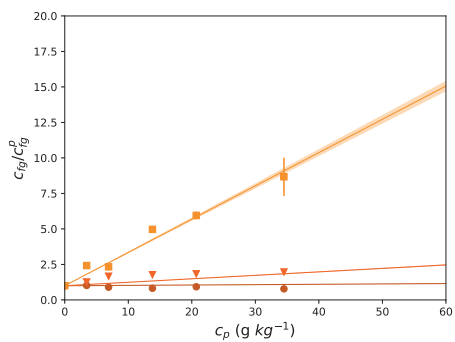
(d) PPI - esters
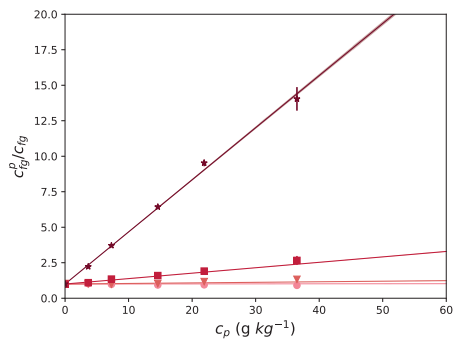
(e) FBPI - ketones
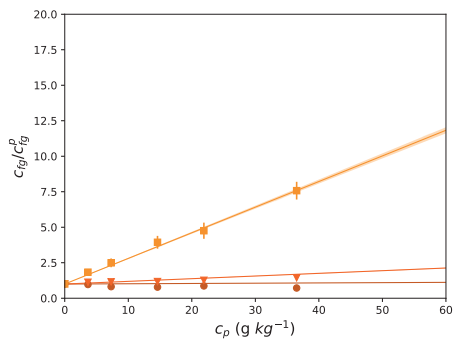
(f) FBPI - esters

Figure 5.3 (continued)

(g) CPPI - ketones

(h) CPPI - esters

(h) WPI - ketones

(i) WPI - esters

Figure 5.3: c_{fg}/c_{fg}^p (headspace concentration of flavor in water/headspace concentration flavor in dispersion) measured with APCI-TOF-MS and model fits of ketones (a, c, e, g, red), and esters (b, d, f, h, orange) as a function of SPI (a, b), PPI (c, d), FBPI (e, f), CPPI (g,h), and WPI (i,j) concentration. Colored lines represent the model fits of the experimental points for C4 (round), C6 (triangle), C8 (square), and C10 (stars, only ketones). Colored areas around the line represent the uncertainty of the fitted parameter. Colored bars represent the standard deviation, n = 3.

5.5   Discussion

The headspace concentrations of esters and ketones with different chain lengths were measured at varying protein concentrations. Subsequently, the results were described with a flavor retention model, using the octanol-water partition coefficients of the flavors and fitting a hydrophobic interaction parameter for SPI, PPI, FBPI, CPPI, and WPI.

This approach based on one fit parameter per class of flavors (esters or ketones) and protein combination allowed a good description of the protein-flavor interactions. The obtained values could therefore be used as a predictive tool.

An increase in the chain length of flavors resulted in a lower relative headspace concentration, which is in accordance with previous studies on the retention of ketones in PPI, and SPI (Gremli, 1974; Heng et al., 2004; K. Wang & Arntfield, 2014), and for esters in WPI dispersions (Viry et al., 2018). The higher flavor retention for longer chain lengths can be explained by the increase in hydrophobicity of these flavors (Table 5.1). These observations are therefore in line with our expectation and approach for the predictive retention model, in which the octanol-water partition coefficient is included as a variable. This could further explain why a more drastic decrease in headspace concentration is seen for the esters since the octanol-water partition coefficients are 1 log higher (Table 5.1). Esters were retained around 30% more than the ketones, depending on the flavor compound. However, the model fits showed a higher hydrophobic interaction parameter for ketones. For ketones, the a_p was around 2-3 x higher than for esters. For CPPI, a_p was even 17x higher for ketones. An ester with a similar log P as the ketone will therefore be less retained.

The model fit parameters make a comparison between the different protein isolates more straightforward. Clearly, the fitted hydrophobic interaction parameter is ordered as follows: CPPI > PPI > FBPI > WPI > SPI. This shows that CPPI and PPI retain more flavor and thus might be harder to flavor, compared to FBPI and SPI. The a_p of CPPI was around 10x higher compared to the other proteins for the ketones. The differences between the tested proteins in their ability to retain flavors could be due to different factors. It could be due to the hydrophobic index of the proteins. Although differences between the hydrophobic indexes are small, they were found to be significant (Table 5.2). A correlation between the hydrophobic index and a_p was also found (0.74 and 0.71). A weaker, negative correlation was found with the solubility of protein isolates (-0.68 and -0.56). In other words, a protein isolate that has a lower solubility, or a higher hydrophobic index, is likely to retain more flavor. It has to be noted that apart from protein, other macro- and micro-molecules could be present in the protein isolate that influence flavor retention. Starch, for example, has been shown to retain flavors by entrapment (Escher et al., 2000). Furthermore, legumes could contain saponins, that can interact with proteins and form hydrophobic patches that influence flavor retention (Heng et al., 2004). In this study, we obtained an a_p for the complete ingredients used, which is expected to be dominated by the high protein content.

In this study, retention was explained with hydrophobic interactions only. However, in addition to hydrophobic interactions, other non-covalent interactions could take place as well. By using different disrupting agents, Wang & Arntfield (2016) showed that ketones (octanone) are retained with hydrophobic interactions to PPI, while acetate esters formed hydrophobic, electrostatic, and hydrogen interactions. This has also been shown for ethyl esters with myofibrillar protein, where hydrogen bonds proved the most dominant interaction (H. Wang et al., 2022). Therefore, hydrogen bonds are thought to play the dominant role in ester retention. Thus, assuming hydrophobic interactions did explain the results convincingly, most likely because esters with a range of hydrophobicities were selected.

Except for WPI, the retention of methyl decanoate could not be explained with the current model, and was thus excluded. The retention was rapid and a reduction of the headspace of more than 50x was seen for the plant proteins (supplementary material). Possibly, the low solubility of methyl decanoate (8.8 mg/kg) affected the experimental results. For butanone and methyl butanoate, the slope was around 0, which means that these small compounds with low P_{ow}^f are not retained.

The obtained parameters show that modeling as a function of the octanol-water partition coefficient is sufficient, without distinguishing between the types of non-covalent reactions. Thus, when flavor retention is mostly dependent on hydrophobic interactions and the protein source is known, flavor retention could be predicted.

5.6   Conclusion

In conclusion, the headspace concentrations of esters and ketones in protein dispersions were measured using five different proteins (PPI, SPI, FBPI, CPPI, and WPI). Results showed that flavor retention was explained by protein content, protein type, and hydrophobicity of the flavor compounds. Flavor partitioning models were successfully applied to the different proteins tested. The models assumed mainly hydrophobic interactions for ketones and esters. The obtained hydrophobic interaction parameters for ketones with different proteins were all in the same order of magnitude, except for CPPI. The highest hydrophobic interaction parameters for ketones and esters were fitted for CPPI (290E-05, 17E-5), followed by PPI (25E-05, 11E-5), FBPI (23E-05, 8.6E-5), WPI (22E-05, 7.2E-5) and SPI (16E-05, 4.8E-5). Although the hydrophobic binding constant of CPPI was clearly higher, the differences between the other plant proteins and whey were small. A correlation between the hydrophobic index of the proteins and the hydrophobic binding constant was found. This led to the conclusion that the retention of esters and ketones is primarily dependent on the flavor compound, and secondary on the protein source.

The assumption of only hydrophobic interactions resulted in good models of the experimental data. The obtained hydrophobic interaction parameter makes it possible to predict flavor-protein interactions for different protein sources to ketones and esters.

5

Appendix A

(a) SPI

(b) PPI
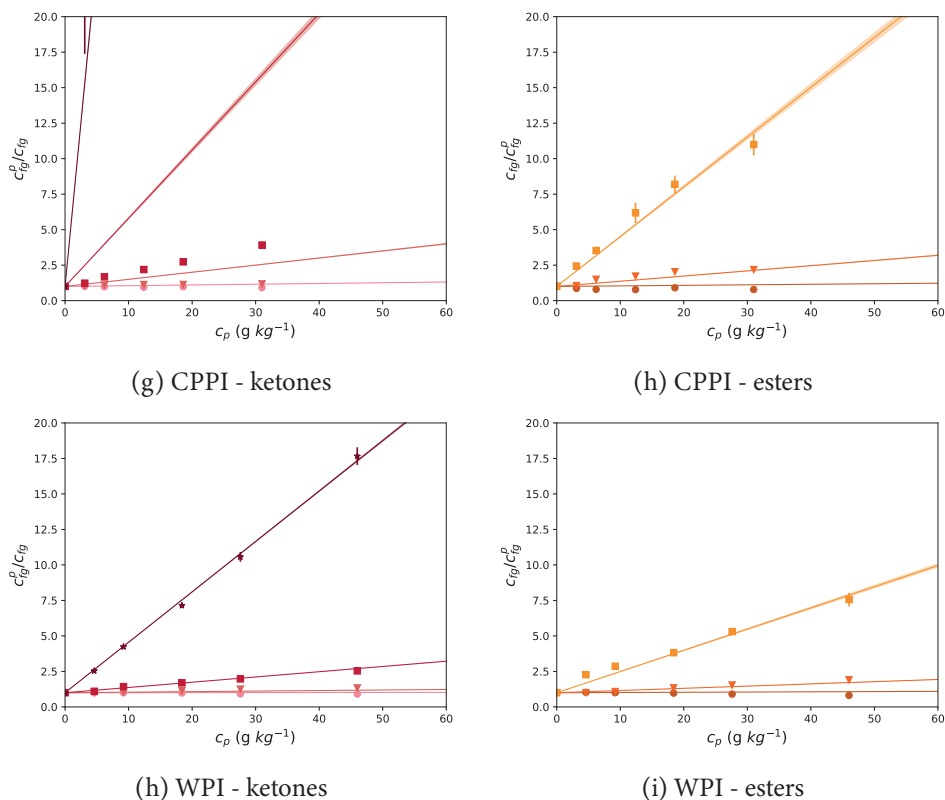
(c) FBPI

(d) CPPI

(e) WPI
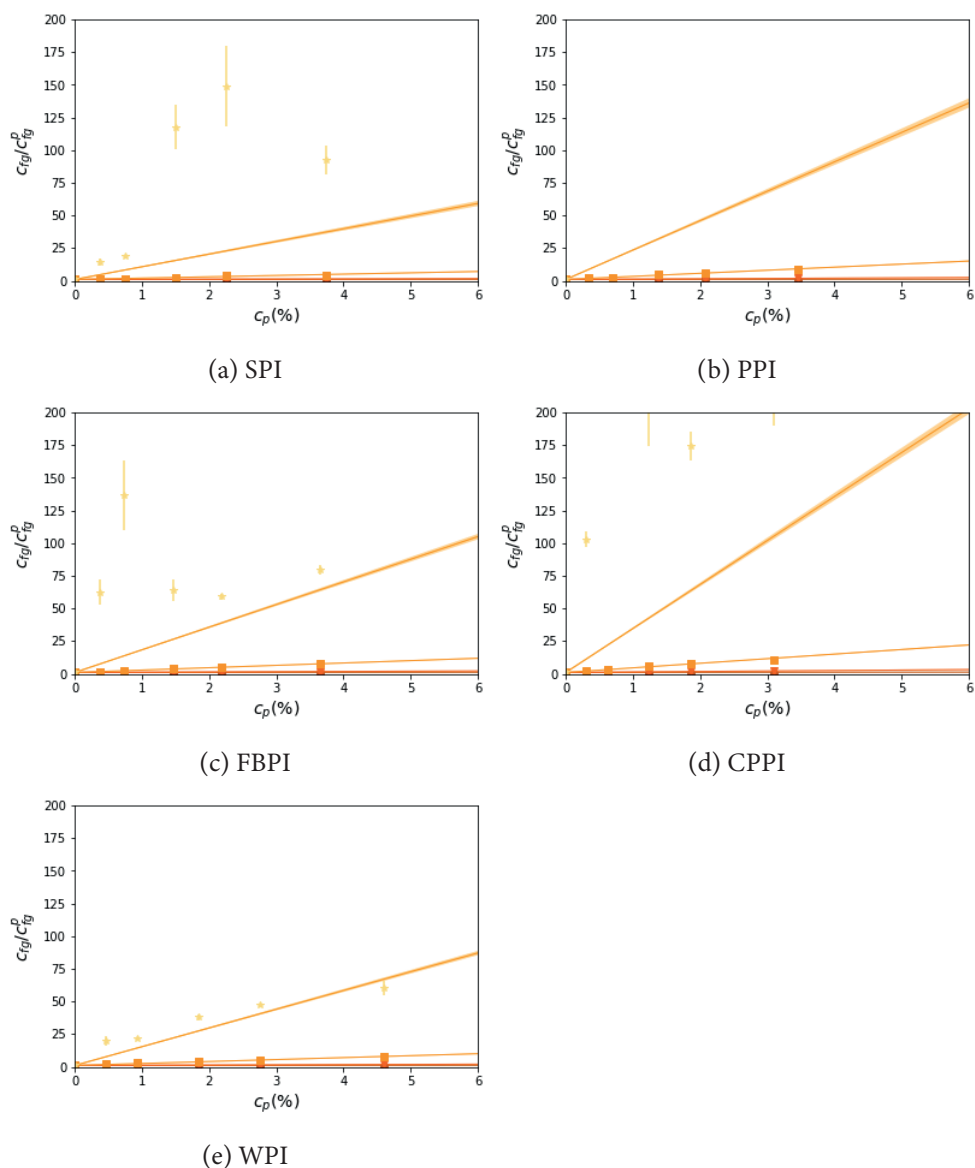
Figure A.2: c_{fg}/c_{fg}^p (headspace concentration of flavor in water/headspace concentration flavor in dispersion) measured with APCI-TOF-MS and model fits of esters as a function of SPI (a), PPI (b), FBPI (c), CPPI (d), and WPI (e) concentration. Colored lines represent the model fits of the experimental points for C4 (round), C6 (triangle), C8 (square), and C10 (stars). Methyl decanoate was predicted with fit parameter obtained with C4, C6, and C8. Colored areas around the line represent the uncertainty of the fitted parameter. Colored bars represent the standard deviation, n = 3

Table A.1: Correlation between hydrophobic index, solubility, pH, and amino acid content of pea, soy, fava bean, and chickpea and their model parameters obtained from fitting the flavor retention model on experimental data. The model parameter is the hydrophobic interaction parameter (a_p) for esters and ketones.

	a_p **Esters**	a_p **Ketones**
a_p	1	1
AUC_rel	-0.09	-0.11
AUC	-0.08	-0.08
hydrophobic.index	0.71	0.74
solubility	-0.68	-0.56
pH	-0.25	-0.42
Ratio	0.17	0.53
Alanine	-0.99	-0.93
Arginine	-0.33	-0.55
Aspartic.acid	-0.98	-0.95
Cystine	-0.66	-0.37
Glutamic.acid	-1	-0.88
Glycine	-0.98	-0.95
Histidine	-0.98	-0.88
Isoleucine	-0.97	-0.96
Leucine	-0.86	-0.94
Lysine	-0.56	-0.87
Methionine	-0.16	0.21
Phenylalanine	0.27	0.48
Proline	-0.97	-0.73
Serine	-0.93	-0.87
Threonine	-0.99	-0.93
Tryptophan	-0.92	-0.65
Tyrosine	-0.93	-0.99
Valine	-0.89	-0.99

5

Table A.2: Fitting results of esters and ketones for soy, yellow pea, fava bean, chickpea, and whey protein isolates, using the flavor partitioning model and P_{ow}^f. Model parameters are the hydrophobic interaction parameter a_p the corresponding residuals squared R^2, and the uncertainty of the parameter a_p

Protein source	Compound	a_p $(10^{-4}\,L/g)$	R^2	Uncertainty a_p $(10^{-4}\,L/g)$
SPI	MeButanoate	0.00	0.00	2.28E+01
	MeHexanoate	0.64	0.71	1.73E+01
	MeOctanoate	0.48	0.87	5.41E+01
	MeDecanoate	1.96	0.28	5.98E+03
PPI	MeButanoate	0.00	0.00	2.04E+01
	MeHexanoate	1.64	0.00	3.80E+01
	MeOctanoate	1.12	0.91	9.85E+01
	MeDecanoate	12.67	0.46	2.71E+04
FBPI	MeButanoate	0.00	0.00	2.51E+01
	MeHexanoate	0.57	0.74	8.20E+00
	MeOctanoate	0.87	0.96	5.49E+01
	MeDecanoate	1.50	0.00	7.71E+03
CKPI	MeButanoate	0.00	0.00	2.92E+01
	MeHexanoate	2.08	0.76	3.10E+01
	MeOctanoate	1.68	0.94	1.22E+02
	MeDecanoate	4.78	0.00	1.78E+04
WPI	MeButanoate	0.00	-0.29	1.19E+01
	MeHexanoate	0.88	0.89	1.16E+01
	MeOctanoate	0.71	0.95	4.61E+01
	MeDecanoate	0.74	0.66	9.43E+02
SPI	Butanone	0.00	0.00	8.97E+00
	Hexanone	4.95	0.70	1.15E+01
	Octanone	1.88	0.96	9.01E+00
	Decanone	1.64	1.00	2.87E+01
PPI	Butanone	0.00	0.00	1.20E+01
	Hexanone	5.32	0.60	1.29E+01
	Octanone	2.50	0.97	1.02E+01
	Decanone	2.47	1.00	2.84E+01
FBPI	Butanone	0.00	0.00	8.48E+00
	Hexanone	4.56	0.68	1.05E+01
	Octanone	2.66	0.95	1.65E+01
	Decanone	2.30	0.99	5.56E+01

Protein source	Compound	a_p $(10^{-4}\,\text{L/g})$	R^2	Uncertainty a_p $(10^{-4}\,\text{L/g})$
CKPI	Butanone	0.00	0.00	7.29E+00
	Hexanone	3.93	0.20	1.11E+01
	Octanone	5.67	0.99	1.15E+01
	Decanone	29.16	0.95	1.62E+03
WPI	Butanone	0.00	0.00	6.82E+00
	Hexanone	4.34	0.77	7.17E+00
	Octanone	2.08	0.98	7.80E+00
	Decanone	2.23	1.00	3.84E+01

5

References

Alexander, P., Brown, C., Arneth, A., Dias, C., Finnigan, J., Moran, D., & Rounsevell, M. D. A. (2017). Could consumption of insects, cultured meat or imitation meat reduce global agricultural land use? *Global Food Security*, *15*(January), 22–32. https://doi.org/10.1016/j.gfs.2017.04.001

Amagliani, L., O'Regan, J., Kelly, A. L., & O'Mahony, J. A. (2017). Composition and protein profile analysis of rice protein ingredients. *Journal of Food Composition and Analysis*, *59*, 18–26. https://doi.org/10.1016/j.jfca.2016.12.026

Anantharamkrishnan, V., Hoye, T., & Reineccius, G. A. (2020). Covalent Adduct Formation between Flavor Compounds of Various Functional Group Classes and the Model Protein β-Lactoglobulin. *Journal of Agricultural and Food Chemistry*, *68*(23), 6395–6402. https://doi.org/10.1021/acs.jafc.0c01925

Anantharamkrishnan, V., & Reineccius, G. A. (2020a). Influence of pH, Temperature, and Water Activity on Covalent Adduct Formation between Selected Flavor Compounds and Model Protein β-Lactoglobulin. *Journal of Agricultural and Food Chemistry*, *68*(47), 13833–13843. https://doi.org/10.1021/acs.jafc.0c06752

Anantharamkrishnan, V., & Reineccius, G. A. (2020b). Method to Characterize and Monitor Covalent Interactions of Flavor Compounds with β-Lactoglobulin Using Mass Spectrometry and Proteomics. *Journal of Agricultural and Food Chemistry*, *68*(46), 13121–13130. https://doi.org/10.1021/acs.jafc.9b07978

Bi, S., Pan, X., Zhang, W., Ma, Z., Lao, F., Shen, Q., & Wu, J. (2022). Non-covalent interactions of selected flavors with pea protein: Role of molecular structure of flavor compounds. *Food Chemistry*, *389*(17), 133044. https://doi.org/10.1016/j.foodchem.2022.133044

Bühler, J. M., Dekkers, B. L., Bruins, M. E., & Goot, A. J. Van Der. (2020). *Modifying Faba Bean Protein Concentrate Using Dry Heat to Increase Water Holding Capacity*. 1–16. https://doi.org/10.3390/foods9081077

Escher, F. E., Nuessli, J., & Conde-Petit, B. (2000). Interactions of Flavor Compounds with Starch in Food Processing. *ACS Symposium Series*, *763*, 230–245. https://doi.org/10.1021/bk-2000-0763.ch019

Gremli, H. A. (1974). Interaction of flavor compounds with soy protein. *Journal of the American Oil Chemists' Society*, *51*(1), 95–97. https://doi.org/10.1007/BF02542100

Guichard, E. (2002). Interactions between flavor compounds and food ingredients and their influence on flavor perception. *Food Reviews International*, *18*(1), 49–70. https://doi.org/10.1081/FRI-120003417

Harrison, M., & Hills, B. P. (1997). Mathematical Model of Flavor Release from Liquids Containing Aroma-Binding Macromolecules. *Journal of Agricultural and Food Chemistry*, *45*(5), 1883–1890. https://doi.org/10.1021/jf9607876

Heng, L., Van Koningsveld, G. A., Gruppen, H., Van Boekel, M. A. J. S., Vincken, J. P., Roozen, J. P., & Voragen, A. G. J. (2004). Protein-flavour interactions in relation to development of novel protein foods. In *Trends in Food Science and Technology* (Vol. 15, Issues 3–4, pp. 217–224). Elsevier Ltd. https://doi.org/10.1016/j.tifs.2003.09.018

Kühn, J., Zhu, X. Q., Considine, T., & Singh, H. (2007). Binding of 2-nonanone and milk proteins in aqueous model systems. *Journal of Agricultural and Food Chemistry*, *55*(9), 3599–3604. https://doi.org/10.1021/jf063517o

Kumar, P., Chatli, M. K., Mehta, N., Singh, P., Malav, O. P., & Verma, A. K. (2017). Meat analogues: Health promising sustainable meat substitutes. *Critical Reviews in Food Science and Nutrition*, *57*(5), 923–932. https://doi.org/10.1080/10408398.2014.939739

Kyriakopoulou, K., Keppler, J. K., & van der Goot, A. J. (2021). Functionality of ingredients and additives in plant-based meat analogues. *Foods*, *10*(3). https://doi.org/10.3390/foods10030600

Linforth, R. S. T., & Taylor, A. J. (1999). *Apparatus and methods for the analysis of trace constituents in gases* (Patent No. 5869344). United States Patent.

Ma, K. K., Grossmann, L., Nolden, A. A., McClements, D. J., & Kinchla, A. J. (2022). Functional and physical properties of commercial pulse proteins compared to soy derived protein. *Future Foods*, *6*(April), 100155. https://doi.org/10.1016/j.fufo.2022.100155

McClements, D. J., & Grossmann, L. (2021). The science of plant-based foods: Constructing next-generation meat,

fish, milk, and egg analogs. *Comprehensive Reviews in Food Science and Food Safety*, *20*(4), 4049–4100. https://doi.org/10.1111/1541-4337.12771

Michel, F., Hartmann, C., & Siegrist, M. (2021). Consumers' associations, perceptions and acceptance of meat and plant-based meat alternatives. *Food Quality and Preference*, *87*(August 2020), 104063. https://doi.org/10.1016/j.foodqual.2020.104063

Monera, O. D., Sereda, T. J., Zhou, N. E., Kay, C. M., & Hodges, R. S. (1995). Relationship of sidechain hydrophobicity and α-helical propensity on the stability of the single-stranded amphipathic α-helix. *Journal of Peptide Science*, *1*(5), 319–329. https://doi.org/10.1002/psc.310010507

Schmidtke, P., & Barril, X. (2010). Understanding and predicting druggability. A high-throughput method for detection of drug binding sites. *Journal of Medicinal Chemistry*, *53*(15), 5858–5867. https://doi.org/10.1021/jm100574m

Van Mierlo, K., Rohmer, S., & Gerdessen, J. C. (2017). A model for composing meat replacers: Reducing the environmental impact of our food consumption pattern while retaining its nutritional value. *Journal of Cleaner Production*, *165*, 930–950. https://doi.org/10.1016/j.jclepro.2017.07.098

Viry, O., Boom, R., Avison, S., Pascu, M., & Bodnár, I. (2018). A predictive model for flavor partitioning and protein-flavor interactions in fat-free dairy protein solutions. *Food Research International*, *109*(December 2017), 52–58. https://doi.org/10.1016/j.foodres.2018.04.013

Wang, H., Guan, H., Zhang, H., Liu, H., Chen, Q., & Kong, B. (2022). Elucidation of interaction mechanisms between myofibrillar proteins and ethyl octanoate by SPME-GC-MS, molecular docking and dynamics simulation. *Lwt*, *154*, 112787. https://doi.org/10.1016/j.lwt.2021.112787

Wang, K., & Arntfield, S. D. (2014). Binding of carbonyl flavours to canola, pea and wheat proteins using GC/MS approach. *Food Chemistry*, *157*, 364–372. https://doi.org/10.1016/j.foodchem.2014.02.042

Wang, K., & Arntfield, S. D. (2015). Binding of selected volatile flavour mixture to salt-extracted canola and pea proteins and effect of heat treatment on flavour binding. *Food Hydrocolloids*, *43*, 410–417. https://doi.org/10.1016/j.foodhyd.2014.06.011

Wang, K., & Arntfield, S. D. (2016). Probing the molecular forces involved in binding of selected volatile flavour compounds to salt-extracted pea proteins. *Food Chemistry*, *211*, 235–242. https://doi.org/10.1016/j.foodchem.2016.05.062

Zhou, Q., & Cadwallader, K. R. (2006). Effect of flavor compound chemical structure and environmental relative humidity on the binding of volatile flavor compounds to dehydrated soy protein isolates. *Journal of Agricultural and Food Chemistry*, *54*(5), 1838–1843. https://doi.org/10.1021/jf052269d

5

Chapter 6

Flavor-protein interactions for four plant proteins with aldehydes

Abstract

Aldehydes are important flavor molecules to consider in plant-based products. Here, the flavor retention of a series of saturated aldehydes and mono-unsaturated aldehydes (2-alkenals) with different chain lengths (C4, C6, C8, and C10) in dispersions with protein isolates of pea, soy, fava bean, chickpea, and whey (as reference) was analyzed with APCI-TOF-MS. The headspace concentrations of alkenals were lower than aldehydes, meaning alkenals were retained more than saturated aldehydes. The retention was modeled by assuming hydrophobic interactions and covalent interactions. The ratio between the hydrophobic interaction parameter and the covalent parameter showed that covalent interactions are mainly important for butanal and butenal (C4). For the other aldehydes, hydrophobic interactions became increasingly important. Correlations were found between the chemical interaction parameters and the cysteine and methionine content of the different proteins. The obtained model parameters for each set of proteins and flavors allow the prediction of flavor retention when developing a flavored product with high protein content.

6.1   Introduction

Diet patterns must change to be able to feed the growing world population in a sustainable matter (Aiking & de Boer, 2018; Broekema et al., 2020). A route to reach this goal is to replace meat and dairy with plant-based products. Nevertheless, plant-based products are considered less appealing by consumers, because of their taste and off-notes (Michel et al., 2021). Currently, a key success factor for plant products that should replace meat is a high similarity in texture, taste, and nutritional value. To reach similarity in taste, flavors are added to plant-based products. However, these products often contain a high protein content and flavors can strongly interact with these proteins (Guichard, 2002). Protein-flavor retention is mostly hydrophobic, but depending on the type of flavor also irreversible covalent interactions, reversible hydrogen bonds, ionic bonds, and Van der Waal's forces can lead to flavor retention (K. Wang & Arntfield, 2014). Aldehydes, for example, can interact covalently with the amine or thiol groups of the proteins, apart from hydrophobic interactions (Anantharamkrishnan & Reineccius, 2020b). Aldehydes can react in Schiff base formation, whereas alkenals are also capable of forming Michael adducts (Anantharamkrishnan et al., 2020).

An efficient route to determine flavor retention is through comparing the equilibrium headspace concentration in a flavored protein dispersion to a control without protein (Gremli, 1974; K. Wang & Arntfield, 2015a; Zhou & Cadwallader, 2006). However, this approach is time-consuming and therefore often only a few chemicals are studied, which makes it challenging to get a full overview of flavor retention in protein products.

A more pragmatic method is to model experimental data to predict flavor partitioning. Harrison & Hills (1997) developed a mathematical model to predict flavor release for both hydrophilic and hydrophobic compounds from a liquid containing macromolecules (Harrison & Hills, 1997). This model was applied to describe flavor retention in whey and sodium caseinate dispersions (Viry et al., 2018). For esters and alcohols, good predictions were obtained by only assuming hydrophobic interactions to explain flavor retention (Viry et al., 2018). For aldehydes, stronger retention was observed, which was attributed to the specific covalent interactions that proteins and aldehydes can undergo (Viry et al., 2018). Therefore, the model was extended with a covalent interaction parameter to describe aldehyde retention (Viry et al., 2018). Recently, this model was applied to predict flavor retention in four plant proteins and whey dispersions with esters, and ketones, assuming hydrophobic interactions only (Snel et al., 2023). Apart from esters and ketones, aldehdyes are an important chemical class to consider for flavoring of plant-based products such as meat analogues. Therefore, probing the interactions between plant proteins and aldehydes is essential and could give great insights in the applicability of the model when covalent interactions are involved. Furthermore, it would highlight the relative contribution of hydrophobic and covalent interactions for aldehyde retention.

This study describes the retention of aldehydes by plant proteins and applies a flavor partitioning model to analyze the results. The proteins studied are pea protein isolate (PPI),

soy protein isolate (SPI), chickpea protein isolate (CPPI), and fava bean protein isolate (FBPI). Besides, whey protein isolate (WPI) will be included as a control. The investigated flavors include a series (C4, C6, C8, C10) of saturated aldehydes and 2-mono-unsaturated aldehydes (alkenals), from now on addressed as aldehydes and alkenals. Furthermore, the obtained partitioning parameters will be correlated with amino acid composition.

6.2 Theory: flavor partitioning models

Harrison & Hills (1997) developed a mathematical model to predict flavor release from an aqueous solution containing polymers. In the case of proteins, flavors can interact with the proteins through either hydrophobic interactions or specific covalent interactions. The flavor-partitioning model will be shortly summarized here. The partition coefficient (K_{wg}^{f}) at equilibrium between flavor concentration in the water phase (c_{fw}^{e}) and gas phase (c_{fg}^{e}) is defined as:

$$K_{wg}^{f} = \frac{c_{fg}^{e}}{c_{fw}^{e}}$$ 6.1

When protein is added to the water phase, part of the flavors could interact with the protein. When we consider that the flavor-protein interaction is a reversible, first-order reaction, the global interaction constant (K_{p}^{f}) between protein P and flavor F is defined as:

$$K_{p}^{f} = \frac{c_{fp}^{e}}{c_{p}^{e} c_{fw}^{e}}$$ 6.2

in which c_{fp}^{e} and c_{p}^{e} are the concentrations of protein-retained flavor in the dispersion at equilibrium, and protein. Since in the experimental set-up protein concentration exceeds the flavor concentration largely, c_{p}^{e} is simplified as the total concentration of protein in the dispersion that thus remains constant during the experiment. Now, the effective partition coefficient K_{wg}^{eff} between flavor in the gas phase and the water-protein phase becomes:

$$K_{wg}^{eff} = \frac{c_{fg}^{e}}{c_{ft}^{e}}$$ 6.3

in which c_{ft}^{e} is the total flavor in the water system. The mass balance reads:

$$c_{ft} = c_{fp} + c_{fw}$$ 6.4

In which c_{ft} equals c_{fw} when no protein is present in the water phase. Using the mass balance and eq. 6.1 and eq. 6.2, we can describe K_{wg}^{eff} as:

$$K_{wg}^{eff} = \frac{K_{wg}^{f}}{1 + K_{p}^{f} c_{p}^{e}}$$ 6.5

When flavor retention is dominated by hydrophobic interactions, we could approach the interaction constant with:

$$K_p^f = a_p P_{ow}^f \qquad\qquad 6.6$$

in which a_p and P_{ow}^f are the hydrophobic interaction parameter and the octanol-water partition coefficient. For aldehydes, the covalent interaction has to be taken into account, leading to (Viry et al., 2018):

$$K_p^f = a_p P_{ow}^f + K_{Ald} \qquad\qquad 6.7$$

in which K_{Ald} is the covalent interaction parameter between aldehydes and proteins. For alkenals, this parameter becomes K_{Alk}. Aldehydes can interact with proteins through a condensation reaction (Schiff base adduct), and alkenals can have an additional conjugate addition (Michael adduct, Figure 6.1) (Anantharamkrishnan et al., 2020). The total contribution of both reactions is captured in the parameters K_{Ald} or K_{Alk}.

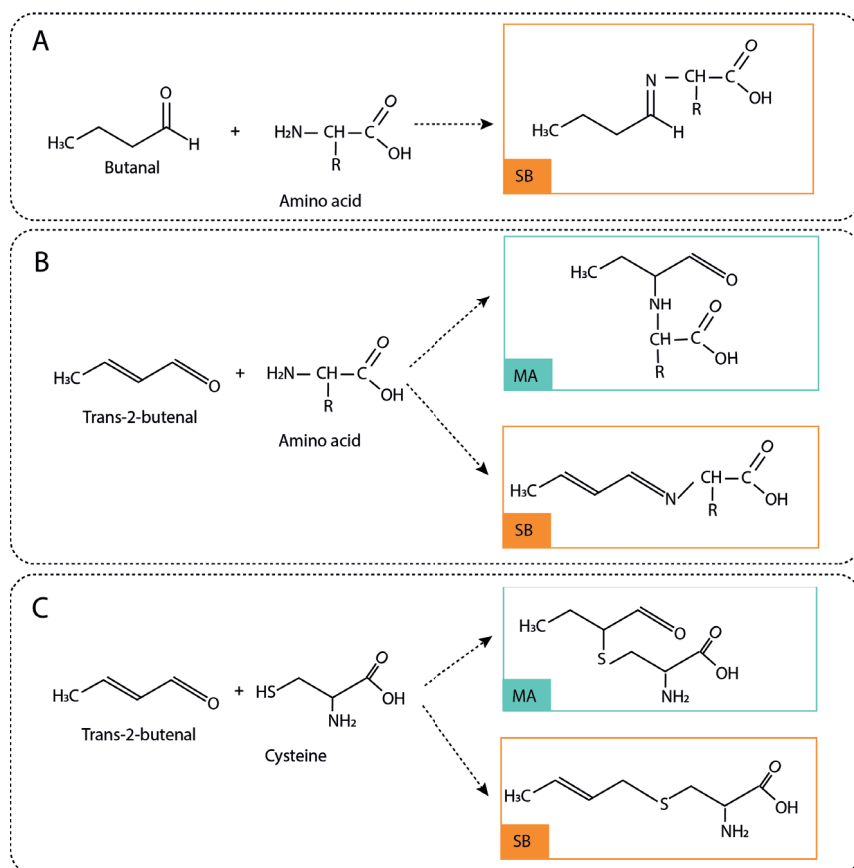*Figure 6.1: Schematical representation of the chemical reactions possible between the amine group of amino acids and butanal (A), and trans-2-butenal (B), and the thiol group of cysteine with trans-2-butenal (C) (Anantharamkrishnan & Reineccius, 2020a). Butanal and trans-2-butenal are chosen in this example to represent aldehydes and alkenals respectively. SB = schiff base, MA = michael adduct.*

6.3   Methods and Materials

6.3.1   Materials

Soy protein isolate (SPI, Supro® 500E A) was obtained from Solae (St. Louis, United States). Pea protein isolate (PPI, Nutralys® F85M) was obtained from Roquette Frères S.A. (Lestrem, France). Fava bean protein isolate (FBPI, FFBP-90-C-EU) and chickpea protein isolate (CPPI, FCPP-70) were both obtained from AGT Foods (Regina, Canada). Whey protein isolate (WPI, BiPRO) was obtained from Davisco Foods International (Minnesota, USA). Amino acid content was measured in a previous study with the same protein isolates, and used to measure protein content (Snel et al., 2023). Furthermore, solubility, pH, and moisture content were measured (Table 6.2). Trans-2-butenal and ethanol were purchased from Sigma-Aldrich (St. Louis, USA). The other flavors listed in Table 6.3 were provided by Firmenich S.A.

Table 6.1: Weighted hydrophobic indexes (WHI), protein content, pH, solubility, and moisture content of soy, pea, faba bean, chickpea and whey protein isolates. Values are means ± standard deviations, letters indicate significant groups (p ≤ 0.05). Amino acids were measured in duplicate, and the protein content, pH, solubility, and moisture content in triplicate. WHI's are a summation of the amino acid weight multiplied by the hydrophobic index.

	Soy	**Yellow pea**	**Faba bean**	**Chickpea**	**Whey** [1]
WHI	147.35 ±0.63 [b]	149.41 ±0.09 [ab]	143.22 ± 1.69 [c]	152.28 ±0.91 [a]	236.18
Protein (g/100g)	83.25 ± 2.77 [a]	77.11 ± 0.29 [b]	80.42 ± 2.99 [ab]	67.03 ±1.83 [c]	89.7
pH	7.1 ±0.01[c]	7.5 ±0.01 [a]	6.4 ±0.02 [e]	6.6 ±0.01 [d]	7.1 ±0.02 [b]
Solubility (g/g)	0.59 ±0.01 [b]	0.41 ± 0.03 [c]	0.12 ±0.01 [d]	0.12 ± 0.00 [d]	1.02 ± 0.00 [a]
Moisture content (g/100g)	8.8 ± 0.0	8.1 ±0.0	8.0 ± 0.1	6.6 ± 0.1	5.2 ± 0.1

[1] *WHI calculated with amino acid composition taken from (Amagliani et al., 2017)*

6.3.2   Preparation flavored protein dispersions

Stock solutions of 50 g/kg were made for each protein and subsequently diluted to obtain dispersions of 5, 10, 20, 30, and 50 g/kg for each protein isolate (in demineralised water). The protein content in the dispersion was then corrected using the protein content and dry matter content. Each flavor compound was first diluted in ethanol, to ensure solubility, and then added to the protein dispersion to reach a concentration in a range from 0.05 to 1.00 mg/kg, depending on their spectra intensity. The flavored dispersions were then vortexed for 30 s. The presence of ethanol in the final solution (1 g/kg) did not affect the MS signal. The mixture was allowed to reach equilibrium for 24h at 21°C.

Table 6.2: *Aldehydes studied with their molecular weight (MW), solubility and octanol-water partition coefficient (Log P), and the concentration in the flavored protein dispersions (mg/kg)*

Name	MW (g/mol)[1]	Solubility (mg/kg)[1]	Log P[1]	Concentration (mg/kg)
Butanal	72.11	23850	0.60	1.00
Hexanal	100.16	3527	1.80	0.75
Octanal	128.22	394	2.78	0.25
Decanal	156.27	43.5	3.76	0.05
Trans-2-butenal	70.09	41480	0.60	5.00
Trans-2-hexenal	98.15	5261	1.58	1.00
Trans-2-octenal	126.2	612	2.57	0.75
Trans-2-decenal	154.25	67.8	3.55	0.50

[1] *Software EPIWEB v4.1, KOWWIN v1.68*

6.3.3 Static headspace measurements

The headspace concentrations were measured as independent triplicates with a G2-XS Q-TOF high definition mass spectrometer (XEVO, Waters, Milford, United States) coupled to a patented Venturi interface (Linforth & Taylor, 1999). An automated PAL system injected 5 mL of the headspace into the mass spectrometer. Mass spectra were collected in centroid mode over the range m/z 20-400 every 1 s. APCI-MS was performed in positive ionization mode with cone voltage of 4.0 kV, source temperature of 105 °C, heated sample transfer line temperature of 130 °C and auxiliary gas flow of 600 L/h. Lock spray (on-the-fly mass calibration) was used to apply a mass correction to measured m/z values during the analysis. All the signal intensities were corrected for the background addition. The relative headspace concentration (RHC) was approximated as:

$$RHC\% = \frac{Peak\ area_{flavored\ dispersion}}{Peak\ area_{flavor\ in\ water}} * 100 \qquad 6.8$$

6

6.3.4 Model fitting

The experimental results were described with the flavor partitioning model (eq 6.5). The relative headspace can be interpreted as $\frac{c_{fg}}{c_{fg}^p}$, since we can assume that $c_{ft} = c_{fw}$ when no protein is added to the dispersion. Equations 6.5 and 6.7 can be combined and rewritten to obtain a linear relation:

$$RHC = \frac{K_{wg}^{eff}}{K_{wg}^f} = \frac{c_{fg}}{c_{fg}^p} = 1 + \left(a_p P_{ow}^f + K_{ald}\right) c_p \qquad 6.9$$

For the alkenals, K_{ald} becomes K_{alk}. The calculated octanol-water partition coefficient was obtained from EPIWEB. The c_p was taken as the concentration of protein, thus corrected with the dry matter and protein content for each isolate. Since in eq 6.9 the slope parameters a_p and K_{ald} can not be extracted as independent parameters, it was chosen to only fit K_{ald}. The a_p was based on previously obtained fitting parameters for esters, for which only hydrophobic interactions were assumed (Snel et al., 2023). These a_p values were 4.8E-5, 1.1E-4, 8.6E-5, 1.7E-4, and 7.2E-5 g/L for SPI, PPI, FBPI, CPPI, and WPI respectively. The fitting was done for each protein and each aldehyde separately. The fitting was performed with Python and the SciPy package. This resulted in a prediction for K_{ald} or K_{alk} and the uncertainties for these predictions. Residuals squared were calculated as the squared Pearson correlation coefficient, which was calculated with the sciPy.stats package. A ratio between K_{ald} or K_{alk} and the hydrophobic contribution was calculated as:

$$Ratio = \frac{K_{ald}}{a_p P_{ow}^f} \qquad 6.10$$

6.3.5 Statistical Analysis

Statistical analysis was performed with R. Normality was tested with descriptive statistics. When the data were normally distributed, a one-way analysis of variance (ANOVA) was done to test if the observed differences between samples were significant. Multiple comparison Tukey tests were done to indicate which treatments were significantly different from each other.

6.4   Results

6.4.1 Influence of protein concentration on flavor retention

The relative headspace concentration (RHC) of aldehydes was measured as a function of protein concentration for SPI, PPI, FBPI, CPPI, and WPI (Figure 6.2). A decrease in RHC is interpreted as an increase in flavor retention. Protein concentrations were corrected with the known protein and moisture content of each protein isolate. The residual polysaccharides are assumed to have only negligible nonspecific molecular interactions (Guichard, 2002).

The RHC of the aldehydes decreased with increasing protein concentration. Furthermore, the RHC decreased when the molecular weight of the aldehydes increased (Table 6.3). The

RHCs of butanal and hexanal were around 90% at low protein concentrations but decreased with increasing protein concentration. Butanal was more retained by FBPI and WPI. Hexanal was also highly retained by FBPI, but less by WPI, and more by CPPI. The RHCs of octanal were around 40-50% at the lowest protein concentrations tested (3-4 g/kg) and decreased with increasing protein concentration. The exception was FBPI, which had an RHC as low as 6.1% at 4 g/kg protein, which first increased slightly at 7 g/kg, followed by a decrease. Decanal had RHCs around 10-20% at low protein concentration, with a lower value for FBPI (1.7%). Both octanal and decanal were more retained by the plant proteins than by WPI.

The RHC of alkenals also depended on protein concentration and octanol-water partition coefficient, and retention was larger compared to the aldehydes. Butenal was more retained than butanal, especially at higher protein concentrations. Butenal was retained the most by SPI. The retention of hexenal and octenal was again higher compared to hexanal and octanal. Hexenal was again more retained by SPI. Octenal was especially highly retained by CPPI, based on the fact that RHC approached 0. Lastly, RHCs of decenal were around 10% and decreased to approximately 0% when protein concentration was increased. Again for CPPI the RHC of decenal was lower compared to the other proteins. Decenal was least retained by FBPI and WPI.

The retention of the alkenals was higher than the retention of aldehydes. Furthermore, the retention increased with the molecular weight of the aldehydes. Differences between flavors were more important than differences between proteins, though differences were observed. Both classes of aldehydes were more retained than the esters and ketones tested in a previous study (Snel et al., 2023).
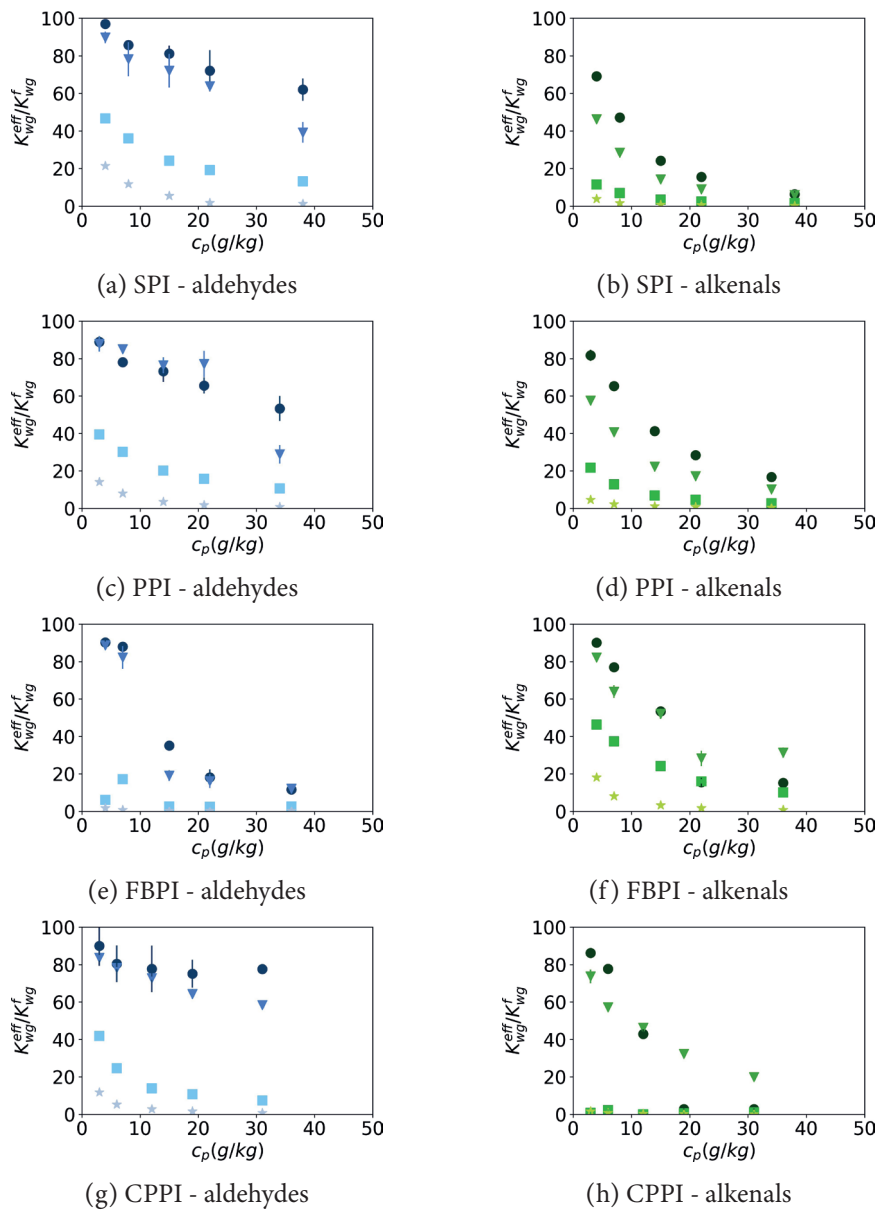
6

(a) SPI - aldehydes

(b) SPI - alkenals

(c) PPI - aldehydes

(d) PPI - alkenals

(e) FBPI - aldehydes

(f) FBPI - alkenals

(g) CPPI - aldehydes

(h) CPPI - alkenals

Figure 6.2 (continued)
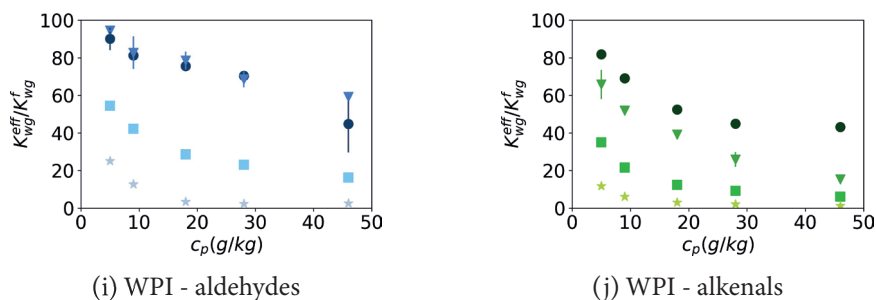
(i) WPI - aldehydes (j) WPI - alkenals

Figure 6.2: K_{wg}^{eff}/K_{wg}^{f} (peak area flavor in dispersion/peak area flavor in water) measured with atmospheric pressure chemical ionization time-of-flight mass spectroscopy of aldehydes (a, c, e, g, blue), and alkenals (b, d, f, h, green) as a function of SPI (a, b), PPI (c, d), FBPI (e, f), CPPI (g, h), and WPI (i, j) concentration. Protein concentration, c_p is the concentration of the isolate corrected for its protein and moisture content. Values are averages for butanal/ butenal (round), hexanal/hexenal (triangle), octanal/octenal (square), and decanal/decenal (star). Colored bars represent the standard error, n = 3.

6.4.2 Flavor partitioning models

Experimental data obtained for aldehydes and alkenals were fitted with eq 6.9 (Figure 6.3). This resulted in fitted values for the chemical interaction parameters K_{ald} and K_{alk} (Table 6.3). It was found that each combination of flavor and protein led to different values for the fitting parameter. It was observed that the fitted values for K_{ald} increased with increasing chain length. The fitted values for K_{ald} for decanal were even a factor of 100 higher than butanal for the plant proteins. For WPI, a factor of 20 was observed. The fitted values for K_{ald} for WPI were the lowest, followed by SPI, PPI/CPPI, and FBPI. The fitted K_{ald} for FBPI was around 10x higher compared to the other proteins. The ratio between K_{ald} and the hydrophobic interactions ($a_p P_{ow}^{f}$) was calculated to illustrate their relative contribution (Table 6.3). Butanal had the highest ratio of aldehydes for each protein. It seemed that for the aldehydes with a chain length longer than 4, the ratio between the binding effect of hydrophobic interactions ($a_p P_{ow}^{f}$) and the covalent binding (K_{ald} or K_{alk}) remained in the same order of magnitude. For WPI, this ratio even remained constant at 2, meaning that the ratio between covalent and hydrophobic interactions was 2:1.

The fitted values for K_{alk} were higher than the values found for K_{ald}, except for FBPI (Table 6.3). As seen for the aldehydes, an increase was seen for K_{alk} with increasing chain length, except for CPPI and FBPI with hexenal, which decreased compared to butenal.

WPI had the lowest fit values for K_{alk} overall, followed by FBPI, PPI, SPI, and CPPI. The ratio between covalent and hydrophobic interactions was highest for butenal, and higher compared to the ratio for the aldehydes. For the alkenals with longer chain lengths, the ratio remained in the same order of magnitude. The high retention of octenal and decenal by CPPI resulted in very low headspace concentrations (Figure 6.2h). This concentration was close to the detection limit of the APCI-TOF-MS, which might explain the high uncertainties for CPPI (Table 6.3, Figure 6.3h).

Table 6.3 Fitting results of aldehydes and alkenals for soy (SPI), yellow pea (PPI), faba bean (FBPI), chickpea (CPPI) and whey (WPI) protein isolates, using the flavor partitioning model. Model parameters are the covalent interaction parameters K_{ald} and K_{alk} for aldehydes and alkenals respectively, and their corresponding residuals squared R^2. Values are reported as fit value ± uncertainty of the fitted parameter (n=3). The ratio between the covalent interaction parameter and hydrophobic interactions is calculated as: $\dfrac{K_{ald}}{a_p P_{ow}^f}$ in which a_p is the hydrophobic interaction parameter per protein and P_{ow}^f the octanol-water partition coefficient of the flavor.

Protein	Aldehyde	K_{ald} (10^{-2} L/g)	R^2	Ratio
SPI	Butanal	0.17 ± 0.01	0.78	87
	Hexanal	0.34 ± 0.03	0.84	11
	Octanal	1.55 ± 0.05	1.00	5
	Decanal	17.88 ± 1.29	0.91	6
PPI	Butanal	0.26 ± 0.02	0.86	58
	Hexanal	0.46 ± 0.08	0.73	7
	Octanal	1.88 ± 0.06	1.00	3
	Decanal	27.03 ± 2.28	0.93	4
FBPI	Butanal	1.96 ± 0.13	0.94	569
	Hexanal	2.12 ± 0.16	0.85	39
	Octanal	13.56 ± 1.56	0.55	26
	Decanal	126.94 ± 13.68	0.60	25
CPPI	Butanal	0.13 ± 0.03	0.10	20
	Hexanal	0.16 ± 0.02	0.96	1
	Octanal	3.24 ± 0.10	0.98	3
	Decanal	25.45 ± 1.04	0.98	3
WPI	Butanal	0.26 ± 0.04	0.55	91
	Hexanal	0.11 ± 0.01	0.88	2
	Octanal	0.75 ± 0.03	1.00	2
	Decanal	6.51 ± 1.01	0.68	2

Alkenal	K_{alk} (10^{-2} L/g)	R^2	Ratio
Butenal	3.40 ± 0.30	0.88	1758
Hexenal	4.40 ± 0.23	0.91	237
Octenal	17.13 ± 0.25	0.99	96
Decenal	95.64 ± 2.87	0.98	56
Butenal	1.32 ± 0.05	0.99	295
Hexenal	2.46 ± 0.05	0.99	57
Octenal	9.81 ± 0.12	0.99	24
Decenal	60.95 ± 1.36	0.98	15
Butenal	1.64 ± 0.17	0.78	476
Hexenal	0.71 ± 0.07	0.69	21
Octenal	2.09 ± 0.05	0.98	7
Decenal	27.40 ± 1.70	0.96	9
Butenal	11.46 ± 1.39	0.76	1709
Hexenal	1.15 ± 0.03	0.98	18
Octenal	112.86 ± 58.56	0.01	183
Decenal	429.36 ± 62.14	0.64	72
Butenal	0.35 ± 0.02	0.84	122
Hexenal	1.10 ± 0.04	0.96	40
Octenal	3.21 ± 0.06	0.99	12
Decenal	14.56 ± 0.15	1.00	6
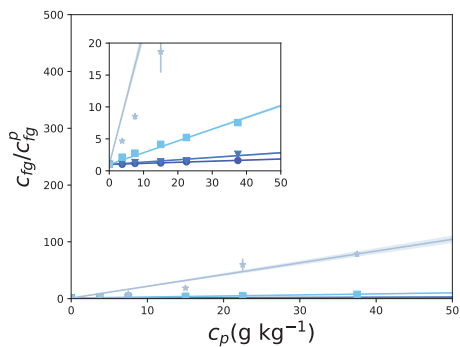
6
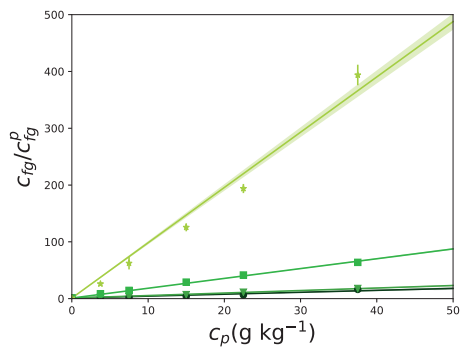
(a) SPI - aldehydes
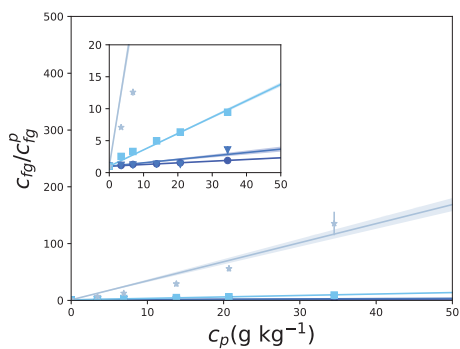
(b) SPI - alkenals
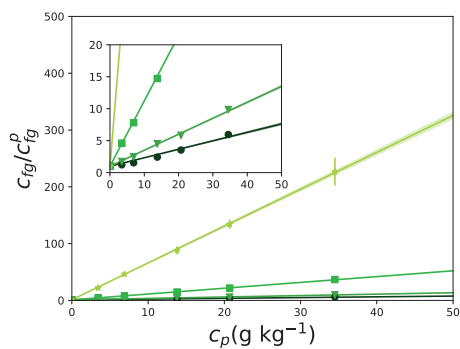
(c) PPI - aldehydes
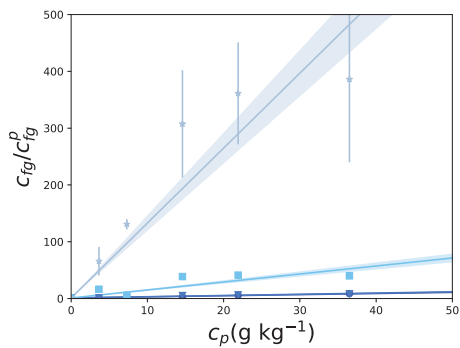
(d) PPI - alkenals

(e) FBPI - aldehydes
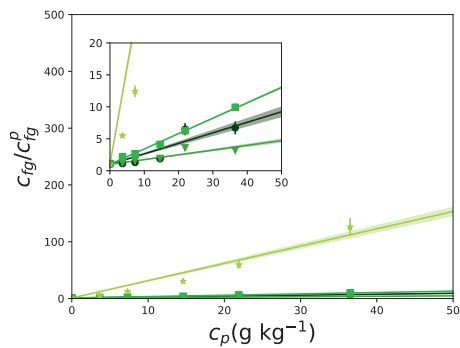
(f) FBPI - alkenals

Figure 6.3 (continued)

(g) CPPI - aldehydes

(h) CPPI - alkenals

(i) WPI - aldehydes

(j) WPI - alkenals
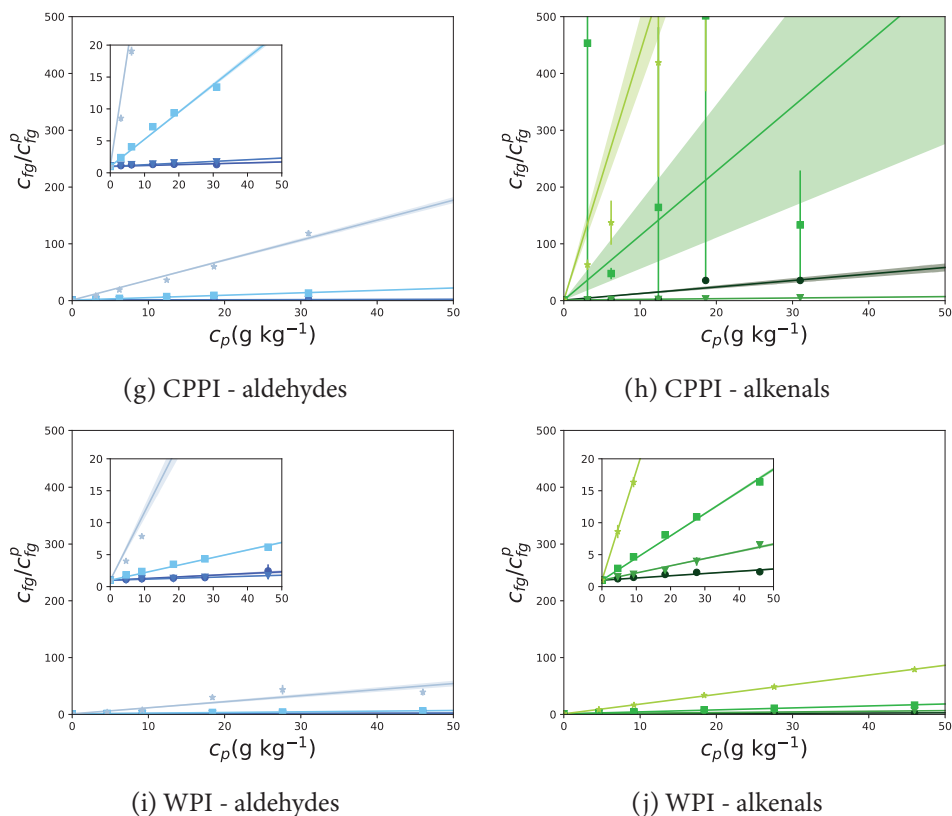
Figure 6.3: c_{fg}/c_{fg}^p *(headspace concentration of flavor in water/headspace concentration flavor in dispersion) measured with atmospheric pressure chemical ionization time-of-flight mass spectroscopy and model fits of aldehydes (a, c, e, g, blue), and alkenals (b, d, f, h, green) as a function of soy (a, b), yellow pea (c, d), fava bean (e, f), chickpea (g,h), and whey (i,j) protein isolate concentrations. Lines represent the model fits of the experimental points for butanal/ butenal (round), hexanal/hexenal (triangle), octanal/octenal (square), and decanal/decenal (star). Colored areas represent uncertainties of the fitted parameters. Colored bars represent the standard error, n = 3. Zoomed-in graphs are included for some graphs.*

6

137

6.4.3 Correlation between amino acid contents and covalent interaction parameters

In a previous study, a complete amino acid profile for the plant proteins was obtained (Snel et al., 2023). To assess whether the amino acid composition could be linked to the retention of aldehydes by proteins, a Pearson test of correlation was performed (Appendix A.1).

The fitted parameter for alkenals, K_{alk} correlated positively with methionine content: 75, 43, 73, and 75% for butenal, hexenal, octenal, and decenal respectively. A smaller positive correlation was found with cysteine content, 30, 84, 26, and 29%. Cysteine and methionine contain a thiol group that can react covalently (Figure 6.1). The thiol group of cysteine has been shown previously to react with aldehydes by forming both Schiff bases and Michael adducts (Hamzalıoğlu & Gökmen, 2018). Methionine can react with 4-hydroxy-trans-2-nonenal (Baker et al., 1998). Fitted values for K_{ald} strongly correlated negatively with cysteine and methionine content (around -80% correlation). This could indicate that other amino acids are more likely to form Schiff bases. Meynier et al. (2004) studied hexanal and hexenal interactions with WPI and caseinate and showed that lysine residues decreased upon both hexanal and hexenal addition, while histidine residues reduced only with hexenal addition. Cysteine and methionine content were not measured, due to limitations of using reversed-phase chromatography to measure amino acids (Meynier et al., 2004).

The fitted parameter K_{ald} showed a slight correlation with histidine content (59, 58, 57, 55%), but no clear correlation with lysine content. Apart from histidine, K_{ald} correlated with arginine (61-73%), leucine (86-89%), and valine content (51-78%). When excluding the hexenal correlations, K_{alk} correlated with alanine (92-95%), aspartic acid (84-90%), phenylalanine (91-95%), and serine content (66-69%). K_{alk} for hexenal did not show the same correlations. This might be a result of the lower value for K_{alk} for CPPI-hexenal and FBPI-hexenal, compared to the K_{alk} for CPPI-butenal and FBPI-butenal.

6.5 Discussion

The headspace concentrations of aldehydes and alkenals with different chain lengths were measured at varying protein concentrations for four different plant proteins and whey. These results were then described with a flavor retention model, using the octanol-water partition coefficients of the flavors, the hydrophobic interaction parameter of the esters, and fitting a covalent interaction parameter for SPI, PPI, FBPI, CPPI, and WPI. Most of the interactions between aldehydes and alkenals with the tested proteins were well described and thus the obtained fitted parameters could be used as a predictive tool. An increased protein concentration resulted in increased flavor retention. Furthermore, an increase in chain length, related to hydrophobicity, of the aldehydes also increased flavor retention. Lastly, alkenals were more bound than aldehydes for the proteins tested in this study.

Wang & Arntfield (2014) found that octanal was 68 % bound to a 10 g/kg PPI dispersion. We found a similar value based on headspace concentrations of 70 % for octanal in a 7 g/kg PPI dispersion. Gremli (1974) showed that hexenal and decenal were more strongly retained than

hexanal and decanal, which is in line with our findings. We observed stronger retention of the alkenals compared to the aldehydes, which can be possibly related to the type of covalent interactions that these chemical classes can undergo. Apart from a Schiff base reaction, alkenals can furthermore form a Michael adduct with nucleophilic sites in proteins (Figure 6.1).

The different proteins tested showed some differences in their retention of aldehydes and alkenals. The smaller flavors, butanal, and butenal, were retained to a higher extent by WPI at low protein concentrations. However, with increasing protein concentration, butenal was more retained by the plant proteins. For the other flavors, higher retention was observed for the plant proteins, especially for chain lengths of 8 and 10. However, in comparison, the effects of flavor on flavor retention were more pronounced than the effect of protein source, although both had an effect. This was observed before for aldehydes when comparing canola, pea, and wheat gluten isolates (K. Wang & Arntfield, 2014). Wang & Arntfield (2014) did see differences between the protein sources, but the effect of the flavor was more pronounced.

A flavor-partition model was used to describe the data. In the model, both the hydrophobic and covalent interaction parameters scale linearly with the protein concentration according to eq. 6.9. It was thus decided to only model the covalent interaction parameter and keep the hydrophobic parameter constant. The hydrophobic parameter was set with obtained fits for the same proteins with esters, which are considered to be retained by hydrophobic interactions only (Snel et al., 2023). The increase in retention of aldehydes with increasing chain length is often attributed to an increase in hydrophobic interactions (Tan & Siebert, 2008; Weel et al., 2003). The observed increase in the covalent interaction parameter in this study suggests that chain length also affects the degree of covalent interactions.

However, when comparing the ratio of hydrophobic interactions to covalent interactions, it was clear that the covalent interactions determine to a larger extent the retention of smaller flavor molecules. Hydrophobic interactions for butenal and butanal seem less important when assuming a constant hydrophobic interaction parameter. For larger flavor molecules, hydrophobic interactions became more important, but still, covalent interactions contributed to a high extent, as seen as the ratio between the reactions remained above 1. Our results, therefore, align well with previous studies, such as Wang & Arntfield (2016) who found that for octanal, both non-covalent and covalent interactions were important for flavor retention, but non-covalent interactions were only responsible for a small part of the flavor retention.

The values for the fitting parameters for alkenals were in general higher compared to the fitting parameters for aldehydes. Except for FBPI, all K_{alk} fits were around 2-10x higher than K_{ald}. This was attributed to the Michael adduct formation in addition to the Schiff base adduct. Michael adducts are expected to have a higher reactivity than Schiff bases (Zou et al., 2016).

The degree of retention, and fits for the covalent interaction parameters differed between the proteins. Most notably, WPI retained the aldehydes and alkenals to a lower extent compared to

the plant proteins. This effect is especially noticeable for the larger flavor molecules. WPI had the lowest parameter estimates for both the aldehydes and alkenals, with the fit for butanal as the only exception. FBPI had the highest parameter estimates for the aldehydes and CPPI for the alkenals. It is known that the protein source and extraction method influence the degree of flavor retention (Viry et al., 2018; K. Wang & Arntfield, 2014). The difference in retention for the different plant proteins could be related to their amino acid profile. It has been suggested that specific amino acids are more likely to interact with aldehydes (Meynier et al., 2004; Zou et al., 2016). To test this, a simple correlation assay was performed on the fitted results and amino acid contents. Interestingly, both cysteine and methionine content correlated with K_{alk}. Cysteine has been shown to have a higher reactivity compared to lysine, and arginine, which was attributed to its thiol group (Hamzalıoğlu & Gökmen, 2018). The correlations found in this study thus suggest that protein isolates with higher contents of sulfur-containing amino acids react more strongly with alkenals. Furthermore, other correlations with amino acids were identified, which might serve as handles for future studies.

In this study, concentrations up to 50 g/kg protein isolate were tested. With the predictive models, it can be calculated that higher protein contents will lead to even higher flavor losses, especially for plant proteins and large flavor molecules. For example, a 100x reduction of the headspace concentration of decanal is already reached at a protein concentration of 48, 30, 8, 28, and 93 g/kg for SPI, PPI, FBPI, CPPI, and WPI respectively. For decenal, these concentrations drop to 10, 15, 33, 2, and 58 g/kg. At 400 kg/kg protein, a relevant concentration for meat analogues, the headspace reduction for decanal is roughly 800, 1300, 5300, 1400, and 400x for SPI, PPI, FBPI, CPPI, and WPI respectively. For decenal, the headspace reduction is roughly 3900, 2600, 1200, 17400, and 700x respectively. These examples illustrate that plant-protein products might be harder to flavor than milk-protein products and this thus causes further challenges in their design.

6.6   Conclusion

This study investigated the flavor retention of aldehydes in protein dispersions, finding that alkenals bound stronger than aldehydes. Aldehydes can undergo a condensation reaction (Schiff base), whereas alkenals can have a further conjugate addition (Michael reaction). The protein source had a secondary effect on the retention. Aldehydes were more retained by FBPI and PPI, whereas alkenals were more retained by SPI and CPPI. The experimental data was fitted with a flavor partitioning model that revealed covalent interaction parameters differed between protein sources and increased with aldehyde chain lengths. The ratio between covalent and hydrophobic interactions was highest for the small aldehydes. This led to the conclusion that butanal and butenal were mostly retained by covalent interactions. For the other aldehydes, the outcomes of the fits suggested that hydrophobic interactions became increasingly important. WPI retained the aldehydes and alkenals to a less extent compared to the plant proteins, with an exception of butanal. Additionally, we found that the fitting parameters for alkenals correlated with the cysteine and methionine content of the plant proteins, suggesting thiol-containing amino acids were more reactive and contribute to a higher retention of alkenals. Our results provide important insights into the mechanisms of flavor retention in protein dispersions.

Appendix A

Table A.1: Correlation between amino acid content (mg/g protein) of pea, soy, fava bean, and chickpea and their model parameters obtained from fitting the flavor retention model on experimental data. The model parameters were the aldehyde partitioning coefficeint for butanal, hexenal, octanal, and decanal (K_{ald}) and the alkenal partitioning coefficient for butenal, hexenal, octenal, and decenal (K_{alk}).

	Butanal	Hexanal	Octanal	Decanal
Alanine	-0.75	-0.8	-0.62	-0.7
Arginine	0.66	0.61	0.73	0.71
Aspartic.acid	-0.52	-0.57	-0.39	-0.45
Cystine	-0.85	-0.84	-0.86	-0.87
Glutamic.acid	0.07	0.1	0	0.01
Glycine	0.41	0.48	0.26	0.34
Histidine	0.59	0.58	0.57	0.55
Isoleucine	0.52	0.56	0.45	0.52
Leucine	0.87	0.86	0.88	0.89
Lysine	-0.12	-0.07	-0.19	-0.11
Methionine	-0.84	-0.88	-0.76	-0.83
Phenylalanine	-0.65	-0.71	-0.52	-0.59
Proline	-0.08	-0.06	-0.13	-0.14
Serine	0.32	0.24	0.48	0.39
Threonine	-0.1	-0.03	-0.25	-0.18
Tryptophan	-0.19	-0.15	-0.27	-0.25
Tyrosine	0.35	0.43	0.18	0.28
Valine	0.63	0.68	0.51	0.6

Butenal	Hexenal	Octenal	Decenal
0.92	-0.01	0.94	0.95
0.14	-0.99	0.18	0.15
0.84	-0.39	0.9	0.89
0.3	0.84	0.26	0.29
-0.36	0.7	-0.47	-0.45
-0.94	0.44	-0.97	-0.97
-0.27	0.12	-0.38	-0.38
-0.65	-0.44	-0.57	-0.59
-0.32	-0.82	-0.29	-0.32
-0.4	-0.13	-0.28	-0.29
0.75	0.43	0.73	0.75
0.91	-0.2	0.95	0.95
-0.18	0.73	-0.28	-0.26
0.69	-0.84	0.68	0.66
-0.74	0.84	-0.77	-0.75
-0.32	0.87	-0.41	-0.39
-0.99	0.39	-0.99	-0.99
-0.89	-0.18	-0.85	-0.86

6

143

References

Aiking, H., & de Boer, J. (2018). The next protein transition. *Trends in Food Science and Technology*, *May*, 0–1. https://doi.org/10.1016/j.tifs.2018.07.008

Amagliani, L., O'Regan, J., Kelly, A. L., & O'Mahony, J. A. (2017). Composition and protein profile analysis of rice protein ingredients. *Journal of Food Composition and Analysis*, *59*, 18–26. https://doi.org/10.1016/j.jfca.2016.12.026

Anantharamkrishnan, V., Hoye, T., & Reineccius, G. A. (2020). Covalent Adduct Formation between Flavor Compounds of Various Functional Group Classes and the Model Protein β-Lactoglobulin. *Journal of Agricultural and Food Chemistry*, *68*(23), 6395–6402. https://doi.org/10.1021/acs.jafc.0c01925

Anantharamkrishnan, V., & Reineccius, G. A. (2020a). Influence of pH, Temperature, and Water Activity on Covalent Adduct Formation between Selected Flavor Compounds and Model Protein β-Lactoglobulin. *Journal of Agricultural and Food Chemistry*, *68*(47), 13833–13843. https://doi.org/10.1021/acs.jafc.0c06752

Anantharamkrishnan, V., & Reineccius, G. A. (2020b). Method to Characterize and Monitor Covalent Interactions of Flavor Compounds with β-Lactoglobulin Using Mass Spectrometry and Proteomics. *Journal of Agricultural and Food Chemistry*, *68*(46), 13121–13130. https://doi.org/10.1021/acs.jafc.9b07978

Baker, A., Žídek, L., Wiesler, D., Chmelík, J., Pagel, M., & Novotny, M. V. (1998). Reaction of N-acetylglycyllysine methyl ester with 2-alkenals: An alternative model for covalent modification of proteins. *Chemical Research in Toxicology*, *11*(7), 730–740. https://doi.org/10.1021/tx970167e

Broekema, R., Tyszler, M., van 't Veer, P., Kok, F. J., Martin, A., Lluch, A., & Blonk, H. T. J. (2020). Future-proof and sustainable healthy diets based on current eating patterns in the Netherlands. *The American Journal of Clinical Nutrition*, *112*(5), 1338–1347. https://doi.org/10.1093/ajcn/nqaa217

Gremli, H. A. (1974). Interaction of flavor compounds with soy protein. *Journal of the American Oil Chemists' Society*, *51*(1), 95–97. https://doi.org/10.1007/BF02542100

Guichard, E. (2002). Interactions between flavor compounds and food ingredients and their influence on flavor perception. *Food Reviews International*, *18*(1), 49–70. https://doi.org/10.1081/FRI-120003417

Hamzalıoğlu, A., & Gökmen, V. (2018). Investigation and kinetic evaluation of the reactions of hydroxymethylfurfural with amino and thiol groups of amino acids. *Food Chemistry*, *240*(May 2017), 354–360. https://doi.org/10.1016/j.foodchem.2017.07.131

Harrison, M., & Hills, B. P. (1997). Mathematical Model of Flavor Release from Liquids Containing Aroma-Binding Macromolecules. *Journal of Agricultural and Food Chemistry*, *45*(5), 1883–1890. https://doi.org/10.1021/jf9607876

Linforth, R. S. T., & Taylor, A. J. (1999). *Apparatus and methods for the analysis of trace constituents in gases* (Patent No. 5869344). United States Patent.

Meynier, A., Rampon, V., Dalgalarrondo, M., & Genot, C. (2004). Hexanal and t-2-hexenal form covalent bonds with whey proteins and sodium caseinate in aqueous solution. *International Dairy Journal*, *14*(8), 681–690. https://doi.org/10.1016/j.idairyj.2004.01.003

Michel, F., Hartmann, C., & Siegrist, M. (2021). Consumers' associations, perceptions and acceptance of meat and plant-based meat alternatives. *Food Quality and Preference*, *87*(August 2020), 104063. https://doi.org/10.1016/j.foodqual.2020.104063

Snel, S. J. E., Pascu, M., Bodnár, I., Avison, S., van der Goot, A. J., & Beyrer, M. (2023). Flavor-protein interactions for four plant proteins with ketones and esters. *Heliyon*, *9*(6), e16503. https://doi.org/10.1016/j.heliyon.2023.e16503

Tan, Y., & Siebert, K. J. (2008). Modeling bovine serum albumin binding of flavor compounds (alcohols, aldehydes, esters, and ketones) as a function of molecular properties. *Journal of Food Science*, *73*(1). https://doi.org/10.1111/j.1750-3841.2007.00591.x

Viry, O., Boom, R., Avison, S., Pascu, M., & Bodnár, I. (2018). A predictive model for flavor partitioning and protein-flavor interactions in fat-free dairy protein solutions. *Food Research International*, *109*(December 2017), 52–58. https://doi.org/10.1016/j.foodres.2018.04.013

Wang, K., & Arntfield, S. D. (2014). Binding of carbonyl flavours to canola, pea and wheat proteins using GC/MS approach. *Food Chemistry*, *157*, 364–372. https://doi.org/10.1016/j.foodchem.2014.02.042

Wang, K., & Arntfield, S. D. (2015). Binding of selected volatile flavour mixture to salt-extracted canola and pea proteins and effect of heat treatment on flavour binding. *Food Hydrocolloids*, *43*, 410–417. https://doi.org/10.1016/j.foodhyd.2014.06.011

Wang, K., & Arntfield, S. D. (2016). Probing the molecular forces involved in binding of selected volatile flavour compounds to salt-extracted pea proteins. *Food Chemistry*, *211*, 235–242. https://doi.org/10.1016/j.foodchem.2016.05.062

Weel, K. G. C., Boelrijk, A. E. M., Burger, J. J., Claassen, N. E., Gruppen, H., Voragen, A. G. J., & Smit, G. (2003). Effect of whey protein on the in vivo release of aldehydes. *Journal of Agricultural and Food Chemistry*, *51*(16), 4746–4752. https://doi.org/10.1021/jf034188s

Zhou, Q., & Cadwallader, K. R. (2006). Effect of flavor compound chemical structure and environmental relative humidity on the binding of volatile flavor compounds to dehydrated soy protein isolates. *Journal of Agricultural and Food Chemistry*, *54*(5), 1838–1843. https://doi.org/10.1021/jf052269d

Zou, Y., Pei, K., Peng, X., Bai, W., Huang, C., & Ou, S. (2016). Possible adducts formed between hydroxymethylfurfural and selected amino acids, and their release in simulated gastric model. *International Journal of Food Science and Technology*, *51*(4), 1002–1009. https://doi.org/10.1111/ijfs.13057

6

Chapter 7

General discussion

7.1   Outline

Current meat analogues on the market are already good alternatives for meat products. The most successful products are comminuted products, like burgers and nuggets, and small pieces that typically resemble chicken meat pieces. However, to maintain the success of meat analogue products, it is important to further innovate analogues for other meat products, for example larger whole cut products. The fact that the products should mimic meat to meet consumer wishes has been recently confirmed in a study by Michel et al. (2021).

One route to develop novel product concepts is to improve the most-used process to make meat analogues, which is extrusion. Innovation should lead to better overall product quality and to the creation of novel product textures and shapes. Another route is based on the use of ingredients to create novel textures. The aim of this thesis was therefore to get a better understanding on the effect of processing and the role of minor ingredients on the structuring of meat analogues. This aim was divided into three objectives, which are: 1) To demonstrate potential of a new, rotating die attached to an extruder; 2) To study the effect of minor ingredients on the structuring potential of soy protein isolate (SPI); 3) To quantify flavor binding to proteinaceous ingredients that are used or have potential for use in meat analogues. In this chapter, first the main findings of the thesis are summarized. Then, the importance of shear on structure formation will be discussed, as well as shear during cooling. The retention of flavors by proteins in meat analogues will be discussed, and the results obtained with a low protein concentration will be extrapolated to high protein concentrations present in meat analogues. Lastly, it will be investigated if flavors could possibly influence the texture properties as well. The chapter ends with an outlook for further research.

7.2   Main findings

In high moisture extrusion (HME), the shear rate in a traditional cooling die is directly determined by the throughput and the die dimensions. Therefore, this thesis describes the introduction of a novel rotating cooling die that was able to apply shear as an independent parameter (**Chapter 2**). The die, consisting of a rotating inner cylinder and a static outer cylinder, was attached to a twin-screw extruder. By changing the rotational speed, the rotational shear was directly affected during processing. Soy protein concentrate (SPC), pea protein isolate (PPI), and vital wheat gluten (VWG) responded differently to the applied rotational shear. Upon the addition of VWG to SPC and PPI, a range of anisotropic structures were obtained. Besides, it was found that each ingredient or combination of ingredients required different shear-values during cooling to obtain a fibrous product. Furthermore, the orientation of the obtained fibers depended on the shear rate applied. In **Chapter 3** the same rotating cooling die was used to test the rework potential of SPI and PPI meat analogues. SPI had the remarkable ability to form fibrous products with similar hardness and anisotropy when extruded twice. Even though the WHC and solubility were clearly affected with each extrusion cycle due to protein aggregation, this was repaired by heating and did thus not

affect the formation of fibrous products. This conclusion was further supported by similar rheological properties after a heat treatment of the extruded powders compared to the untreated isolates.

Chapter 4 described how the fibrousness of soy protein-based products can be improved through the addition of pectins from different sources. The products were formed with the shear cell. The addition of high methyl-esterified citrus (HMC) and soybean pectin (SYB) to SPI led to very pronounced fibrous products. It was concluded that pectin could have two main effects in the products: pectin droplets can coalesce and form a dispersed phase, which leads to anisotropy, and pectin can lead to inclusion and deformation of air bubbles.

The interactions between flavors and a range of plant proteins were quantified in **Chapter 5 and 6. Chapter 5** focused on the non-covalent interactions that are expected between proteins and esters and ketones. It was found that the retention of esters and ketones depended primarily on chain length of the flavor compounds. To model the interactions, it was sufficient to assuming only hydrophobic interactions to fit the results well. The difference between SPI, PPI, faba bean protein isolate (FBPI), and chickpea protein isolate (CPPI) were rather small, although the differences between the protein sources correlated to the hydrophobic index and solubility of the proteins. In **Chapter 6** mono-unsaturated and saturated aldehydes were examined. Now, the flavor retention model had to be extended with a covalent interaction parameter. It was found that the covalent interactions were mainly important for small aldehydes. Furthermore, a correlation between sulfur-containing amino acids present in proteins and the covalent interaction parameter was found.

7.3   Shear in the extruder cooling die

7.3.1   Influence on structure

Most of the current meat analogues are produced using high moisture extrusion cooking combined with a slit die in which the product is deformed and cooled (Cheftel et al., 1992; van der Sman & van der Goot, 2023). In the cooling die, shear stresses arise that are dependent on the throughput and die dimensions (Cornet et al., 2021). The shear might be responsible or enhance the fibrous structure formation in the meat analogue. However, the shear rate in the cooling die is not directly controllable. The introduction of a novel rotating cooling die could be a new route to texture plant proteins into meat analogues (**Chapter 2**). The rotation of the inner cylinder induced a rotational shear, which is controlled by the rotational speed. The rotating die consists of two sections that can both rotate and their rotational speed can be controlled with two independent motors. Different commonly used ingredients, SPC, PPI, and VWG, were structured with the rotating die into fibrous structures. The process exhibited consistent stability, with the maximally attainable throughputs being determined by the type of extruder used. When employing a twin-screw extruder with a 25 mm screw diameter, a maximum throughput of 40 kg/hr was attained for PPI, reaching the water pump's capacity limit. However, when utilizing a larger extruder with a 32 mm screw diameter, a maximum

throughput of 100 kg/hr was achieved for SPC, while PPI could be processed at a maximum throughput of 60 kg/hr. The maximum throughputs for the 32 mm screw with the rotating die were twice as high as those achieved with the slit die. Notably, the larger extruder could not run a stable process at a 0 rpm rotation of the inner rotating cylinder. Conversely, the extruder with the 25 mm screws maintained stability at 0 rpm, though no layer formation was observed. This suggests that the enhanced throughput is facilitated by the rotation within the cooling die. It is plausible that at this increased throughput and longer retention time (approximately 90 s for maximum throughput), the rotation contributed to improved cooling.

The rotating die applies additional shear during the cooling of the protein blend. Shearing during cooling in shear cell experiments conducted on PPI/VWG blends have demonstrated that moderate shear rates can promote the formation of fibrous structures (Köllmann et al., 2023). However, it was observed that shearing during the heating phase led to even more pronounced fibrous textures (Köllmann et al., 2023). In the context of the rotating die, it is possible that the initial section of the rotating die, where the material is still in a hot and deformable state, plays the dominant role in structure formation. This suggests that the application of shear forces during this stage is primarily responsible for the desired fibrous structure development. This has been indicated for the slit die as well, where mainly the inlet of the cooling die could induce the onset of fibrous structure formation (Wittek, Ellwanger, et al., 2021). Once the material solidifies, it is expected that the rotational shear would have limited impact on further structure development.

7.3.2   Comparison with shear cell and extruder with slit die

The novel rotating cooling die can be seen as a combination of high moisture extrusion cooking and a shearing device, such as the shear cell. In the shear cell, the shear is applied while heating, and shearing during cooling was not beneficial. In the rotating die, high mechanical stresses and shear are applied in the extruder barrel, whereas in the rotating cooling die the material is cooled and moderately sheared. A comparison between the two processes is not straightforward since they require different optimal settings. In general, a dry matter of 40% is preferred for shear cell structuring, and a shear rate of 39 s^{-1} for 15 min, although deviations of these settings are possible (Grabowska et al., 2016). In the experiments described in this thesis a dry matter content of 38 % for SPI and 40-42 % for PPI was used, and shear rate ranged between 31 s^{-1} and 71 s^{-1} (**Chapter 2 and 3**). In Figure 7.1 different samples from the two processes are compared. In general, it seems that the rotating cooling die induces more layer formation compared to the shear cell, while the color is lighter. The latter is probably due to the higher moisture content during processing and the shorter residence time at high tempeartures. As a reference, also a picture is added that was obtained for PPI with the slit die (Figure 7.1c), and for SPI with a slit die (Figure 7.1d) (Wittek, Zeiler, et al., 2021). The PPI sample was thinner (3 mm) compared to the sample obtained with the rotating die for the same extruder. Some thin fibers can be observed, but the material was softer and easily deformed between two fingers. The SPI sample was more layered compared to the sample

of the rotating die and shear cell, but the higher dry matter content might have led to more layer formation. For these three processes, it is plausible that layers are mainly formed due to elongational or shear flow (Wittek, Ellwanger, et al., 2021) and further enhanced by syneresis (van der Sman & van der Goot, 2023). The adjustable shear in the rotating cooling die could enhance layer formation. Then, when cooling down, the reduced WHC of the protein might result in expulsion of water and a further enhanced layer formation (Cornet et al., 2021).
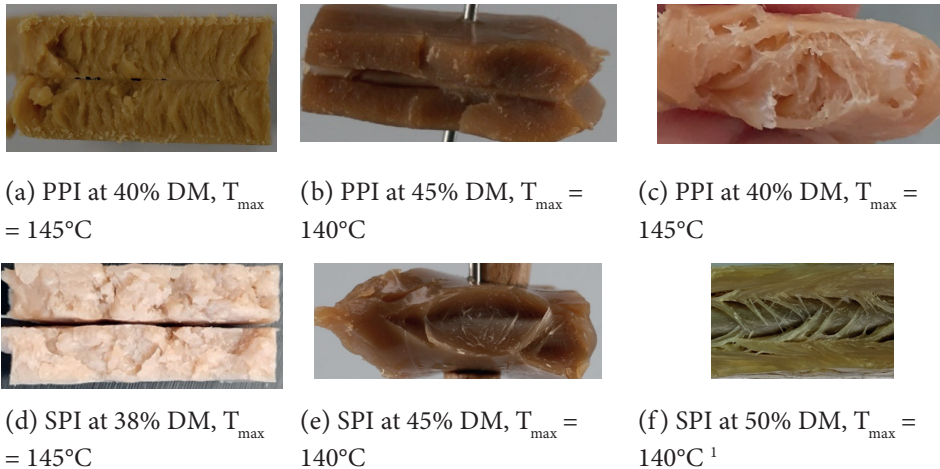

(a) PPI at 40% DM, T_{max} = 145°C

(b) PPI at 45% DM, T_{max} = 140°C

(c) PPI at 40% DM, T_{max} = 145°C

(d) SPI at 38% DM, T_{max} = 145°C

(e) SPI at 45% DM, T_{max} = 140°C

(f) SPI at 50% DM, T_{max} = 140°C [1]

Figure 7.1. Examples of samples obtained with the rotating cooling die with a shear rate of 51 s^{-1} (a, d), with a slit die (c, f), and with the shear cell at a rotation of 39 s^{-1} (b,e). Samples are made from either PPI (a, b, c) or SPI (d, e, f).

[1]*SPI produced with twin-screw extruder and slit die of 30 x 6 mm (Wittek et al., 2021)*

7.4   Flavoring meat analogues

Meat analogues are flavored to mask off-flavors and to improve the hedonistic properties of the product. These flavors generally consists of esters, ketones, aldehydes, and alkenes (Kale et al., 2022). Unfortunately, plant proteins have the tendency to bind with these flavors, thereby reducing their functionality in the product (**Chapter 5 and 6**). To quantify the interactions, a range of model mixtures that each contained only one plant protein and one flavor compound were used in this thesis. However, current meat analogues contain a much higher protein content and are a soft-solid and not a 'liquid' product. Those differences could hinder direct extrapolation of our results since both the higher protein concentration and the solid structure could influence protein-flavor interactions. Nevertheless, we think that the trends observed and main conclusions are still relevant for flavors in meat analogues, based on which assumption the obtained model is used to predict the retention at higher protein content. Apart from the concentration effect, other ingredients could also induce flavor retention, either actively or as a secondary effect by for example modifying pH or salt concentration.

7.4.1 Flavor retention during extrusion

When extrapolating the results of **Chapter 5 and 6** to high moisture extrusion cooking, at least three factors have to be taken into account: the higher protein concentration, the high temperatures in the extruder barrel, and the combination of different flavor compounds. These effects will be discussed below.

The protein concentrations tested in **Chapter 5 and 6** were between 0.5 and 5 %. These concentrations are thus much lower compared with the protein concentrations relevant for meat analogues. With the obtained model parameters for the different proteins and chemical classes, we can predict how much of the flavor will be retained at higher protein concentrations. A relevant isolate concentration for meat analogues to consider is 40% (DM basis). When assuming an average of 80% protein, we would thus expect a protein content of 32%. Then, we can calculate for the different chemical classes how much of the headspace will be reduced compared to when the compound is added in water. As an example, relative headspace concentration (RHC) was calculated for flavor compounds with a carbon count of 6 and 8 (Table 7.1). The RHC is predicted to be drastically reduced for all compounds, with a maximum RHC of 53%. For CPPI, the RHC's are especially low, with (almost) no concentration left for the compounds with a chain length of 8. In other words, to achieve the desired flavor concentration in a CPPI meat analogue, a 100x higher concentration should be added for octanone and octanoate, which is probably not feasible for several reasons. Some tests with PPI and hexanal in a HME setting were performed and the headspace concentration was measured. However, no detectable concentration in the headspace was found, even though according to our prediction in Table 7.1 we should have 21% left. It is thus concluded that the higher protein concentration has a drastic effect on the final flavor concentration, but other factors during processing reduce this concentration even further.

An example of a processing factor that is expected to affect the flavor concentration is the high processing temperature. The flavor retention in this thesis was measured at ambient temperature. During extrusion, elevated temperatures are applied of around 140 °C. This elevated temperature can affect flavor losses in three ways: 1) higher volatility of the flavors at higher temperatures (Khio et al., 2012); 2) an increase of covalent interactions;

Table 7.1. Prediction of the relative headspace concentration (%) of different flavor compounds when the protein concentration is 32% in the meat analogue. For example, for Hexanone and SPI, the relative headspace concentration compared to hexanone in water is 53%, thus the concentration is almost halved

RHC (%)	Hexanone	Hexanoate	Hexanal	Hexenal
SPI	53	23	33	6
PPI	42	11	21	10
FBPI	44	14	11	23
CPPI	6	8	20	15

and 3) weakening of protein-protein interactions, exposing hydrophobic regions that can interact with the flavor.

Interactions as a result of covalent reactions can increase upon heating and the effect of this increase on total retention depends on the specific compound. For the compounds studied in this thesis, aldehydes are expected to form covalent interactions in addition to hydrophobic interactions (Anantharamkrishnan et al., 2020). The covalent interactions could thus increase, while hydrophobic interactions are not expected to be influenced by temperature, except as a secondary effect due to changes to the protein structure, which will be discussed below. The retention of hexanal by canola protein increased gradually when heated to 95 °C for 60 min (Wang & Arntfield, 2015). However, the retention of nonanal to whey protein was found to be constant when heating to 80 °C for the first 10 min, and only increased slightly after 20 min (Kühn et al., 2008). This effect was attributed to an equilibrium between the release of reversibly retained nonanal, and the increase of irreversibly bound nonanal (Kühn et al., 2008). This would mean that for hexanal, covalent interactions are more important than hydrophobic interactions, while for nonanal the interactions are not dominated by covalent interactions. That would be in line with our hypothesis that smaller aldehydes are retained mainly by covalent interactions, whereas larger aldehydes are retained dominantly by hydrophobic interactions (**Chapter 6**). It is thus expected that heating will lead to more retention especially for the smaller aldehydes.

The effect of heating on hydrophobic interactions is caused by an effect on the protein itself. Initially, the retention increases because hydrophobic groups are exposed upon unfolding, but upon longer heating the protein starts to aggregate and retention will decrease (Kühn et al., 2008). As an example, 2-octanone was retained more by canola protein when heating for 2 min, after which the retention decreased upon continued heating at 95 °C (K. Wang & Arntfield, 2015a).

7

Octanone	Octanoate	Octanal	Octenal
11	3	7	2
7	1	4	2
8	2	2	6
1	1	2	0

7.4.2 Soluble versus insoluble protein

In **Chapter 5** a correlation between protein solubility and flavor retention was observed. This effect was studied further by separating the soluble proteins with a two-step centrifugation (16,000 x *g*, 30 min) in a 0.01 M phosphate buffer at pH 8. A difference was observed between the retention of esters between the soluble and insoluble fraction (Figure 7.1). For esters, retention by the soluble protein fraction was less compared to the insoluble and total fraction at both 0.5 and 2 % protein. This effect was most pronounced for octanoate. This indicates that higher protein solubility leads to less protein-flavor interactions, possibly due to less hydrophobic regions for the ester to interact with. For hexanoate and octanoate with SPI, the retention to the total protein fraction was in between soluble and insoluble retention indicating that the insoluble fraction is more responsible for retention of esters. Similarly, when solubilizing PPI at pH 3 or 11, less retention of ketones was found compared to pH 5, at which pH the protein was less soluble (K. Wang & Arntfield, 2015b).
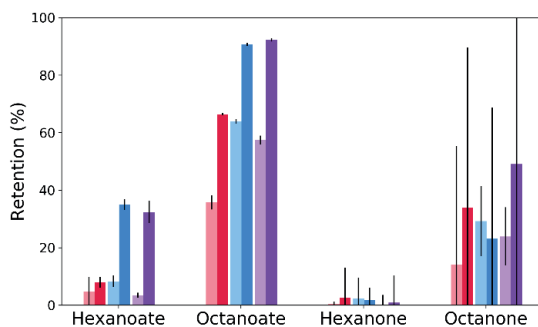
(a) PPI
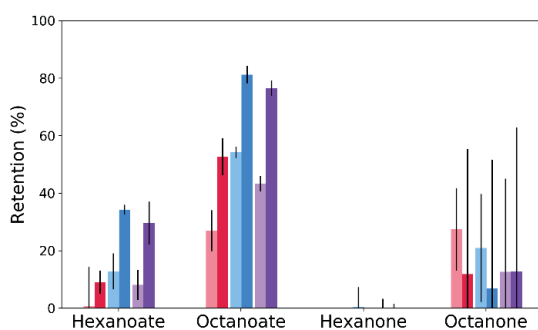
(b) SPI

Figure 7.2. The relative headspace concentration of esters and ketones in the soluble protein fraction (red), insoluble protein fraction (blue), and the total protein fraction (purple) for PPI (a) and SPI (b). Light colors represent a protein concentration of 0.5%, and darker colors a protein concentration of 2%. Fractions were separated with centrifugation.

7.4.3 Influence of flavor on texture

Aldehydes interact with the proteins through both hydrophobic and covalent interactions (Anantharamkrishnan & Reineccius, 2020). The interaction could induce changes to the protein and possibly its behavior during a structuring process (K. Wang & Arntfield, 2015c). To investigate if aldehydes could indeed induce changes to the protein matrix, a strain-sweep was performed on a 45% PPI dispersion with and without 0.1% butanal added. The test was performed both at 30 °C and after heating to 140 °C followed by cooling to 30 °C. The latter was included to mimic the temperature profile during HME. Butanal was chosen, since especially the small aldehydes are expected to form dominantly covalent interactions (**Chapter 6**). It was found though that the storage and loss moduli of PPI were not changed when 0.1% of butanal was added (Figure 7.2). This was somewhat unexpected, since in another study the addition of 0.1% octanal to 14.5% PPI increased G' and G'' in a plate-plate oscillatory frequency sweep (K. Wang & Arntfield, 2015c). However, the flavor concentration of 0.1% is much higher than the relevant concentration for flavoring meat analogues. Therefore, at lower concentrations, no effects on texture are expected upon the addition of aldehydes and ketones. It is thus unlikely that flavor addition will affect the texture of meat analogues during production.
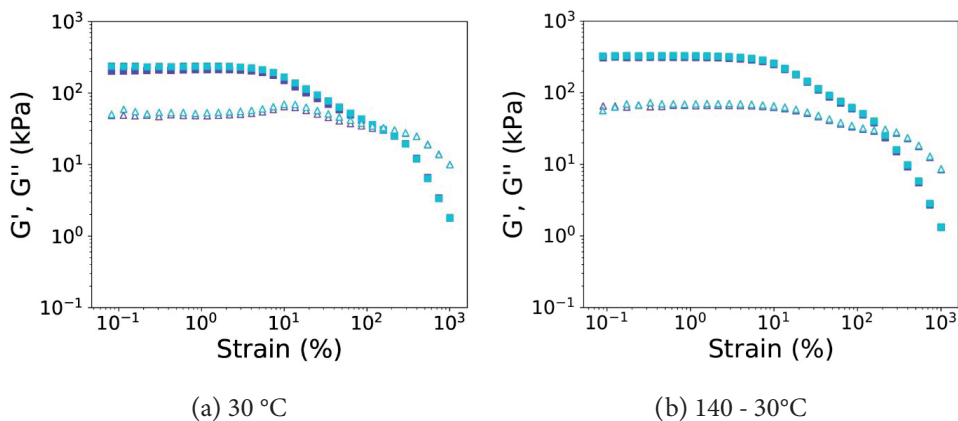

(a) 30 °C   (b) 140 - 30°C

Figure 7.3. Storage (G') and loss (G'') moduli obtained from an oscillatory strain sweep of PPI at 45% dry matter content (purple) and PPI with 0.1% butanal added (blue) measured at 30 °C (a) or after heating to 140 °C and cooling to 30 °C (b).

7.5   Suggestions for future research

As described in section 7.3, extrusion is mostly used to make meat analogue products industrially. However, a trend can be observed that researchers become interested in non-extrusion based methods to make next generation products. Examples of non-extrusion, mild processes are the manual elongation of zein in protein-starch blends (Dobson et al., 2023), and coacervation of pea protein with gellan gum at acidic conditions under shear (Ryu et al., 2023). Also, in the production of meat analogues there is a notable trend to investigate non-extrusion based techniques. 3D-printing and shear cell technology are examples of methods that are currently developed to produce meat analogues. (Ben-Shitrit et al., 2022; Köllmann et al., 2023; Qiu et al., 2023). Nevertheless, extrusion is already applied and used to produce fibrous products for several decades (Kyriakopoulou et al., 2019b). Therefore, the rotating die is of interest since it can be attached to an existing twin-screw extruder. The application of shear in the cooling die could allow for milder conditions in the extruder barrel. Indeed, when extruding with a screw diameter of 32 mm, a lower barrel temperature of approximately 125 °C was still successful in forming fibrous products, compared to temperatures of >135 °C in a conventional extruder set-up. To develop the technology further, it has to be understood how the design of the rotating die can be further improved.

In future research, it is crucial to investigate new process designs and updates for the rotating die used in extrusion. The current die design has limitations, such as fixed locations for motors and a reliance on two motors to be able to rotate the two sections separately. This makes the design somewhat complex, and a single motor design might simplify the process. A single motor is probably sufficient, since we observed that mainly in the first section of the rotating die the shear stress is beneficial. It is probable that mild shear is sufficient to aid in the structure formation, which could be achieved by one rotational speed that is not too destructive.

As mentioned, milder conditions in the extruder barrel are possible due to the extra added shear in the rotating die. In addition, higher throughputs were possible. Therefore, it would be of interest to rethink the complete process overall and investigate if the complexity of the twin-screw extruder is needed for the productions of fibrous products using the rotating cooling die. Since the structure formation is mainly expected to take place in the cooling die, any process that could transport proteins in a liquified form should be a good option to be coupled with the rotating die. Possibly, a single screw extruder could process the protein-water blend sufficiently well to transport the blend into the rotating die. The use of single screw extruder in combination with the rotating die simplifies the process considerably and probably require less energy. Both factors will lead to cost reductions. Comparative studies between the existing extruders and the single screw extruder coupled with the rotating die can provide valuable insights into the advantages and limitations of each process set-up. For example, different ingredients used for meat analogues could be tested in both settings and the obtained fibrous products could be compared in their anisotropy and hardness.

A broader understanding of the behavior of plant-based proteins is crucial in advancing our knowledge of structuring processes. As observed in **Chapter 2** different proteins respond in a specific manner on shear. To better understand the behavior of plant-based proteins behavior under shear, rheology seems the most relevant analytical technique. The results could be extrapolated using models to understand the flow behavior of the protein in the extruder dies (van der Sman et al., 2023). Further advancements in measuring in-line during extrusion, or preferably in the rotating die itself could increase our understanding. It is possible that different ingredients require different structuring mechanisms. The minor ingredient pectin induced fibrous texture formation when using shear cell technology (**Chapter 6**). It is possible that similar results could be obtained in extrusion. As hypothesized by van der Sman et al. (2023), the addition of a dispersed phase is not essential for extrusion, but could enhance fibrous structure. Further research is needed to validate the ability of pectins to induce fibrous texture formation in extrusion trials. Overall, it can be concluded that a better understanding of the behavior of the plant-based ingredients under processing conditions could help to select the right ingredients and design the right process (conditions) to develop the next generation products. A strong retention of flavors by plant-based proteins in meat analogues can be also expected in the rotating die or other non-extrusion-based processes. To still obtain a flavored meat analogue, a much higher concentration of flavors should be added as a consequence, with is not desired for multiple reasons including costs. Therefore, the addition of the flavor in a post-processing step seems more appropriate, and possibly the only feasible way to effectively add the flavor. The meat analogue could be marinated under vacuum and as such improve the juiciness of the meat analogues as well (Cornet et al., 2021). In the marinating solution, the flavors could be added. However, this mainly works for small meat analogue pieces. Alternatively, efforts can be made to develop plant proteins that possess cleaner taste profiles, eliminating the need for flavor maskers altogether. New plant breeding strategies, and novel extraction and processing techniques for plant proteins may help in creating cleaner-tasting alternatives that align with consumer preferences.

7.6   Concluding remarks

The main challenge for meat analogues is to create novel products with new structures or product dimensions. For this purpose, new processing technologies should be examined, and a better control over protein-flavor interactions is crucial. Therefore, this thesis introduced a novel rotating cooling die, which allows additional shearing in the cooling section to produce meat analogues with different structure and dimensions. Furthermore, a strong retention of flavors by different plant proteins was observed, especially for flavor compounds with larger molecular weight. It is concluded that the rotating die is a promising new processing technique to create other product structures, but this was not the solution to prevent strong protein-flavor interactions. Thus, flavoring of meat analogues still require other solutions like addition of flavors after structuring the plant proteins or the development of precurses that form flavor at the process conditions used to make the fibrous products.

References

Anantharamkrishnan, V., Hoye, T., & Reineccius, G. A. (2020). Covalent Adduct Formation between Flavor Compounds of Various Functional Group Classes and the Model Protein β-Lactoglobulin. *Journal of Agricultural and Food Chemistry*, *68*(23), 6395–6402. https://doi.org/10.1021/acs.jafc.0c01925

Anantharamkrishnan, V., & Reineccius, G. A. (2020). Method to Characterize and Monitor Covalent Interactions of Flavor Compounds with β-Lactoglobulin Using Mass Spectrometry and Proteomics. *Journal of Agricultural and Food Chemistry*, *68*(46), 13121–13130. https://doi.org/10.1021/acs.jafc.9b07978

Ben-Shitrit, E., Tomsov, A., Mandelik, D., Dikovsky, D., & Silberstein, S. (2022). *Meat analogues and methods of producing the same* (Patent No. US20220125072A1).

Cheftel, J. C., Kitagawa, M., & Queguiner, C. (1992). New Protein Texturization Processes by Extrusion Cooking at High Moisture Levels. *Food Reviews International*, *8*(2), 235–275. https://doi.org/10.1080/87559129209540940

Cornet, S. H. V., Snel, S. J. E., Lesschen, J., van der Goot, A. J., & van der Sman, R. G. M. (2021). Enhancing the water holding capacity of model meat analogues through marinade composition. *Journal of Food Engineering*, *290*, 110283. https://doi.org/10.1016/j.jfoodeng.2020.110283

Cornet, S. H. V., Snel, S. J. E., Schreuders, F. K. G., Van der Sman, R. G. M., Beyrer, M., & Van der Goot, A. J. (2021). Thermo-mechanical processing of plant proteins using shear cell and high-moisture extrusion cooking. *Critical Reviews in Food Science and Nutrition*, *0*(0), 1–18. https://doi.org/10.1080/10408398.2020.1864618

Dobson, S., Stobbs, J., Laredo, T., & Marangoni, A. G. (2023). A facile strategy for plant protein fiber formation without extrusion or shear processing. *Innovative Food Science and Emerging Technologies*, *86*. https://doi.org/10.1016/j.ifset.2023.103385

Grabowska, K. J., Zhu, S., Dekkers, B. L., De Ruijter, N. C. A., Gieteling, J., & Van Der Goot, A. J. (2016). Shear-induced structuring as a tool to make anisotropic materials using soy protein concentrate. *Journal of Food Engineering*, *188*, 77–86. https://doi.org/10.1016/j.jfoodeng.2016.05.010

Kale, P., Mishra, A., & Annapure, U. S. (2022). Development of vegan meat flavour: A review on sources and techniques. *Future Foods*, *5*. https://doi.org/10.1016/j.fufo.2022.100149

Khio, S. W., Cheong, M. W., Zhou, W., Curran, P., & Yu, B. (2012). Characterization of the volatility of flavor compounds in alcoholic beverages through headspace solid-phase microextraction (HS-SPME) and mathematical modeling. *Journal of Food Science*, *77*(1). https://doi.org/10.1111/j.1750-3841.2011.02474.x

Köllmann, N., Schreuders, F. K. G., Zhang, L., & van der Goot, A. J. (2023). On the importance of cooling in structuring processes for meat analogues. *Journal of Food Engineering*, *350*(March), 111490. https://doi.org/10.1016/j.jfoodeng.2023.111490

Kühn, J., Considine, T., & Singh, H. (2008). Binding of flavor compounds and whey protein isolate as affected by heat and high pressure treatments. *Journal of Agricultural and Food Chemistry*, *56*(21), 10218–10224. https://doi.org/10.1021/jf801810b

Kyriakopoulou, K., Dekkers, B., & van der Goot, A. J. (2019). Plant-Based Meat Analogues. In *Sustainable Meat Production and Processing*. Elsevier Inc. https://doi.org/10.1016/B978-0-12-814874-7.00006-7

Michel, F., Hartmann, C., & Siegrist, M. (2021). Consumers' associations, perceptions and acceptance of meat and plant-based meat alternatives. *Food Quality and Preference*, *87*(August 2020), 104063. https://doi.org/10.1016/j.foodqual.2020.104063

Qiu, Y., McClements, D. J., Chen, J., Li, C., Liu, C., & Dai, T. (2023). Construction of 3D printed meat analogs from plant-based proteins: Improving the printing performance of soy protein- and gluten-based pastes facilitated by rice protein. *Food Research International*, *167*. https://doi.org/10.1016/j.foodres.2023.112635

Ryu, J., Xiang, X., Hu, X., Rosenfeld, S. E., Qin, D., Zhou, H., & McClements, D. J. (2023). Assembly of plant-based meat analogs using soft matter physics: A coacervation-shearing-gelation approach. *Food Hydrocolloids*, *142*. https://doi.org/10.1016/j.foodhyd.2023.108817

van der Sman, R. G. M., Chakraborty, P., Hua, N. P., & Kollmann, N. (2023). Scaling relations in rheology of proteins present in meat analogs. *Food Hydrocolloids*, *135*(September 2022), 108195. https://doi.org/10.1016/j.

foodhyd.2022.108195

van der Sman, R. G. M., & van der Goot, A. J. (2023). Hypotheses concerning structuring of extruded meat analogs. In *Current Research in Food Science* (Vol. 6). Elsevier B.V. https://doi.org/10.1016/j.crfs.2023.100510

Wang, K., & Arntfield, S. D. (2015a). Binding of selected volatile flavour mixture to salt-extracted canola and pea proteins and effect of heat treatment on flavour binding. *Food Hydrocolloids*, *43*, 410–417. https://doi.org/10.1016/j.foodhyd.2014.06.011

Wang, K., & Arntfield, S. D. (2015b). Effect of salts and pH on selected ketone flavours binding to salt-extracted pea proteins: The role of non-covalent forces. *Food Research International*, *77*, 1–9. https://doi.org/10.1016/j.foodres.2015.03.017

Wang, K., & Arntfield, S. D. (2015c). Interaction of selected volatile flavour compounds and salt-extracted pea proteins: Effect on protein structure and thermal-induced gelation properties. *Food Hydrocolloids*, *51*, 383–394. https://doi.org/10.1016/j.foodhyd.2015.05.044

Wittek, P., Ellwanger, F., Karbstein, H. P., & Emin, M. A. (2021). Morphology development and flow characteristics during high moisture extrusion of a plant-based meat analogue. *Foods*, *10*(8). https://doi.org/10.3390/foods10081753

Wittek, P., Zeiler, N., Karbstein, H. P., & Emin, M. A. (2021). High Moisture Extrusion of Soy Protein: Investigations on the Formation of Anisotropic Product Structure. *Foods*, *10*(1), 102. https://doi.org/10.3390/foods10010102

7

Summary

English summary

Meat analogues can replace meat in the human diet and as such are thought to lower the environmental food print of current diets. Yet, the lack of similarity in texture and flavor makes the consumer hesitant to transition from meat to meat analogues. The process to produce many of the current meat analogues is based on extrusion technology. Extrusion can be used to create (ingredients for) products with low and high moisture and can as such mimic products such as burgers, nuggets, and chunks. However, to cover the full scope of meat products, other process solutions should be developed. Novel technologies are shear cell structuring, spinning, and 3D printing. However, those techniques are still in development or only applied on small scale. Another route to develop new production methods for meat analogues is to investigate the combination of different texturing processes. Therefore, a combination between high moisture extrusion and the shear cell technology was explored in this thesis, as a possible new route for texturing plant proteins. Apart from texture, meat analogues often lack similarity in terms of flavor. Off-flavors arise during the isolation and processing of plant-based ingredients. In addition, the proteins are known to interact with (added) flavors, which make them less available. It explains why protein-flavor interactions are studied in more detail in this thesis. The overall aim was to increase understanding on the effect of processing and minor ingredients on the structuring process of dense protein blends.

In **Chapter 2**, the rotating die attached to a twin-screw extruder was introduced as a new technology that allows the application of shear as an independent parameter in high moisture extrusion. The rotating die consists of an inner rotating cylinder and an outer cylinder that can be cooled. In this chapter, results are described with common ingredients for meat analogues to understand the potential of this rotating die. Three different rotational speeds of the inner cylinder were tested, which resulted in a range of textures for soy protein concentrate (SPC), pea protein isolate (PPI) and vital wheat gluten (VWG). Both SPC and combinations of PPI and VWG could be transformed into layered and fibrous products when using the rotating die, but the optimum process settings turned out to be dependent on the ingredients used. It was further concluded that the shear stress applied induced a different angle of the obtained fibers. In **Chapter 3** the same set-up of HME and the rotating die was used to investigate the rework potential of SPI and PPI. Despite the fact that HME had an impact on the protein through creating additional crosslinks, the material could be reworked in a second HME step without clear changes in the appearance of the fibrous product. Cross-link density decreased the solubility and WHC of the protein. Changes in rheological properties were also observed, but the changes were largely reversed after heat treatment. Rework is thus deemed to be possible for both SPI and PPI.

Chapter 4 describes the effect of minor ingredients on the fibrous structure formation of SPI. As a minor ingredient, different pectins were selected and their ability to induce fibrous structure formation in SPI was Investigated. The shear cell was used to form the fibrous products. It was found that the use of a different pectin led to products with various structures. Pectins obtained from soybean and citrus peel (high methyl-esterified pectins) induced fibrous structure formation, which was probably a result of the presence of highly

deformed air bubbles. It was concluded that the addition of pectin led to the creation of a second phase, but it also preserved the elastic properties of the continuous SPI-phase, which led to elongation of the dispersed phase.

The interactions between flavor and protein components were studied in **Chapter 5** and **Chapter 6.** The protein-flavor interactions were quantified by first studying flavor retention, and secondly describing flavor retention with the Harrison & Hills model. In **Chapter 5** non-covalent interactions were studied by adding esters and ketones to four different plant proteins. The retention of esters and ketones was described well by assuming solely hydrophobic interactions between the flavors and the proteins. In addition, a correlation between the solubility of the proteins and the fitting parameter in the mathematical model was found. In **Chapter 6** mono-unsaturated and saturated aldehydes were tested with the same plant proteins. As expected, the descriptive model had to be extended with the inclusion of a covalent interaction parameter. Experiments revealed that the type of aldehyde and chain length affected the retention of the flavors by the protein the most. The model outcomes showed that covalent interactions were mainly important for small aldehydes. The protein source had also an effect, but this effect was smaller. A correlation between sulfur-containing amino acids and the covalent interaction parameter hinted at a possible explanation for differences between protein sources.

Chapter 7 describes a reflection on the results and insights obtained in this thesis. The effect of shear in the cooling die was discussed. It was observed that additional shear in the cooling die could be beneficial for structure formation, especially when novel ingredients are used. It was hypothesized that the shear is probably especially important in the initial section of the cooling die, where the material is still hot and deformable. Furthermore, the relevance of the flavor studies was discussed. The use of a diluted protein system at equilibrium might pose difficulties when extrapolating the results to real meat analogues. However, the study shows that a certain classification of flavors and proteins was possible. Additional experiments described in chapter 7 revealed that the interactions between proteins and flavors hardly affected the structure formation process. However, the strong interactions between flavors and proteins, as well as the high temperatures applied, make it still a great challenge to maintain the functionality of flavors when added during processing in HME.

In conclusion, the use of a novel rotating die is a promising processing technique that can be directly applied in HME to produce fibrous products. Minor ingredients such as pectin could enhance fibrous structure formation, but it is advised to add minor flavor components after HME.

S

List of abbreviations

Abbreviation	Meaning
3D	Three-dimension
ANOVA	Analysis of variance
APCI-TOF-MS	Atmospheric pressure chemical ionization time-of-flight mass spectroscopy
CCR	Closed cavity rheometer
CLSM	Confocal laser scanning microscope
CPPI	Chickpea protein isolate
CTRW	Continuous time random walk
DM	Dry matter content
FBPI	Fava bean protein isolate
FC	Foaming capacity
FG	Flavor in the gas phase
FP	Flavor bound to protein
FW	Flavor in water
GC	Gas chromatography
HCL	Hydrochloric acid
HMC	High methyl-esterified citrus pectin
HME	High moisture extrusion
HPLC	High-performance liquid chromatography
LAOS	Large amplitude oscillatory shear
LMC	Low methyl-esterified citrus pectin
Log P	Octanol-water partition coefficient (log)
LVE	Linear viscoelastic
MC	Moisture content
MC	Moisture content
MW	Molecular weight
NaCl	Sodium chloride
P	Protein
pI	Isoelectric point
PPI	Pea protein isolate
RHC	Relative headspace concentration
SC	Shear cell
SDS-PAGE	Sodium dodecyl sulfate-polyacrylamide gel electrophoresis
SGB	Sugarbeet pectin

Abbreviation	Meaning
SME	Specific mechanical energy
SPC	Soy protein concentrate
SPI	Soy protein isolate
SYB	Soybean pectin
TF	Total flavor
TPA	Texture profile analysis
VWG	Vital wheat gluten
W	Water
WHC	Water-holding capacity
WHI	Weighted hydrophobic index
WPI	Whey protein isolate
XRT	X-ray microtomography

L

Acknowledgements

I have fantasized about writing these acknowledgements often while being on a hike or looking out of the train window. But now that I am actually writing it, it is difficult to find words that truly express the impact people made over the last years. Even choosing the language proofed difficult, which has resulted in a mixture of English, Dutch and French. I am so humbled by all the help and support I received, and I hope that my gratitude comes across on these pages for everyone that contributed, participated, or supported me during my journey.

Firstly, I want to express my immense gratitude to my supervisors **Michael** and **Atze Jan**. **Michael**, I cannot thank you enough for giving me the incredible opportunity to work on this exciting subject under your supervision. I am truly grateful for your openness to my ideas and for creating a welcoming space for me, even opening your house when I needed a place to stay. Your trust in me and this project have been a driving force behind my growth as a researcher. **Atze Jan**, ik wil je bedanken voor je steun en betrokkenheid tijdens mijn PhD. Je was altijd beschikbaar als ik hulp nodig had, en dacht mee over de juiste oplossingen. Ik heb ook veel geleerd van jouw feedback en ik voelde me gehoord en gemotiveerd.

Igor, bedankt dat je me zo warm hebt ontvangen bij Firmenich, voor al je enthousiasme, goede raad, en humor waarmee je alles goed wist te relativeren. Ik ben heel dankbaar dat ik zo veel met jou en je team heb kunnen samen werken. **Mirela** and **Shane**, it was such a pleasure to work together with you, I enjoyed all our discussions and your positive attitude always made me smile. **Narendra,** thank you for your help with the extrusion trials, and for the nice chats we had on numerous topics.

Sylvie, c'était vraiment un plaisir de travailler avec vous chez Firminy. Merci pour votre aide avec la filiere et pour m'inviter à travailler avec ton équipe. **Emmanuel, Nadege, Juna, Sylvain, Raffael** et tout le reste de l'équipe de Clextral, merci pour me laisser sentir bienvenue dans Firminy.

Denis and **Gordon** thank you for introducing me with a lot of enthusiasm to extrusion, helping out with theory and calculations, and for kindly giving me reading material.

Je tiens à remercier Hes-So Valais de m'avoir accueillie et mes collègues qui m'ont aidée tout au long de mon parcours. **Sergio**, merci d'avoir guidé et soutenu mon travail. **Anne** et **Alexia**, merci pour le soutien administratif. **Frédéric**, **Dimitri**, **Ysamar** et **Maria**, merci pour votre aide dans les travaux de laboratoire. **Thierry**, merci pour ton aide dans la commande des ingrédients. **Julien** et **Véronique**, merci de m'avoir permis d'utiliser les installations de votre laboratoire. **Wilfried**, **Stefan** et **Pascal**, merci de m'avoir accueilli dans le laboratoire de chimie et de m'avoir aidé avec les machines d'analyse. **Nancy**, merci pour ton aide avec Kjeldahl et pour les bons cafés. **Christoph** et **David**, merci de m'avoir aidé à mettre en place la méthode analytique et pour vos conseils avec Comsol. **Matthias**, merci de m'avoir inclus dans les discussions sur le Raman et pour nos discussions agréables. **Sandra**, **Laetitia** et **Laurence**, merci pour vos conseils et vos discussions fructueuses. **Gerrit**, merci pour les brèves

A

167

Miek and **Cora**, thank you for being my paranymphs. **Miek**, I am so grateful to have met you early on in my PhD, I have learned with and from you, and our almost daily contact gave me the feeling you were always there to give support. I also enjoyed our dinners, which you almost always ended up cooking for me and which never failed to be delicious. **Cora**, tu es mon lien entre Wageningen et Sion. C'était vraiment cool de passer une semaine ensemble à Wageningen, et nous avons essayé la plupart des restaurants. Merci aussi de m'aider avec mon français, en m'écoutant toujours patiemment.

Ik wil al mijn lieve vrienden bedanken die hun huizen voor mij beschikbaar maakten om te werken, te logeren of simpelweg in goed gezelschap te zijn (met heel erg lekker eten): **Charlotte, Bram, Sabine, Xanthe, Eline, Hinne, Shan, Pippi-Lotte** en **Tessa.** Jullie zijn stuk voor stuk fantastisch en altijd welkom bij mij. Mijn lieve vrienden van de Nascie: bedankt dat ik mee mocht op weekend en voor de leuke diners. **Rosa**, we zien elkaar veel te weinig maar ik ben super dankbaar voor alle spraakberichten, het videobellen, het weekend op het strand en de tijd in Australië. **Alina**, your decision to come to Switzerland for half a year was one of the highlights of my PhD and I loved walking next to lake Geneva with you. **Tati**, thank you for your help on anything plant-based, for staying with me in Switzerland for a while and for the nice trips. **Simone**, bedankt voor de lieve kaartjes.

Mijn lieve familie, misschien wel de belangrijkste om te bedanken omdat zij mij de ruimte hebben gegeven om mijn eigen pad te kiezen. **Pap** en **mam**, jullie hebben mij altijd aangemoedigd zonder verwachtingen. **Ole** en **Viggo**, bedankt voor jullie humor, voor de gezelligheid en voor jullie ontembare interesse. **Oskar** en **Cas**, bedankt dat jullie mijn ouders een beetje in de gaten houden. Ik ben trots op wat jullie hebben bereikt. **Quinta**, bedankt dat ik bij jou tot rust mocht komen.

Bardiya, *Azizam,* من از آن روز که دربند توام آزادم

IN MEMORIAM

Gijs Ruttenberg

1995-2022

Camiel Zwart

1980-2021

Fred Snel

1944-2022

Author

About the author

About the author

Silvia Snel was born on the 25th of July 1995 in Alkmaar, the Netherlands. Her pronounced aversion against meat finally drove her to become a vegetarian at 8 years old. Being a vegetarian in 2003 meant dealing with several low quality meat replacers, which she would criticize at the dinner table at the amusement of her brothers and slight despair of her parents. She went to high school at the Zaanlands Lyceum where her chemistry teacher planted the seed that beta studies might be the way to go.

She started her bachelor's study in Nutrition & Health at Wageningen University in 2013. Still vegetarian, she was interested to know the consequences of her own diet and decided to perform her BSc thesis on the possible health effects of replacing meat with pulses in the Dutch diet. The results convinced her to become vegan.

Still consuming and criticizing meat replacers regularly, she became curious about the production of food, which made her follow a minor on Food Technology. This sparked her interest, and she enrolled in the MSc Food Technology at Wageningen University in 2016. During her MSc she specialized in Product Design. As juiciness was one of the lacking aspects of meat replacers on the market, she studied the water holding capacity of meat analogues for her MSc thesis at the department of Food Process Engineering at Wageningen University. She went to do an internship at the Not Company in Santiago, Chile, to develop plant-based blood, which led to a patent. After completing her MSc degree, she continued working at the Not Company as Product Developer, where she worked on developing a plant-based burger, and helped out with other vegan products.

In 2020, she decided to come back to academia and continued her studies as a PhD candidate at Wageningen University. She performed her PhD externally at HES-SO University of Applied Sciences and Arts Western Switzerland.

List of publications

This thesis:

S.J.E. Snel, Y. Bellwald, A.J. van der Goot, and M. Beyrer. Novel rotating die coupled to a twin-screw extruder as a new route to produce meat analogues with soy, pea and gluten. *Innovative Food Science & Emerging Technologies* 81 (2022): 103152.

S.J.E. Snel, Y. Amroussi, A.J. van der Goot, and M. Beyrer. Rework Potential of Soy and Pea Protein Isolates in High-Moisture Extrusion. *Foods* 12, no. 13 (2023): 2543.

S.J.E. Snel, M. Pascu, I. Bodnár, S. Avison, A.J. van der Goot, and M. Beyrer. Flavor-protein interactions for four plant proteins with ketones and esters. *Heliyon* 9, no. 6 (2023) : e16503.

S.J.E. Snel, M. Pascu, I. Bodnár, S. Avison, A.J. van der Goot, and M. Beyrer. Flavor-protein interactions for four plant protein isolates and whey protein isolate with aldehydes. *LWT* 185 (2023): 115177.

S.J.E. Snel, K. Otto, M. Schlangen, A.J. van der Goot, and M. Beyrer. Type of pectin determines structuring potential of soy proteins into meat analogue applications. *Food Hydrocolloids* (2023): 109262.

Other publications:

S.H.V. Cornet, **S.J.E. Snel**, J. Lesschen, A.J. van der Goot, and R.G.M. van der Sman. Enhancing the water holding capacity of model meat analogues through marinade composition. *Journal of Food Engineering* 290 (2021): 110283.

S.H.V. Cornet, **S.J.E. Snel**, F.K.G. Schreuders, R.G.M. van der Sman, M. Beyrer, and A.J. van der Goot. Thermo-mechanical processing of plant proteins using shear cell and high-moisture extrusion cooking. *Critical Reviews in Food Science and Nutrition* 62, no. 12 (2022): 3264-3280.

C. De Gol, **S.J.E. Snel**, Y. Rodriguez, and M. Beyrer. Gelling capacity of cell-disrupted Chlorella vulgaris and its texture effect in extruded meat substitutes. *Food Structure* (2023): 100332.

A

Overview of completed training activities

Discipline specific activities

Courses

 Food Extrusion Technology, Sion, Switzerland (2020)
 Design of Food Extrusion Dies, Sion, Switzerland (2020)
 Food Proteins, Copenhagen , Denmark (2020)
 Rheology: the do's and don'ts, Wageningen, the Netherlands (2020)
 Online lecture series, Wageningen, the Netherlands (2020)
 Advanced food analysis, Wageningen, the Netherlands (2021)
 Big data analysis, Wageningen, the Netherlands (2021)
 Winter school on physical chemistry, Han sur Lesse, Belgium (2022)
 School of rheology, Leuven, Belgium (2022)

Conferences

 EFFoST conference, Lausanne, Switzerland (2021)[a]
 Meat analogues conference, Wageningen, the Netherlands (2021)[a]
 Food structure and functionality symposium, Cork, Ireland (2021)[b]
 Food structure and functionality symposium, Cork, Ireland (2022)[a]
 EFFoST conference, Dublin, Ireland (2022)[b]
 European PhD workshop, Copenhagen, Denmark (2023)[a]

General courses

 VLAG PhD week, Baarlo, the Netherlands (2020)
 Analyzing data with Python, edX (2020)
 Female leadership, Movielearning (2020)
 Scientific writing, Wageningen, the Netherlands (2020)
 Introduction to R, Wageningen, the Netherlands (2021)
 Applied statistics, Wageningen, the Netherlands (2021)
 Presenting online, Wageningen, the Netherlands (2021)
 Research data management, Wageningen, the Netherlands (2021)
 Scientific artwork, data visualization and infographics with Adobe Illustrator, Wageningen, the Netherlands (2022)
 Adobe indesign, Wageningen, the Netherlands (2023)

Other activities

Preparation of research proposal (2020)

HMEC Seminar (2021)[a]

PhD study tour to Singapore (2022)[a,b]

[a] Oral presentation

[b] Poster presentation